LATERAL CREEP BEHAVIOUR OF DISCRETE "WINKLER" PILE ELEMENTS IN ICE

by

Robert M. Kenyon

A Thesis
Presented to the University of Manitoba
in Partial Fulfilment of the Requirements
for the Degree of **Doctor of Philosophy**
in the Department of Civil and Geological Engineering

Winnipeg, Manitoba

January, 1994

ISBN 0-315-92203-6

Name _____

Dissertation Abstracts International is arranged by broad, general subject categories. Please select the one subject which most nearly describes the content of your dissertation. Enter the corresponding four-digit code in the spaces provided.

	0428 U·M·I
SUBJECT TERM	SUBJECT CODE

Subject Categories

THE HUMANITIES AND SOCIAL SCIENCES

COMMUNICATIONS AND THE ARTS
Architecture 0729
Art History 0377
Cinema 0900
Dance 0378
Fine Arts 0357
Information Science 0723
Journalism 0391
Library Science 0399
Mass Communications 0708
Music 0413
Speech Communication 0459
Theater 0465

EDUCATION
General 0515
Administration 0514
Adult and Continuing 0516
Agricultural 0517
Art 0273
Bilingual and Multicultural 0282
Business 0688
Community College 0275
Curriculum and Instruction 0727
Early Childhood 0518
Elementary 0524
Finance 0277
Guidance and Counseling 0519
Health 0680
Higher 0745
History of 0520
Home Economics 0278
Industrial 0521
Language and Literature 0279
Mathematics 0280
Music 0522
Philosophy of 0998
Physical 0523
Psychology 0525
Reading 0535
Religious 0527
Sciences 0714
Secondary 0533
Social Sciences 0534
Sociology of 0340
Special 0529
Teacher Training 0530
Technology 0710
Tests and Measurements 0288
Vocational 0747

LANGUAGE, LITERATURE AND LINGUISTICS
Language
- General 0679
- Ancient 0289
- Linguistics 0290
- Modern 0291

Literature
- General 0401
- Classical 0294
- Comparative 0295
- Medieval 0297
- Modern 0298
- African 0316
- American 0591
- Asian 0305
- Canadian (English) 0352
- Canadian (French) 0355
- English 0593
- Germanic 0311
- Latin American 0312
- Middle Eastern 0315
- Romance 0313
- Slavic and East European 0314

PHILOSOPHY, RELIGION AND THEOLOGY
Philosophy 0422
Religion
- General 0318
- Biblical Studies 0321
- Clergy 0319
- History of 0320
- Philosophy of 0322

Theology 0469

SOCIAL SCIENCES
American Studies 0323
Anthropology
- Archaeology 0324
- Cultural 0326
- Physical 0327

Business Administration
- General 0310
- Accounting 0272
- Banking 0770
- Management 0454
- Marketing 0338

Canadian Studies 0385
Economics
- General 0501
- Agricultural 0503
- Commerce-Business 0505
- Finance 0508
- History 0509
- Labor 0510
- Theory 0511

Folklore 0358
Geography 0366
Gerontology 0351
History
- General 0578
- Ancient 0579
- Medieval 0581
- Modern 0582
- Black 0328
- African 0331
- Asia, Australia and Oceania 0332
- Canadian 0334
- European 0335
- Latin American 0336
- Middle Eastern 0333
- United States 0337

History of Science 0585
Law 0398
Political Science
- General 0615
- International Law and Relations 0616
- Public Administration 0617

Recreation 0814
Social Work 0452
Sociology
- General 0626
- Criminology and Penology 0627
- Demography 0938
- Ethnic and Racial Studies 0631
- Individual and Family Studies 0628
- Industrial and Labor Relations 0629
- Public and Social Welfare 0630
- Social Structure and Development 0700
- Theory and Methods 0344

Transportation 0709
Urban and Regional Planning 0999
Women's Studies 0453

THE SCIENCES AND ENGINEERING

BIOLOGICAL SCIENCES
Agriculture
- General 0473
- Agronomy 0285
- Animal Culture and Nutrition 0475
- Animal Pathology 0476
- Food Science and Technology 0359
- Forestry and Wildlife 0478
- Plant Culture 0479
- Plant Pathology 0480
- Plant Physiology 0817
- Range Management 0777
- Wood Technology 0746

Biology
- General 0306
- Anatomy 0287
- Biostatistics 0308
- Botany 0309
- Cell 0379
- Ecology 0329
- Entomology 0353
- Genetics 0369
- Limnology 0793
- Microbiology 0410
- Molecular 0307
- Neuroscience 0317
- Oceanography 0416
- Physiology 0433
- Radiation 0821
- Veterinary Science 0778
- Zoology 0472

Biophysics
- General 0786
- Medical 0760

EARTH SCIENCES
Biogeochemistry 0425
Geochemistry 0996
Geodesy 0370
Geology 0372
Geophysics 0373
Hydrology 0388
Mineralogy 0411
Paleobotany 0345
Paleoecology 0426
Paleontology 0418
Paleozoology 0985
Palynology 0427
Physical Geography 0368
Physical Oceanography 0415

HEALTH AND ENVIRONMENTAL SCIENCES
Environmental Sciences 0768
Health Sciences
- General 0566
- Audiology 0300
- Chemotherapy 0992
- Dentistry 0567
- Education 0350
- Hospital Management 0769
- Human Development 0758
- Immunology 0982
- Medicine and Surgery 0564
- Mental Health 0347
- Nursing 0569
- Nutrition 0570
- Obstetrics and Gynecology 0380
- Occupational Health and Therapy 0354
- Ophthalmology 0381
- Pathology 0571
- Pharmacology 0419
- Pharmacy 0572
- Physical Therapy 0382
- Public Health 0573
- Radiology 0574
- Recreation 0575
- Speech Pathology 0460
- Toxicology 0383

Home Economics 0386

PHYSICAL SCIENCES
Pure Sciences
Chemistry
- General 0485
- Agricultural 0749
- Analytical 0486
- Biochemistry 0487
- Inorganic 0488
- Nuclear 0738
- Organic 0490
- Pharmaceutical 0491
- Physical 0494
- Polymer 0495
- Radiation 0754

Mathematics 0405
Physics
- General 0605
- Acoustics 0986
- Astronomy and Astrophysics 0606
- Atmospheric Science 0608
- Atomic 0748
- Electronics and Electricity 0607
- Elementary Particles and High Energy 0798
- Fluid and Plasma 0759
- Molecular 0609
- Nuclear 0610
- Optics 0752
- Radiation 0756
- Solid State 0611

Statistics 0463

Applied Sciences
Applied Mechanics 0346
Computer Science 0984
Engineering
- General 0537
- Aerospace 0538
- Agricultural 0539
- Automotive 0540
- Biomedical 0541
- Chemical 0542
- Civil 0543
- Electronics and Electrical 0544
- Heat and Thermodynamics 0348
- Hydraulic 0545
- Industrial 0546
- Marine 0547
- Materials Science 0794
- Mechanical 0548
- Metallurgy 0743
- Mining 0551
- Nuclear 0552
- Packaging 0549
- Petroleum 0765
- Sanitary and Municipal 0554
- System Science 0790

Geotechnology 0428
Operations Research 0796
Plastics Technology 0795
Textile Technology 0994

PSYCHOLOGY
General 0621
Behavioral 0384
Clinical 0622
Developmental 0620
Experimental 0623
Industrial 0624
Personality 0625
Physiological 0989
Psychobiology 0349
Psychometrics 0632
Social 0451

LATERAL CREEP BEHAVIOUR OF DISCRETE "WINKLER" PILE ELEMENTS IN ICE

BY

ROBERT M. KENYON

A Thesis submitted to the Faculty of Graduate Studies of the University of Manitoba in partial fulfillment of the requirements of the degree of

DOCTOR OF PHILOSOPHY

ABSTRACT

This experimental thesis tests the applicability of power law creep theory to model the creep behaviour of laterally loaded piles. This thesis also tests the use of pressuremeter creep tests to predict the creep behaviour of laterally loaded piles.

The experimental program consisted of forcing a short, cylindrical, rigid bar to translate laterally through a disc of polycrystalline ice at -2°C. Both single stage tests and a multi-stage test were performed over equivalent frontal pressures (load/projected frontal area) ranging from 1.0 MPa to 2.25 MPa. Creep test durations ranged from 100 hrs (2.25 MPa) to 1,000 hrs (1.0 MPa). The rigid bar was of the same diameter and a similar length as an NX-sized OYO pressuremeter probe, which had also been used (Kjartanson, 1986) to test the creep behaviour of similar ice.

The experimental program was unique in that it modelled directly the behaviour of a short section of a laterally loaded pile, under controlled laboratory conditions. It was also unique in its direct test result comparison to pressuremeter test results.

The test results of the rigid bar experiments were analyzed in terms of power law creep theory using engineering solutions to model the creep behaviour of a laterally translating cylinder. Test results were also compared directly with the results of pressuremeter creep tests. The conclusion of the analysis is that power law creep theory describes the behaviour of the bar adequately. The thesis also finds a direct correspondence between the bar behaviour and the pressuremeter creep tests.

ACKNOWLEDGEMENTS

This study was carried out under the direct supervision of Dr. D.H. Shields, Department of Civil Engineering, University of Manitoba. This author wishes to express his sincere gratitude to Dr. Shields for suggesting this research topic, and for his continued guidance, encouragement and support.

This author wishes to thank Dr. J. Graham, Dr. S. Rizkalla, and Dr. G. Sims who, as members of the Advisory Committee, provided useful ideas, constructive criticism, and positive encouragement. While visiting at this university, Mr. F. Baguelin and Dr. R. Frank provided many helpful comments, as did Dr. L. Fransson.

Financial support of the author, in the form of scholarships and fellowships, was provided by the Roads and Transportation Association of Canada, Mobil Oil Corporation, Gulf Canada Ltd., and the Natural Sciences and Engineering Research Council. Financial support by the University of Manitoba, through postgraduate teaching assistantships, is also acknowledged.

This experimental thesis could not have been completed without the excellent help of Mr. E. Lemke, Chief Technician, and the technical support staff of the Civil Engineering Department. Mr. J. Clark and Mr. S. Meyerhoff fabricated the experimental apparatus. Mr. D. Fedorowich and Mr. M. Green assembled the instrumentation and the data acquisition system. A very special "thank you" is owed to Mr. B. Turnbull for all his assistance during the experimental program.

Gratitude is expressed to Mrs. I. Trestrail for her efficient typing and preparation of the manuscript.

Finally, thank you to my family who persevered through the trials and tribulations of this thesis. In particular, thank you to my mother, Mary Kenyon, and to my wife, Robin Allison, for their support and encouragement.

TABLE OF CONTENTS

LIST OF TABLES

LIST OF FIGURES

LIST OF PHOTOS

CHAPTER 1

INTRODUCTION

Since the late 1960's, major resource development projects in the Canadian and Alaskan arctic have required that geotechnical engineers design and construct large engineering projects in areas underlain by permafrost (perennially frozen ground). Much of this permafrost is classified as "dirty ice" or "ice-rich".

The design of vertical piles subjected to lateral loads is one of the problems which geotechnical engineers have been investigating in permafrost. Piles of this kind are used to carry elevated pipelines over warm, thermally-sensitive permafrost, to support bridge piers, and to found offshore structures subjected to lateral ice loads.

In more conventional, unfrozen soils, the design of piles subjected to lateral loads generally follows the beam-on-elastic foundation concept attributed to Winkler (1867). Hetenyi (1946) gives a detailed description of this approach. Analytically, the pile is considered to consist of a series of independent segments or Winkler elements, each of which is supported by some kind of "spring". In the case of frozen soils or ice, the Winkler "springs" are assumed to be non-linear and to have a deformation modulus which is time-dependant (Rowley et al., 1973, 1975; Nixon, 1984; Neukirchner and Nixon, 1987). In another approach, a dashpot is added in series with a spring (Foriero and Ladanyi, 1990; Morin et al., 1991).

In either approach it is necessary to define the load-time-displacement relationship for each Winkler layer. The definition of the load-time-displacement relationship is based upon the results of uniaxial compression creep tests in the laboratory, on in situ

creep tests such as pressuremeter tests (Rowley et al., 1973, 1975), or by conducting full-scale pile load tests.

In reviewing the published literature regarding the creep of laterally loaded piles, this author concluded that since the late 1960's the modelling of laterally loaded piles in permafrost has grown increasingly sophisticated. There is, unfortunately, no way to tell if the increase in sophistication is warranted because so few measurements have been made of actual pile behaviour.

Virtually all models rely on a volumetric transformation from cylindrical cavity expansion (the pressuremeter) to the volume displaced by a laterally translating cylinder, to solve the problem of laterally loaded piles (Rowley et al., 1973, 1975; Nixon, 1984; Neukirchner and Nixon, 1987). The assumption is that if a long, semi-cylindrical cavity is loaded radially (the pressuremeter), and another long cylindrical bar is loaded laterally, both under equivalent pressure, then the volume displaced by the semi-cylinder would equal the volume displaced by the projected vertical area of the cylindrical bar over a given time period. Implicit in this assumption is the belief that pressuremeter test results can be used to predict the creep behaviour of a laterally loaded pile.

Prior to this thesis, there had been no experimental verification of this fundamental assumption. One objective of this thesis, therefore, was to test the hypothesis regarding the volume transformation from cylindrical cavity expansion to a laterally translating cylindrical pile element, under carefully controlled laboratory conditions. The experimental plan was to create a single Winkler layer of polycrystalline ice, and to force this single Winkler pile element to translate through the ice. Analytically, the objective was to determine the validity of Rowley et al.'s (1973)

transformation by comparing directly the results of the Winkler pile element tests with the results of pressuremeter creep tests conducted by Kjartanson (1986) in similar ice. A second objective was to compare directly the expansion rate of the pressuremeter probe and the displacement rate of the pile element at various times. The third objective was to test the applicability of power law creep theory to the bar displacement phenomenon.

This thesis represents an extension to our fundamental knowledge regarding the use of the pressuremeter to predict the behaviour of laterally loaded piles in ice or ice-rich frozen soils.

CHAPTER 2

CREEP OF LATERALLY LOADED PILES IN WARM ICE OR ICE-RICH FROZEN SOILS

2.1 INTRODUCTION

This chapter reviews the published literature regarding the behaviour of laterally loaded piles in ice or ice-rich frozen soils. The review concludes that although modelling techniques have become increasingly sophisticated in the last 20 years, there is at present no way to tell if this increase in sophistication is warranted. Part of this problem can be attributed to the very small amount of test data in the literature, which contains a total of 8 load test results under various conditions. Part of the problem may also be due to the low experimental quality of half of those 8 tests. This chapter concludes that experimental testing of the fundamental assumptions of these models is necessary. Only then can the question of the predictive accuracy be properly addressed.

This chapter opens with a short description of the behaviour of ice and a review of power law creep theory. Power law creep theory is reviewed because it has been used in the modelling of the creep behaviour of virtually all permafrost foundation problems investigated so far. Next, examples of how power law theory has been applied to various boundary value problems are summarized. These examples include solutions for the pressuremeter and for the translation of a discrete "Winkler" element, plus a number of common foundation problems. The chapter continues with a review of the creep of laterally loaded piles, both from a modelling and from an experimental basis. No modellers have checked experimentally their fundamental assumptions regarding how a

short finite length of pile actually translates through a creeping mechanism. Hence the models are not validated, and there is a need for high quality testing of this fundamental problem.

2.2 SOME GENERAL CHARACTERISTICS OF ICE

The following subsection is a short general description of the crystallography of ice, and of the nature of the physical processes occurring during its deformation at high homologous temperatures. The description is meant as background to the thesis, and is not a review of the extensive literature of ice physics or ice mechanics. This author has drawn primarily from Sego (1980), Mellor (1979), Gold (1978) and Michel (1978) in preparing this subsection.

The general type of creep curve shown in Figure 2.1a is typical of the creep behaviour of many polycrystalline materials, including ice and ice-rich frozen soils (Ladanyi, 1972). Figures 2.1b and 2.1c show the corresponding strain versus time, and strain rate versus time, respectively, when the yield strength of the material is exceeded. The stress-strain behaviour consists of an instantaneous elastic strain, ϵ_o, followed by 3 phases of creep. These phases are characterized as:

(I) Primary creep, where strain rate decreases with time

(II) Secondary creep, where the strain rate remains constant with time

(III) Tertiary creep, where the strain rate accelerates.

Not all polycrystalline materials exhibit all three phases of creep. For polycrystalline ice, true secondary creep does not appear to occur, at least not at high homologous temperatures and compressive or shear stresses from 1.0 to 2.5 MPa (Mellor

and Cole, 1982(a); Kjartanson et al., 1988). Instead, the secondary creep phase consists of a single inflection point separating primary from tertiary creep. For engineering purposes, failure of ice can be generally defined as the end of primary creep.

In order to understand the deformation mechanisms occurring within the ice during creep, it is necessary to first consider a single ice crystal. A single crystal of ice can be visualized as having an appearance similar to that of a wooden pencil. The lead of the pencil forms the c-axis of the ice crystal, and the plane perpendicular to the c-axis, i.e. the cross-section of the pencil, is termed its basal plane.

An ideal ice crystal consists of oxygen and hydrogen atoms arranged tetrahedrally at a separation of 2.76 Å. This gives rise to hexagonal symmetry about the c-axis. Adjoining molecules lie in a set of parallel planes which form the basal planes of the crystal. A single unit cell of the crystal structure contains 4 molecules and has a theoretical density of 0.917 Mg/m^3 at 0°C.

The mechanical behaviour of a single crystal is markedly anisotropic. The basal plane is the sole glide plane of the lattice. Shear stress applied parallel to the plane results in strain rates at least two orders of magnitude greater than that resulting from shear normal to the plane (Mellor, 1979). In terms of its mechanical behaviour, a single crystal of ice can be compared to a new deck of playing cards, where the resistance to shear along the plane of the cards is much lower than normal to the plane.

This anisotropy can have a marked influence on the mass behaviour of polycrystalline ice. Random orientation of strongly anisotropic individual crystals results in variable compliance from crystal to crystal, depending on how individual basal planes are oriented relative to the shear stresses.

Even the purest form of ice contains impurities such as solid particles, ionic impurities (such as salt), and air bubbles. Concentrations of these impurities occur within and along grain boundaries, and affect grain boundary movements. Depending on the purity and temperature, there may also be a thin liquid layer surrounding individual crystals (Michel, 1978). These impurities are in addition to dislocations which are inherent to any crystalline material. Dislocations are defects in the crystal lattice structure. They may occur as point defects in an individual crystal, as line defects, or they may be stacking defects.

Pure elastic deformation of ice is characterized primarily by straining of the molecular bonds of individual ice crystals, and some instantaneous movement along grain boundaries. In a polycrystalline arrangement, not all crystals will be strained by the same amount initially, so there remains the potential for delayed elastic deformation.

True static values of Young's modulus, E, are difficult to measure, due to the creeping nature of the ice. Therefore, statically determined values vary widely, but range from 1 to 10 GPa (Michel, 1978). Higher values occur when the load is applied very quickly, say at the speed of elastic waves, while lower values are recorded under static load tests. Dynamic values of E are in the order of 10 GPa. Gold (1978) gives a concise summary of the elastic characteristics of ice (see also Michel, 1978). On the other hand, Mellor (1979) notes that applying large stresses "instantaneously" leads to premature damage of the test specimen, and recommends loading the ice slowly when its creep characteristics are to be determined.

Primary creep is a delayed elastic (classical visco-elastic) strain hardening phenomenon which is dominated by delayed elastic molecular straining, plus grain

boundary sliding, a reorientation of crystals in the shear zone, the development of microcracking, and the migration of dislocations.

Tertiary creep begins when there is no delayed elastic action remaining, so that strain softening processes can dominate. Softening processes include increased microcrack formation and propagation, the multiplication of dislocations at larger strains, and syntectonic recrystallization. Recrystallization results in a preferred reorientation of basal planes aligned with shear stresses, and hence a dramatic increase in deformation rate. Researchers allude to a theoretical maximum creep rate, or a finite limit to the softening processes, but this area has not been studied in detail.

2.3 POWER LAW CREEP THEORY

The power law creep model is a phenomenological or engineering model (Hult, 1966) which was based upon the observed behaviour of metals at high homologous temperatures. Power law creep theory has been described as macroanalytical (Ladanyi 1972, 1981; Andersland et al., 1978), versus a micromechanistic theory which is based upon established laws of physics at the molecular, atomic, or sub-atomic level.

Historically, the first published creep study is attributed to Andrade (1910). Andrade reported the results of lead wires subjected to dead weight loading at room temperature. His work established the general nature of the creep process from a macroanalytical point of view, but engineers continued using elastic theory until the 1920's.

During the 1920's, engineers began to measure the creep behaviour of building materials such as iron, steel, and concrete. These creep experiments led to the first

development in engineering creep theory when Bailey (1929) and Norton (1929) proposed that a power law relationship, relating secondary creep rate and stress, be used to replace Hooke's Law in analyzing the creep of uniaxially loaded bodies. The theory was generalized to multiaxial states of stress by Odqvist (1933), and Bailey (1935). The study of creep of metals intensified following World War II, resulting in a number of monographs on creep such as those by Finnie and Hellor (1959), Odqvist (1962), Hult (1966), and Odqvist (1966). Each of these monographs presented the theory of power law creep, and then applied the theory to solve select boundary value problems.

In the late 1960's and early 1970's, major development projects occurred in the Canadian and Alaskan arctic, associated primarily with discovery of major hydrocarbon deposits off the north slope of Alaska and in the Mackenzie Delta in Canada. These developments required that geotechnical engineers design and construct large structures on sites underlain by permafrost. Much of the permafrost was ice-rich, leading researchers such as Nixon (1978), Morgenstern et al. (1980), Ladanyi (1981), and Weaver and Morgenstern (1981) to conclude that the creep behaviour of polycrystalline ice constituted an upper bound to the creep of ice-rich frozen soil.

Ladanyi (1972) may be credited for introducing power law creep theory to geotechnical engineers. In 1972 he published "An engineering theory of creep of frozen soils", a paper which borrowed extensively from Hult (1966) and Odqvist (1966) in terms of the constitutive model for uniaxial and multiaxial states of creep of ice-rich frozen soils and ice. Following the publication of the 1972 paper, power law creep theory was applied to a number of foundation boundary value problems including:

1. The pressuremeter problem (Ladanyi and Johnston, 1973).

2. Laterally loaded piles (Rowley et al. 1973, 1975).
3. Strip footings (Ladanyi, 1975, 1983).
4. Circular footings and plate anchors (Ladanyi and Johnston, 1974).
5. Deep end bearing piles and plate anchors in frozen soils (Ladanyi and Johnston, 1974; Ladanyi and Paquin, 1978).
6. Friction piles (Morgenstern at al. 1980).

The references shown represent only the first published research regarding a particular boundary problem. The pressuremeter test, for example, has since been examined by Ladanyi and Saint-Pierre (1978), Ladanyi et al. (1979), Ladanyi (1982), Ladanyi and Eckardt (1983), Huneault (1984), Fensury (1985), Murat et al. (1986), Kjartanson (1986), and Kjartanson et al. (1988). Power law creep theory is therefore widely used today in permafrost engineering, and forms the basis for the modelling of most foundation engineering problems in creep sensitive frozen soils.

2.3.1 Constitutive Equations: Uniaxial State of Stress

As discussed in the previous section, power law creep theory evolved initially based upon the behaviour of metals in uniaxial creep. Historically, the creep laws were developed first in terms of uniaxial creep, and then were generalized to solve multiaxial boundary value problems. This subsection mirrors that historical progression from uniaxial creep to a generalized model for multiaxial creep.

2.3.1.1 Secondary Creep

Many analytic and numerical models of creep assume that secondary creep forms the dominant creep mechanism. Analytically, this represents the simplest assumption, and so historically has been considered first. Figure 2.2 shows a series of creep curves, each obtained at constant temperature, and each from a material loaded under a series of constant stresses $\sigma_1 < \sigma_2 < \sigma_3 < \sigma_4$. According to Hult (1966) and Ladanyi (1972), secondary creep is approximated by a straight line, the slope of which is extended back to the ordinate at t = 0. The intercept is termed the pseudo-instantaneous strain. Assuming this approximation, the strain ϵ at any time, t, is given by:

$$\epsilon = \epsilon^{(i)} + \dot{\epsilon}^{(c)}\, t \tag{2.1}$$

where $\epsilon^{(i)}$ and $\dot{\epsilon}^{(c)}$ are functions of applied stress and temperature. The pseudo-instantaneous strain $\epsilon^{(i)}$ consists of an elastic (reversible) portion $\epsilon^{(ie)}$, plus a plastic (irreversible) portion $\epsilon^{(ip)}$. The elastic portion can be expressed as:

$$\epsilon^{(ie)} = \frac{\sigma}{E'} \tag{2.2}$$

where E' is a temperature-dependent fictitious Young's modulus. The fictitious Young's modulus, E', is smaller than the instantaneous elastic modulus, because $\epsilon^{(ie)}$ contains some delayed elasticity. The plastic portion may be approximated by a power law (Odqvist, 1952):

$$\epsilon^{(ip)} = \epsilon_k \left[\frac{\sigma}{\sigma_k}\right]^k, \quad k \geq 1 \tag{2.3}$$

where ϵ_k is an arbitrary small strain introduced for normalization purposes, σ_k plays the

role of a normalizing stress, and $k \geq 1$.

The total pseudo-instantaneous strain is therefore given by:

$$\begin{aligned} \epsilon^{(i)} &= \epsilon^{(ie)} + \epsilon^{(ip)} \\ &= \frac{\sigma}{E^{I}} + \epsilon_k \left[\frac{\sigma}{\sigma_k}\right]^k \end{aligned} \tag{2.4}$$

In practise, the pseudo-instantaneous strain is typically taken at the end of 1 minute (Ladanyi and Johnston, 1978). Its pseudo-elastic creep $\epsilon^{(ie)}$ can be taken as the initial tangent modulus of the 1-minute stress-strain readings, and the plastic creep component taken as the difference between $\epsilon^{(i)}$ at 1 minute and $\epsilon^{(ie)}$. Hult (1966) suggests that at small stresses, pseudo-elastic strain may tend to dominate such that (2.3) can be ignored. Conversely, at large stresses, the plastic response may tend to dominate.

The relationship between the steady secondary creep rate $\dot{\epsilon}^{(c)}$ and stress σ is found to follow a power law formulation, known commonly as Norton's law (Norton, 1929), where:

$$\dot{\epsilon}^{(c)} = \dot{\epsilon}_c \left[\frac{\sigma}{\sigma_c}\right]^n \tag{2.5}$$

The quantity $\dot{\epsilon}_c$ is an arbitrary small creep strain rate, introduced to give the creep parameter σ_c the dimension of stress. The creep parameter σ_c is termed the creep proof stress, and is the stress which would cause the creep strain rate $\dot{\epsilon}_c$. In log-log space, Equation (2.5) linearizes to:

$$\log \left[\frac{\dot{\epsilon}^{(c)}}{\dot{\epsilon}_c} \right] = n \log \sigma - n \log \sigma_c \ . \qquad (2.6)$$

Once $\dot{\epsilon}_c$ has been arbitrarily assigned, then the secondary creep parameters σ_c and n are determined from the log-log plot as shown in Figure 2.3.

Finally, substituting (2.4) and (2.5) into (2.1), the strain at any time, t, is given by:

$$\epsilon = \frac{\sigma}{E'} + \epsilon_k \left[\frac{\sigma}{\sigma_k} \right]^k + \dot{\epsilon}_c \left[\frac{\sigma}{\sigma_c} \right]^n t \qquad (2.7)$$

The constitutive Equation (2.7) may be solved by conducting a series of constant stress controlled creep tests, or alternately, multi-stage tests may be conducted to solve the constitutive equation (Ladanyi, 1972). Ladanyi proposed a graphical summation procedure, as shown on Figure 2.4, to determine the equivalent accumulated pseudo-instantaneous and secondary creep strains. Examples showing how to solve the constitutive creep Equation (2.7) are given by Hult (1966) and Andersland et al. (1978). The foregoing model of linearized secondary creep formed the constitutive creep model for Ladanyi's 1972 paper.

2.3.1.2 Primary Creep

When the lifetime of the structure is of the same order of time as the duration of primary creep, then Ladanyi's (1972) linearized secondary creep model is not applicable. Now, the requisite constitutive equations must describe more precisely the decreasing creep rate of the primary creep period. The primary creep model which follows, was

proposed by Ladanyi and Johnston (1973), again following the formulation of Hult (1966). Their purpose was to extrapolate from a series of short-term multistage pressuremeter creep tests, what the longer term secondary creep behaviour might be.

Ladanyi and Johnston (1973) started with the strain-hardening, primary space power law creep expression from Hult (1966):

$$\epsilon^{(c)} = K\,\sigma^{n}\,t^{b}\ ,\ (b<1). \tag{2.8}$$

Differentiation with respect to time, with constant stress, and elimination of t, yields the strain-hardening creep law:

$$\frac{d\epsilon^{(c)}}{dt} = K^{1/b}\,b\,\sigma^{n/b}\,(\epsilon^{(c)})^{-(1-b)/b}, \tag{2.9}$$

which, for convenience, can be written:

$$\frac{d}{dt}\,(\epsilon^{(c)})^{1/b} = \left[\frac{\dot{\epsilon}_c}{b}\right]\left[\frac{\sigma}{\sigma_c}\right]^{n/b}. \tag{2.10}$$

For a constant-stress creep test, it follows that the creep strain becomes:

$$\epsilon^{(c)} = \left[\frac{\dot{\epsilon}_c}{b}\right]\left[\frac{\sigma}{\sigma_c}\right]^{n} t^{b} \tag{2.11}$$

where $\epsilon^{(c)}$, $\dot{\epsilon}_c$, and σ_c are as defined for the secondary creep Equation (2.5), and b is the primary creep parameter. Note that for b=1, Equation (2.11) degenerates to the secondary creep Equation (2.5).

Worked examples for processing data are given by Andersland, Sayles, and Ladanyi (1978). Data processing in this thesis is as follows. First, on a log-log graph, plot $\epsilon^{(c)}$ versus t for each stress increment. For a constant stress test, equation (2.11)

in log-log space becomes:

$$\log \epsilon^{(c)} = \log C + b \log t \tag{2.12}$$

where:

$$C = \left[\frac{\dot{\epsilon}_c}{b}\right] \left[\frac{\sigma}{\sigma_c}\right]^n \tag{2.13}$$

If the model is valid, then the data of $\epsilon^{(c)}$ versus t should plot as a series of straight, separate, and parallel lines. The arithmetic slope of the lines gives the creep exponent b.

Next, note that at t=1 time unit, Equation (2.11) becomes:

$$\epsilon^{(c)}_{t=1} = \left[\frac{\dot{\epsilon}_c}{b}\right] \left[\frac{\sigma}{\sigma_c}\right]^n \tag{2.14}$$

From the previous plot, determine the values of $\epsilon^{(c)}$ at t=1 time unit for each stress level σ. Plot $\epsilon^{(c)}$ at t=1 versus σ in log-log space. Now Equation (2.14) in log-log space becomes:

$$\log \epsilon^{(c)}_{t=1} = \log D + n \log \sigma \tag{2.15}$$

where:

$$D = \frac{\dot{\epsilon}_c}{b} \sigma_c^{\frac{1}{n}} \tag{2.16}$$

The data plots as a single straight line of arithmetic slope n. The intercept at σ=1 results in D, and the remaining creep parameter σ_c can be obtained by substitution back into (2.16).

At this point it should be noted that the specific format of the constitutive

equations for primary and secondary creep do vary, particularly in terms of the arbitrary creep strain rate $\dot{\epsilon}_c$, and the corresponding creep proof stress. The format of the equations shown above is consistent with Andersland, Sayles, and Ladanyi (1978). There are two other formats which appear in the literature. For example Hult (1966) presents Equation (2.11) as:

$$\epsilon^{(c)} = \frac{1+\mu}{\tau^{\frac{1}{(1+\mu)}}} \left[\frac{\sigma}{\sigma_c}\right]^{\frac{m}{(1+\mu)}} t^{\frac{1}{(1+\mu)}} \tag{2.17}$$

where:

$$\frac{1}{1+\mu} = b$$

$$\frac{m}{1+\mu} = n$$

$$\tau = \frac{1}{\dot{\epsilon}_c}$$

In Hult's format, μ represents the strain hardening in primary creep. For secondary creep μ becomes equal to zero. On the other hand, Morgenstern et al., (1980) express (2.11) as:

$$\epsilon^{(c)} = B\ \sigma^n\ t^b \tag{2.18}$$

where B has dimensions of stress^{-n}.time^{-b}.

2.3.2 Multiaxial States of Stress: Constitutive Equations

Generalization of the uniaxial primary and secondary creep constitutive equations to multiaxial states of stress follows Hult (1966), Odqvist (1966), and Andersland, Sayles and Ladanyi (1978). For the multiaxial stress state, σ, ϵ, and $\dot{\epsilon}$ are replaced by the

equivalent stress σ_e, the equivalent creep strain ϵ_e, and the equivalent strain rate $\dot{\epsilon}_e$, respectively.

The equivalent multiaxial stress, strain, and strain rates are given below in terms of principal stresses, strains and strain rates:

$$\sigma_e^2 = \tfrac{1}{2}\left[(\sigma_1-\sigma_2)^2 + (\sigma_2-\sigma_3)^2 + (\sigma_3-\sigma_1)^2\right] \tag{2.19}$$

$$\epsilon_e^2 = 2/9\left[(\epsilon_1-\epsilon_2)^2 + (\epsilon_2-\epsilon_3)^2 + (\epsilon_3-\epsilon_1)^2\right] \tag{2.20}$$

$$\dot{\epsilon}_e^2 = 2/9\left[(\dot{\epsilon}_1-\dot{\epsilon}_2)^2 + (\dot{\epsilon}_2-\dot{\epsilon}_3)^2 + (\dot{\epsilon}_3-\dot{\epsilon}_1)^2\right] \tag{2.21}$$

The above constitutive equations for multiaxial creep assume the validity of the von Mises (1928) relationship for isotropic solids under a multiaxial state of stress:

1. The directions of principal creep strains and principal stresses coincide.
2. The rates of shear strains and shear stresses are proportional.
3. The creep flow depends on deviatoric stress, and is independent of hydrostatic pressure.
4. Incompressibility of the material.

2.3.3 Stress Redistribution During Creep

The constitutive equations for primary and secondary creep assume that the material is undergoing stationary creep. The term stationary creep means that the spatial distribution of stress remains constant with time. It does not mean that the creep rate is

constant. This assumption is correct for the simple case of uniaxial compression tests of small right cylindrical samples, when load compensation is made for the increased cross-sectional area of the specimen, but is not valid, say, for the pressuremeter case, nor is it valid for laterally loaded piles.

In order to resolve this problem, a numerical solution for stress redistribution, based upon finite element modelling, has been proposed for the pressuremeter by Murat et al. (1986). The technique has been tested by Shields et al. (1989), who concluded that the pressuremeter determined values of n and b are in good agreement with those deduced from uniaxial compression tests, when this technique is applied. To date there is no similar numerical solution for a laterally loaded Winkler element of a laterally loaded pile.

2.3.4 Solutions to Selected Boundary-Value Problems

This subsection presents solutions to a number of boundary value problems, as applied to foundation engineering in ice-rich frozen soils. Its purpose is to show that power law creep theory is frequently used in foundation design of frozen soils, and to indicate the nature of the solutions. The section starts with the solution of the pressuremeter test, follows with solutions for a discrete Winkler element, and concludes with examples of several other foundation problems.

2.3.4.1 The Pressuremeter Test

In permafrost engineering, sampling and transporting of frozen soil samples over long distances to a laboratory for testing is difficult, due to the likelihood of thermal

disturbance of the samples during transport (Baker, 1976; Ladanyi and Johnston, 1978). On the other hand, in situ testing reduces the possibility of such thermal degradation. It is for this reason that the pressuremeter creep test as proposed by Ladanyi and Johnston (1973), and improved by Fensury (1985) and Kjartanson (1986), is considered the preferred method of measuring the constitutive creep properties of frozen soil.

The pressuremeter problem is modelled as the expansion of a vertical, infinitely long cylindrical cavity in an infinite half-space. Plane strain conditions are assumed. The solution to this boundary value problem is given by Hult (1966) and Ladanyi and Johnston (1973) for primary creep as:

$$\ln\left[\frac{r}{r_o}\right] = \left[\frac{\sqrt{3}}{2}\right]^{n+1} \left[\frac{\dot{\epsilon}_c}{b}\right]^{b} \left[\frac{2(p-p_o)}{n\sigma_c}\right]^{n} t^{b} \qquad (2.22)$$

where:

r = current cavity radius

r_o = cavity radius at t=0

p = cavity pressure

p_o = cavity pressure at r=∞, and

n, σ_c, $\dot{\epsilon}_c$, b are as defined previously.

For secondary creep, b=1, and Equation (2.22) becomes:

$$\frac{d}{dt}\left[\ln\frac{r}{r_0}\right] = \left[\frac{\sqrt{3}}{2}\right]^{n+1} (\dot{\epsilon}_c) \left[\frac{2(p_c-p_o)}{n\sigma_c}\right]^{n} \qquad (2.23)$$

Note that at small strains, $\ln\frac{r}{r_o} = \frac{r-r_o}{r_o} = \frac{\Delta r}{r_o}$. Equation (2.22) for primary creep,

and (2.23) for secondary creep have the same form as the constitutive Equations (2.11) and (2.5). The techniques for solving for σ_c, n, and b are as discussed previously.

2.3.4.2 A Single Winkler Element of a Laterally Loaded Pile

A Winkler element of a beam or pile is a short rigid section of the beam or pile. Numerical solutions generally assume that the beam or pile can be considered as a series of such Winkler elements. There are three papers in the literature proposing engineering solutions to the creep behaviour of a laterally loaded discrete Winkler element.

Rowley et al. (1973, 1975) present test results of lateral pile load tests on cylindrical piles in ice-rich silt near Inuvik, N.W.T. The tests were of relatively short duration (typically 2 hours per stage), and so the observed creep was of a primary type. The authors proposed transforming the radial expansion of a semi-cylinder cavity (the pressuremeter) to the lateral creep translation of the same cavity (the pile), by assuming the volumetric expansion of the semi-cylinder equals the volume displaced by the projected vertical area of a laterally translating cavity of the same diameter.

Assuming this volumetric transformation is valid, then the volume displaced by the semi-cylinder is:

$$\Delta V = \frac{\pi}{2}\left[(r_o + \Delta r)^2 - r_o^2\right] \tag{2.24}$$

where:

r_o = initial radius of the semi-cylinder

Δr = increase in radius expansion.

On the other hand, the volume displaced by the projected frontal area of the translating cylinder is:

$$\Delta V = y * B \tag{2.25}$$

where:

y = the lateral displacement of the cylinder

B = diameter.

Equating the two volumes yields:

$$y = \frac{\pi}{8} B \left[\left[1 + \frac{\Delta r}{r_o} \right]^2 - 1 \right] \tag{2.26}$$

Backsubstituting into (2.22) gives:

$$\frac{y}{B} = \frac{\pi}{8} \left[\left[1 + \left[\frac{\sqrt{3}}{2} \right]^{n+1} \left[\frac{2}{n} \right]^n \left[\frac{p - p_o}{\sigma_c} \right]^n \left[\frac{\dot{\epsilon}_c}{b} \right]^b t^b \right]^2 - 1 \right] \tag{2.27}$$

where:

p = equivalent frontal pressure acting against the projected vertical area of the bar

p_o = in situ lateral earth pressure

B = pile diameter, and

b, n, σ_c are the creep parameters for a given $\dot{\epsilon}_c$.

Nixon (1978) proposed that a cylindrical tube or strip-loaded area embedded in a viscous medium at a depth of several diameters will displace during secondary creep at a rate $\dot{u}$ given by:

$$\dot{u} = I \, a \, \dot{\epsilon}_c \left[\frac{p}{\sigma_c} \right]^n \tag{2.28}$$

where:

a = pile radius

p = horizontal pressure on the projected vertical area of the bar loaded area

n, σ_c = creep parameters for a given $\dot{\epsilon}_c$, and

I is an influence factor.

Nixon proposed that the value of I be taken from Ladanyi's (1975) analysis for a deep strip footing. The expression for I is:

$$I = \left[\frac{2}{n}\right]^n \left[\frac{\sqrt{3}}{2}\right]^{n+1} \tag{2.29}$$

Nixon (1978) had conducted a finite element analysis of the problem, which confirmed the appropriateness of Ladanyi's approach.

Foriero and Ladanyi (1989) present a streamlined solution for a rigid cylinder moving laterally within a nonlinear viscoelastic medium. The solution is based upon the constitutive model for secondary creep, a simulation of flow in the vicinity of the cylinder, and a general bound theorem. The simulation of the flow pattern was based upon the Vivatrat et al. (1984) model for flow of a cylinder through ice, and Baguelin et al.'s (1977) solution for stress distribution in front of the cylinder.

The resulting solution for a rigid cylinder translating through an ice mass is identical in form to (2.26), but now the influence factor is given by:

$$I = \left[\frac{2\ (n+1)\ (n+3)}{\pi\ n^2\ (\frac{4}{\sqrt{3}})^{\frac{(n+1)}{n}}} \right]^3 \qquad (2.30)$$

Foriero and Ladanyi report good agreement between the influence factor I calculated from (2.27), and the influence factor calculated by (2.26). For the case of n=3 for ice (Morgenstern et al., 1980), I = 0.172 is calculated from (2.27) and I = 0.167 calculated from (2.26).

2.3.4.3 Grouted Rod Anchors and Vertically Loaded Friction Piles in Permafrost

The creep of deep, grouted rod anchors has been modelled by Johnston and Ladanyi (1972). The grouted anchors, which are long and cylindrical in shape, are used to support transmission and communication towers in the arctic. The model assumes that there is no slippage at the anchor-soil interface, and that the frozen soil or ice deforms in simple shear. For these assumptions, the steady state or secondary displacement rate is given by:

$$\dot{u}_a = a\ \frac{3^{(n+1)/2}}{n-1}\ \dot{\epsilon}_c \left[\frac{\tau_a}{\sigma_c} \right]^n \qquad (2.31)$$

where:

$\dot{u}_a$ = secondary displacement rate of the anchor

a = anchor (or pile) radius

τ_a = average applied tangential shear stress

σ_c, n = creep parameters for a given $\dot{\epsilon}_c$

The distribution of shear stresses at any radial distance r was taken from Nadai (1963) as:

$$\tau = \tau_a \ (a/r) \tag{2.32}$$

This same solution has been applied to the problem of vertically loaded friction piles in ice-rich frozen soils by Nixon and McRoberts (1976), Morgenstern et al. (1980) and Weaver and Morgenstern (1981).

2.3.4.4 Shallow Foundations

Solutions for both strip and circular footings have been developed from cylindrical and spherical cavity expansion theories, respectively. Ladanyi (1975) developed the solution for a strip footing by applying the exact solution for creep of a semi-cylinder (Ladanyi and Johnston, 1973), and assumed the volume displacements of the semi-cylinder are equal to those of the strip footing. This solution is the same approach as for the laterally loaded pile. To model the secondary creep of strip footings, Nixon (1978) developed influence factors based upon the footing shape and depth of embedment. The influence factors were calculated following a finite element analysis of various shapes of footings and spanning a range of creep parameters, n.

Ladanyi (1983) reviewed Nixon's (1978) approach, and concluded that the secondary settlement rate of a footing in ice or ice-rich frozen soil can be expressed as:

$$\dot{S} = I \frac{B}{2} \dot{\epsilon}_c \left[\frac{q}{\sigma_c}\right]^n \tag{2.33}$$

where:

$\dot{S}$ = secondary creep rate of the strip footing

I = influence factor based on footing shape

B = foundation width or diameter

q = applied vertical pressure

n, σ_c = creep parameters for a given $\dot{\epsilon}_c$.

Approximate values of I, as estimated from cavity expansion theories are:

$$I = \left[\frac{3}{2n}\right]^n \text{ for circular footings} \tag{2.34}$$

and

$$I = \left[\frac{\pi\sqrt{3}}{4}\right]\left[\frac{\sqrt{3}}{n}\right]^n \text{ for strip footings} \tag{2.35}$$

2.3.4.5 Plate Anchors and/or End Bearing Piles

The problems of deeply embedded single-helix type plate anchors, to support transmission towers, was modelled by Ladanyi and Johnston (1974), assuming the deformation of the ice or ice-rich frozen soil approximates that of an expanding spherical cavity of radius a. This same solution has also been proposed (Weaver and Morgenstern, 1981) to solve the creep of end bearing piles. Here the settlement rate is given by:

$$\dot{\mu}_a = a\,\frac{2}{3}\left[\left[1 - \frac{\dot{\epsilon}_c}{2}\left[\frac{3(p_i - p_o)}{2n\,\sigma_c}\right]^n\right]^{-3} - 1\right] \tag{2.36}$$

where:

a = plate anchor or pile radius

p_i = cavity expansion pressure

p_o = original ground pressure at the anchor level or pile top

n, σ_c = creep parameters.

Interestingly, each of the foregoing solutions to the various foundation problems represented some volumetric transformation from either cylindrical cavity expansion, or spherical cavity expansion to the volume displaced by some particular foundation shape.

2.4 REVIEW OF PUBLISHED STUDIES OF LATERALLY LOADED PILES IN ICE OR ICE-RICH FROZEN SOILS

This subsection reviews what has been published regarding the creep behaviour of laterally loaded piles in ice or ice-rich frozen soils. This problem is more complex than that of a discrete Winkler element; here an attempt is made to model how a vertical elastic beam (a series of discrete Winkler elements) interacts with the ice under lateral loading.

Historically, there have been two basic approaches to modelling the behaviour of laterally loaded piles in frozen soils.

1. Analytic approaches, using the theory of subgrade reaction.
2. Numerical solutions, using the Winkler model (Winkler, 1867), and considering the pile as a series of discrete pile segments.

Four published studies have examined the creep of laterally loaded piles in ice or ice-rich frozen soils[1]. Chronologically, they have included: the work by Rowley et al.

---

1 Papers published as a result of the work in this thesis (Kenyon et al., 1991; Morin et al., 1991) are not included in this review. Instead, these papers are referred to in Chapter 5.

(1973, 1975); the work by Nixon (1984), and Neukirchner and Nixon (1987); the work by Foriero and Ladanyi (1989, 1990, 1991), and the work by Domaschuk et al. (1988, 1991).

Investigators have proposed either analytic solutions, (Rowley et al. 1973; Nixon, 1984; Foriero et al., 1989), or numerical solutions (Nixon, 1984; Foriero et al., 1990; Morin et al., 1991). There have been, however, very few reliable experimental data against which investigators could check their models. To date there has been a total of eight published lateral pile load tests. The tests consisted of: four full-scale pile load tests under field conditions (Rowley et al., 1973, 1975); three model pile (12.7 mm in diameter by 200 mm long) tests in ice under controlled laboratory conditions (Nixon, 1984); and one large-scale pile load test in frozen sand under controlled laboratory conditions (Domaschuk et al., 1988, 1991).

2.4.1 Lateral Pile Load Test Study by Rowley, Watson, and Ladanyi (1973, 1975)

Rowley et al. (1973, 1975) reported on 4 full-scale lateral pile load tests, and 6 pressuremeter creep tests completed near Inuvik, N.W.T. in 1971 and 1972. The hypothesis of their study was that the creep of laterally loaded piles could be predicted from the results of pressuremeter creep tests, assuming that Equation (2.24) was valid.

The frozen soils at the site are summarized by Table 2.1. They consisted primarily of peat in an ice matrix (ice content of 180-570%), and an ice-rich clayey silt (ice content of 180%). According to Weaver's (1979) permafrost classification system, the soils are classified as dirty ice, and ice-rich frozen soils, respectively. Ladanyi (1981) suggests that the flow laws for ice constitute the upper bound of creep for such

materials.

Ground and air temperatures during the pile load testing program are summarized on Figure 2.5. The testing was completed during late November 1971. At that time, ground temperatures at the datum station were steady and ranged from 0.0°C to -0.4°C. In contrast to the datum station ground temperatures, average daily air temperatures ranged from -20°C to -30°C, and were dropping steadily. Ground temperatures measured adjacent to two timber piles (poor thermal conductivity) were approximately -2°C, but no measurements were taken adjacent to the steel piles. The two types of piles have different thermal conductivities, and it is most likely that the permafrost temperatures surrounding the two pile types were different. The investigators analyzed the data for both types of piles assuming the permafrost was -2°C.

General information regarding the piles is summarized on Table 2.2. Piles were installed in 0.46 m diameter holes augured down to the gravel till at the 2.75 m depth. A 10 to 11 cm thick annulus between the augured hole and the piles was back-filled with a medium to coarse sand. This method of pile installation is significant experimentally, because the sand was an ice-poor frictional material, much less sensitive to creep than the surrounding in situ dirty ice.

A total of six pressuremeter creep tests were performed the following year, each at a depth of 1.5 m in the dirty ice (peat in an ice matrix). The tests consisted of two standard pressuremeter tests, three multistage creep tests with 15 min duration per stage, and one multistage test with 10 hours under load for the last stage. The constitutive creep parameters were given as: σ_c = 0.31 MPa, n = 3.38, and b = 0.86, for $\dot{\epsilon}_c = 10^{-5}$ min^{-1}.

Figures 2.6 and 2.7 show typical pile load test results for the timber and steel piles, respectively. The piles were stage-loaded, each stage held either until movement ceased, or for a period of 24 hours. Creep curves for individual stages have the shape of primary creep curves.

The analysis of the pile creep data followed the analytic subgrade reaction solution of Broms (1964) for piles in unfrozen soils. The Broms solution is for a linear elastic time-independent displacement, but at any particular time t, the subgrade reaction modulus K was solved as the secant modulus of the load-deflection creep curve.

In order to test their hypothesis, an equivalent time-dependant value of K was also calculated from the pressuremeter creep tests, assuming Equation (2.27) was valid. Figure 2.8 compares the time-dependant values of K determined from the pile load tests, versus K, as determined from the pressuremeter creep tests.

There were two apparent problems with the comparison. First, the value of K is different for the steel piles (S-5-L and S-4-L) than for the timber piles (T-2-L and T-3-L). Calculated K values for the two pile types plot as separate parallel lines. Secondly, the K value from the pressuremeter tests decays much more rapidly than for the pile load tests.

The discrepancy between K determined from the steel pile data versus K determined from the timber pile data suggests that the two piles were tested at different temperatures. If both piles were tested at the same temperature, then both sets of data should plot on one line. As discussed previously, it is most likely that the frozen soil surrounding the steel pile was colder than for the timber pile.

The discrepancy between K determined from the pile tests versus K from the

pressuremeter tests, may be due to the method of installing the piles. The 10 to 11 cm of frozen sand backfilled around the piles could be classified either as ice-poor or even as an unsaturated frozen soil (Weaver, 1979). In terms of the test data, the result is to skew the test data to suggest that the permafrost was less sensitive to creep.

In spite of these fundamental experimental problems, this data continues to be used by researchers to calibrate their models. Neukirchner and Nixon (1987) used the data to calibrate their finite difference model, as did Foriero and Ladanyi (1990) to calibrate their finite element model.

The foregoing discussion has not been to suggest that pressuremeter creep tests cannot be used to predict the behaviour of laterally loaded piles. Ladanyi and Johnston's (1973) volumetric transformation of semi-cylindrical cavity expansion to an equivalent translating cylinder, may in fact be a valid model. However, the experimental problems encountered in this field program point to the need to examine the model under carefully controlled laboratory conditions.

The observation that K decays or softens with time did provide a new understanding of the behaviour of the creep of laterally loaded piles. The decreasing K values suggested to Rowley et al. that piles embedded in a creep sensitive material may start to deform or creep as a "perfectly flexible pile", but as the material softens the pile will behave more and more in a "perfectly rigid" fashion. This implies that there will be a redistribution of stresses down the pile, as the characteristic length L/l_o decreases, and suggests that in the long term virtually any pile can be modelled as rigid.

2.4.2 Laterally Loaded Pile Studies by Nixon (1984) and Neukirchner and Nixon (1987)

Nixon (1984) reported the results of a study which included three lateral model pile load tests conducted on small diameter steel rods. The model pile study consisted of three model pile tests using 12.7 mm diameter steel rods, each embedded approximately 200 mm in ice. All testing was conducted under controlled laboratory conditions at -3°C for durations of 2 to 4 weeks. Test results are summarized on Figure 2.9. The creep displacements are characterized by a steadily decreasing creep rate (primary creep), with no evidence of stationary or secondary creep displacements even after 4 weeks duration.

In the same paper, Nixon advanced two models based upon the flow law of (2.28). The first model was an analytical solution for perfectly rigid piles under stationary creep. Solutions were presented for both rigid free-headed and rigid fix-headed piles. These solutions are applicable only after a constant secondary creep rate has been obtained, and so are of limited value. The model was not tested against his test data, nor any other data.

The 1984 paper also presented a finite-difference solution to the classical beam equation, with Equation (2.28) relating soil pressure to secondary creep rates at each node. Based upon this model, Nixon suggested that when a flexible elastic pile, such as the 12.7 mm diameter steel rods, is embedded in a creeping medium and loaded laterally, a relatively long period of stress redistribution elapses before the pile achieves an equilibrium shape. Nixon argues implicitly that the long period of apparent primary creep illustrated by the steel rod tests was due more to stress redistribution in the flexible

elastic pile, than to primary creep of the ice. The fundamental flaw is that the finite-difference solution ignores instantaneous and primary creep.

Neukirchner and Nixon (1987), and Neukirchner (1987) published two companion papers which compare predictive capability versus test data using the finite difference model of the preceding (1984) paper. The analysis consisted of comparing the finite-difference model versus the full-scale field data by Rowley et al. (1973, 1975), and the model pile data by Nixon (1984).

Figure 2.10 shows the comparison of measured versus predicted pile creep rates for a steel pipe pile from Rowley et al.'s (1975) Inuvik field tests. Note that the predictive model has been run for a series of temperatures, and for two different pile diameters. The former was an attempt to examine the previously discussed problem of estimating the actual temperatures surrounding the steel piles, while the latter attempts to account for the method of installing the piles.

The finite difference model appears to predict closely the shape of the primary creep rate curve, but nevertheless overpredicts the creep rate at any point in time. For example, at the reported test temperature of -2.2°C, and assuming a 273 mm pile diameter, the measured creep rate is approximately half the calculated rate. Better agreement might have occurred if permafrost temperatures of say -10°C had been modelled (given that the -5°C calculations show closer agreement with the test results), but the actual test temperatures around the steel piles are not in fact known.

It is not known what assumptions regarding pile stiffness were made when the possibility of a larger effective (457 mm assumed versus 273 mm actual) pile diameter was input into the model. The change in assumed effective diameter does allow the

model to better predict the measured creep rate.

The comparison of the model versus Nixon's model pile data is shown on Figure 2.11. Again the model appears to overpredict creep rates during virtually all of this preliminary period of declining creep rates. Nixon and Neukirchner concluded that the model "predicts the actual behaviour of the field and lab tests reasonably well", but when the model sometimes predicts displacement rates which are in the order of twice the measured rates, then it is hard to support these conclusions.

This study, or sequence of studies, clearly demonstrated the need for more carefully controlled pile load testing, but it also suggested that future modelling should consider pseudo-elastic displacement, plus the primary creep flow laws when attempting to model primary type creep displacements of the pile.

2.4.3 The Studies by Foriero and Ladanyi, 1989, 1990, 1991

Foriero and Ladanyi published a series of three papers which presented a streamline solution for rigid laterally loaded piles in permafrost (1989); introduced a quasi-three-dimensional finite-element model incorporating pseudo-instantaneous displacements and the primary creep laws; and then modified the 1990 solution to model the behaviour of a pile under combined horizontal, vertical, and moment loading (1991).

The first (1989) paper presented an analytical model described as a streamlined solution for rigid laterally loaded piles in permafrost. The model for the pile-soil interaction assumed a rigid cylinder translating laterally, under stationary creep, according to Equation (2.28), with the influence factor, I, defined by (2.30). The form of this analytic model is very similar to Nixon's (1984) analytic model for rigid piles in

stationary creep. Foriero and Ladanyi compare their solution with Nixon's, and conclude that the two models predict virtually the same behaviour. There was no actual comparison to experimental test data.

The second paper (1990) presents a finite element model to simulate the creep of a laterally loaded pile in a viscoelastic layered medium. This model was significant in two ways. First the model is approximately three-dimensional, and secondly it is the first model which incorporates pseudo-instantaneous displacements and primary creep behaviour.

The three-dimensional aspect of the model was achieved by coupling Baguelin et al.'s (1977) solution for the stress state in the vicinity of a laterally loaded discrete Winkler element, to the classic one-dimensional Winkler model. Baguelin et al. (1977) modelled the Winkler element as a finite disc embedded in a much larger finite disc of soil, and developed an analytical solution for the stress state in the vicinity of the Winkler element. The solution assumes the soil adheres perfectly to the pile.

The reaction mechanism consisted of a spring in series with a dashpot, to account for the instantaneous displacement, plus primary creep. The primary creep law used was Equation (2.11) generalized to the multiaxial state of stress. Required input to the program include the instantaneous or pseudo-elastic subgrade reaction modulus, K, plus the primary creep parameters σ_c, n, and b.

The model was evaluated by comparison with the Inuvik test data from Rowley, Watson and Ladanyi (1973, 1975). The comparison is shown on Figure 2.12 for the timber piles. While it is true that the measured versus predicted results compare favourably for T-3-L, there is a 2:1 discrepancy for T-2-L. Comparison with the other

test results from this site were not reported.

Morin (1992) reviewed the Foriero and Ladanyi finite element model and concluded that the sophistication of this numerical model did not appear to improve the predictive capabilities over a simpler finite-difference approach.

2.4.4 The Studies by Domaschuk et al., 1988, 1991 and 1992

Domaschuk et al. present the results of a large-scale pile load creep test carried out under carefully controlled laboratory conditions at the University of Manitoba. The pile load test was carried out for a duration of 435 days. The researchers also reported pressuremeter and plate creep tests. No analysis or modelling are presented in the paper.

The test pile was described as a square tubular pipe, 150 mm square by 1,800 mm long. Mounted to the pile were nine rectangular pressure plates used to measure the reactive pressures against the pile.

The test pile was embedded in a large pit of frozen medium-grain sized sand, at moisture contents ranging from 20 to 24%, and at ice saturations ranging from 90 to 98%. According to Weaver's (1979) permafrost classification system, the material is classified as ice-poor or partially saturated frozen soil. In terms of creep behaviour, such frozen soil represents the lower bound of creep sensitive material (Ladanyi, 1981), but the experimental results are nevertheless an important step in providing researchers with good quality data to calibrate their models against.

The single test was a multi-stage loaded creep test with applied load increments of 36, 61, 114, and 146 kN. Each load increment was maintained until either the creep rates approached zero (first three stages), or until the creep rates began to accelerate into

tertiary creep (stage 4). Figure 2.13 presents a summary of applied lateral loads and displacements versus time.

The experiment measured the change in reactive pressure versus time for each applied load increment. These data are summarized on Figure 2.14. This test is significant because it shows experimentally that as the pile creeps under a given applied load, the distribution of soil reaction does indeed move down the pile. This behaviour had been suggested by Nixon (1984) and Foriero and Ladanyi (1990), but had not been physically observed before.

2.5 SUMMARY AND STATEMENT OF THE PROBLEM

The review of the previously published research has shown clearly a progressive increase in the level of sophistication in the modelling of laterally loaded piles. The modelling began with the work of Rowley, Watson and Ladanyi (1973, 1975) who extended the simple analytical solution of Broms (1964) for unfrozen soils, by incorporating a subgrade reaction modulus which was time dependant. They further proposed that the creep behaviour of the pile could be deduced directly from pressuremeter creep test results. Their modelling allowed for instantaneous and primary creep.

Rowley et al.'s work was followed by Nixon (1984) who also proposed an analytical solution for a laterally loaded pile, also based upon the transformation of semi-cylindrical cavity creep (the pressuremeter) to an equivalent cylindrical cavity translation. This model was simpler to follow, but incorporated only secondary creep. Nixon (1984) then proposed a finite-difference model, applying his analytic solution at each finite

difference node. Neukirchner and Nixon (1987) applied this secondary creep model to predict the stress redistribution which occurs in a pile prior to the attaining of secondary creep displacements.

More recently Foriero and Ladanyi (1990) proposed a finite element model which couples the Winkler model with theory describing the stress state in the plane in front of the pile (Baguelin et al., 1977). This finite element formulation appears to account for instantaneous deflection, and primary creep.

While the sophistication of the modelling has increased, the predictive capacity may not have increased correspondingly. There is simply too little meaningful test data against which the models can be tested.

Domaschuk et al. (1991) carry this assessment one step further by stating "the reliability of the various solutions to the laterally loaded pile problem cannot be properly assessed because none of them are used in a class A prediction, i.e., where the behaviour is predicted before the performance is measured".

The only full-scale field test data (Rowley et al., 1973, 1975) are difficult to analyze because of the unknown temperature conditions surrounding the piles, and because of the method of installing the piles. If these data are discounted, then the only remaining data available to modellers consists of three small-scale tests by Nixon on 12.7 mm diameter steel rods, plus the one large-scale model pile test by Domaschuk et al. (1991). Clearly there is a need for more lateral pile load tests under carefully controlled conditions.

This author has chosen the subject of this experimental thesis based upon the perceived need for high-quality, controlled tests. The approach, outlined in the following

chapters, is to conduct experiments on discrete "Winkler" elements which have the same diameter as a pressuremeter. Thus it is possible to test directly the fundamental hypothesis that the creep of laterally loaded pile can be predicted by transforming semi-cylindrical cavity creep to cylindrical creep translation, such as assumed by Rowley et al. (1973) and Nixon (1984). Once this problem is addressed experimentally, then modellers will have a better appreciation of one of the fundamental assumptions on which their solutions are based.

Description of soil strata	Depth below ground surface (ft)	(m)	Frozen bulk density (p.c.f.)	(kg/m³)	Water or ice content (%)
Organics	0–0.5	0–0.15		Not sampled	
Clayey silt (organic)	0.5–1.5	0.15–0.46	90–110	1440–1760	100–45
Peat in ice matrix	1.5–5	0.46–1.52	69–80	1100–1280	570–180
Grey clayey silt with ice lenses and layers to 2 in. (5 cm) thick	5–9	1.52–2.75	80	1280	180
Gravelly till	9–14	2.75–4.26	110	1760	45

2.1 Soil profile at the Inuvik lateral pile load test site (after Rowley et al., 1975).

Pile No.	Type	B, in. (cm)	L, in. (cm)	e, in. (cm)	e/L	I_p, in.⁴ (cm⁴)	E_p, 10⁶ p.s.i. (GPa)	E_pI_p, 10⁶ lb in.² (MN m²)
T-2-L	Timber	11.0 (28.0)	105 (267)	24 (61)	0.228	719 (29 927)	1.5 (10.3)	1077 (3.09)
T-3-L	Timber	10.25 (26.1)	106 (270)	20 (51)	0.189	541 (22 518)	1.5 (10.3)	811 (2.33)
S-4-L	Steel pipe	10.75 (27.4)	103 (262)	21 (53)	0.204	164 (6 826)	30 (207)	4920 (14.12)
S-5-L	Steel pipe	10.75 (27.4)	96 (245)	14.5 (37)	0.151	164 (6 826)	30 (207)	4920 (14.12)
S-6-L	Steel pipe	10.75 (27.4)	96 (245)	16.5 (42)	0.172	164 (6 826)	30 (207)	4920 (14.12)

2.2 General information on the laterally loaded piles at the Inuvik test site (after Rowley et al., 1975).

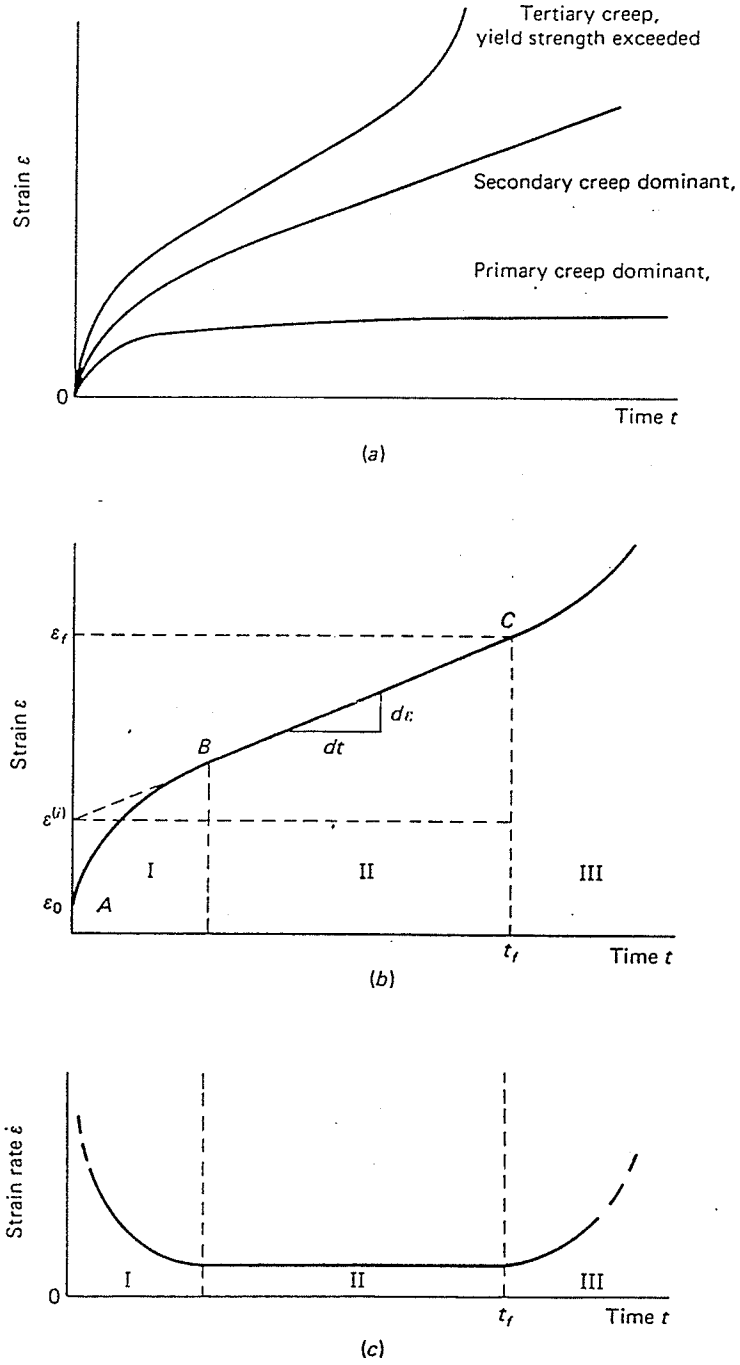

Figure 2.1 Typical constant stress creep test curves for uniaxial creep (after Andersland, Sayles and Ladanyi, 1978).

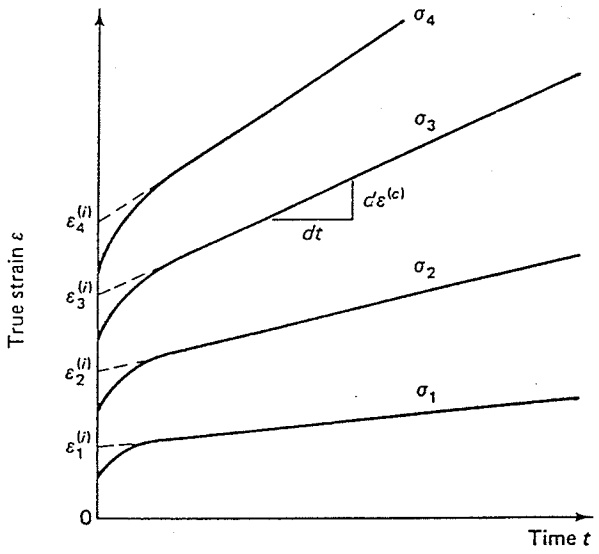

Figure 2.2 "Linearized" secondary creep curves for uniaxial creep (after Hult, 1966).

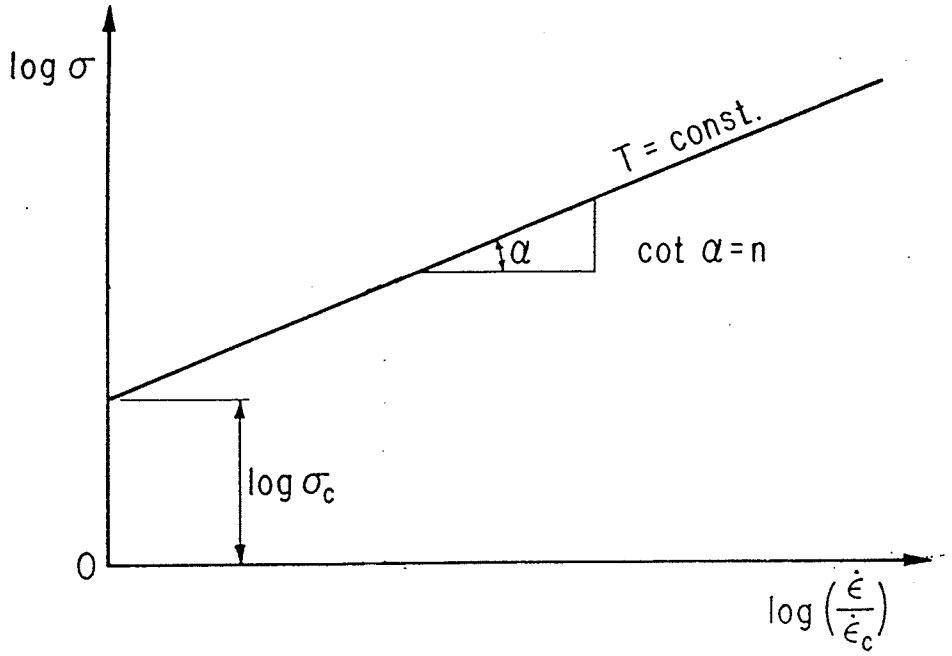

Figure 2.3 Determination of secondary creep parameters σ_c and n (after Andersland, Sayles and Ladanyi, 1978).

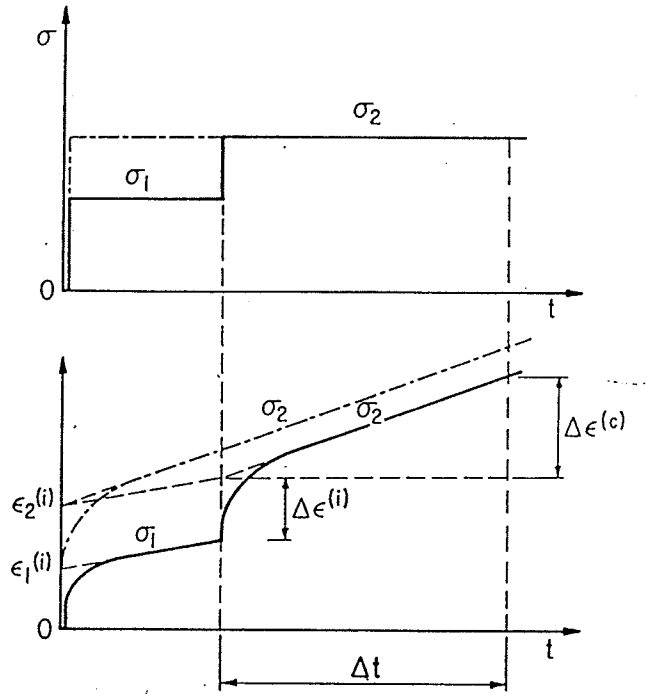

Figure 2.4 Graphical summation technique to determine secondary creep parameters from a multistage test (after Ladanyi, 1972).

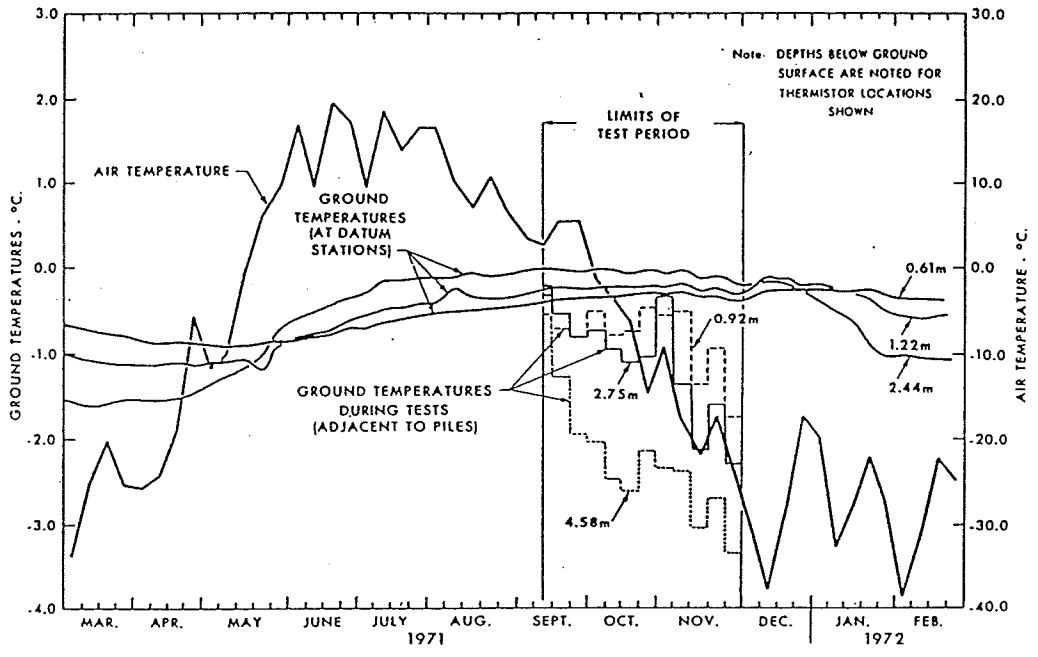

Figure 2.5 Air and ground temperatures during the Inuvik lateral pile load tests (after Rowley et al., 1973). LIMITS OF TEST PERIOD shown on graph are for vertical and lateral pile load tests. Lateral pile load testing was performed during late November, 1971.

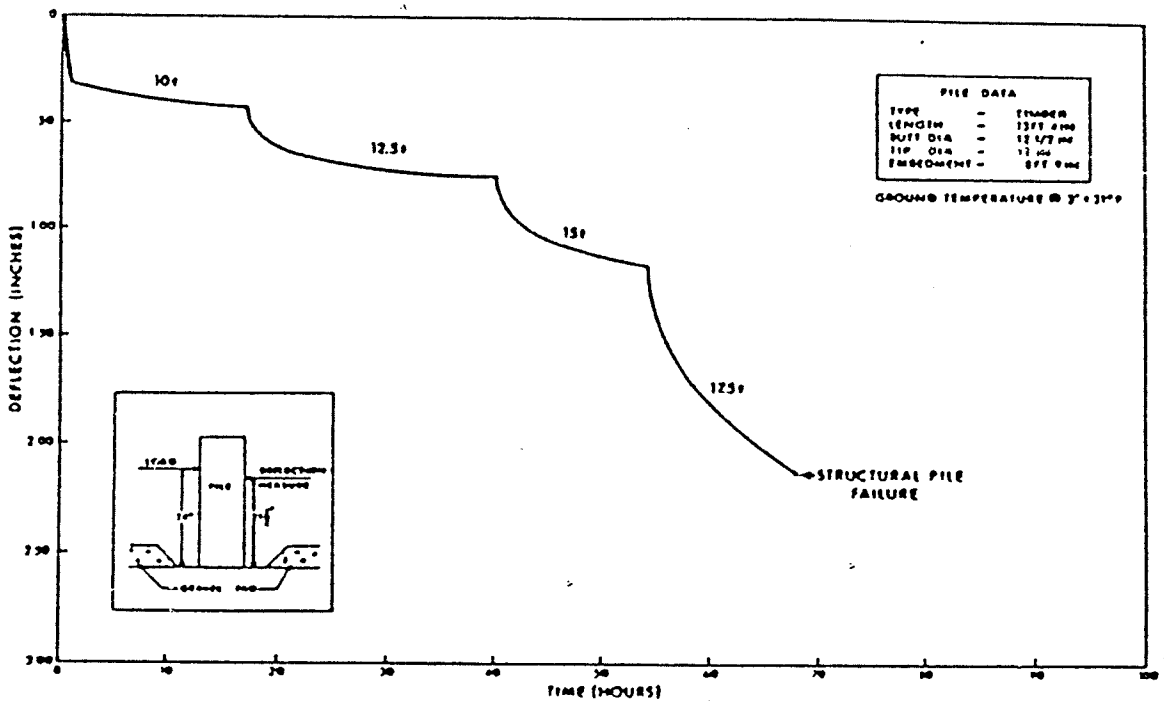

FIG. 1. Lateral test results: pile No. T-2-L.

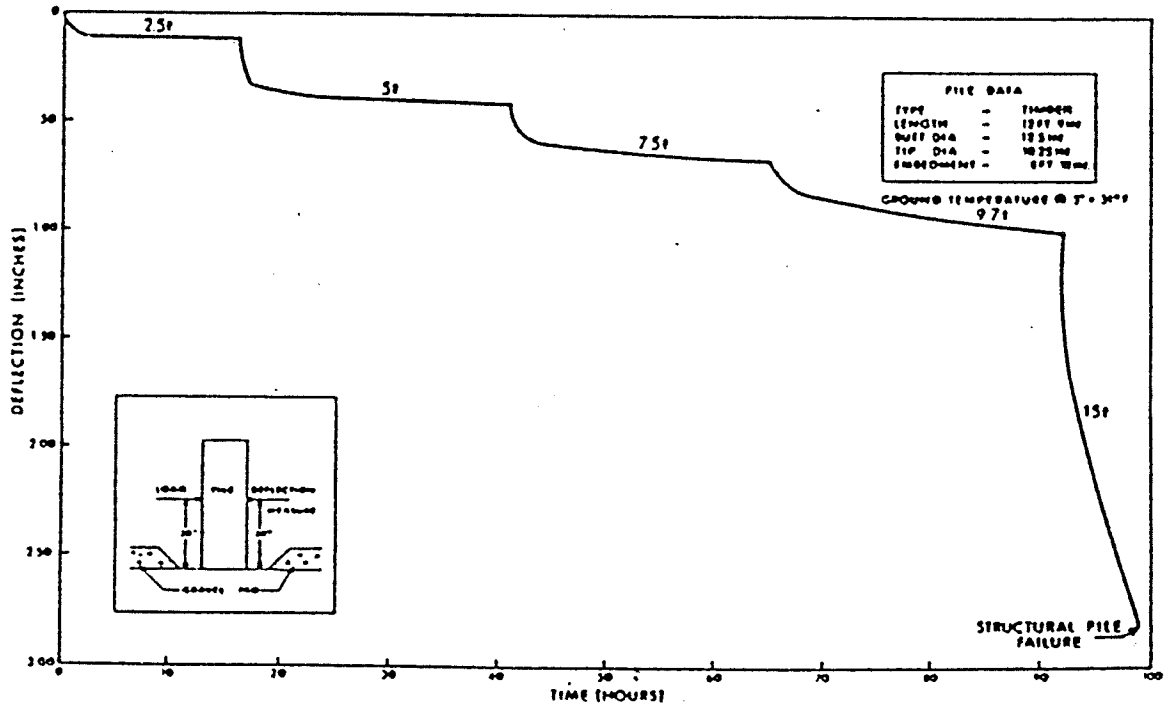

Figure 2.6 Typical lateral pile load test on timber pile at Inuvik, N.W.T. (after Rowley et al., 1975).

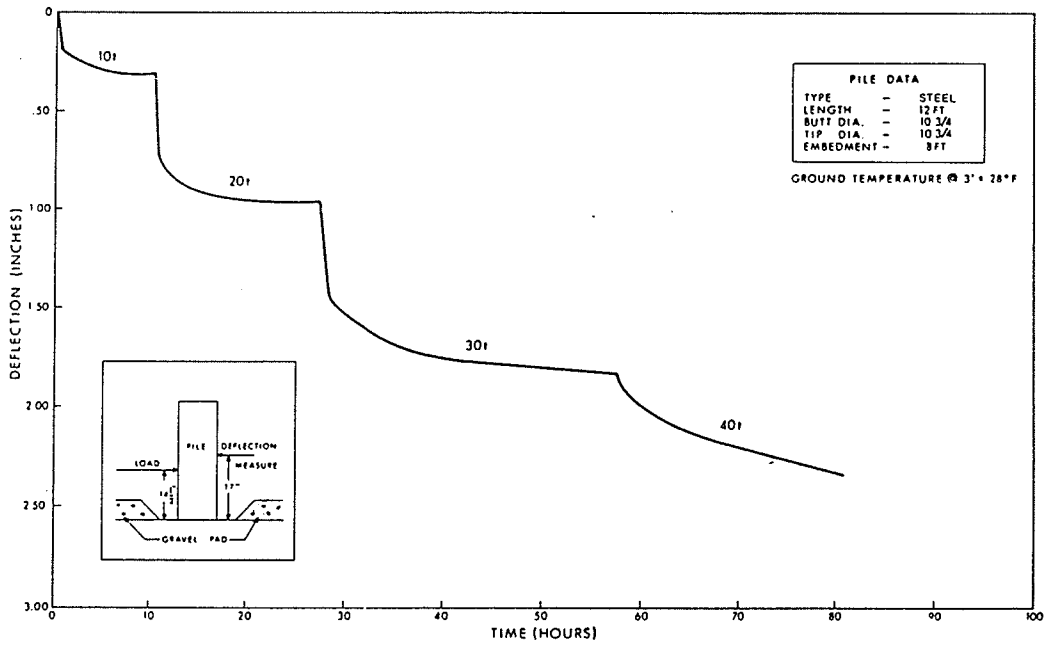

Figure 2.7 Typical lateral pile load test on steel pipe pile at Inuvik, N.W.T. (after Rowley et al., 1975).

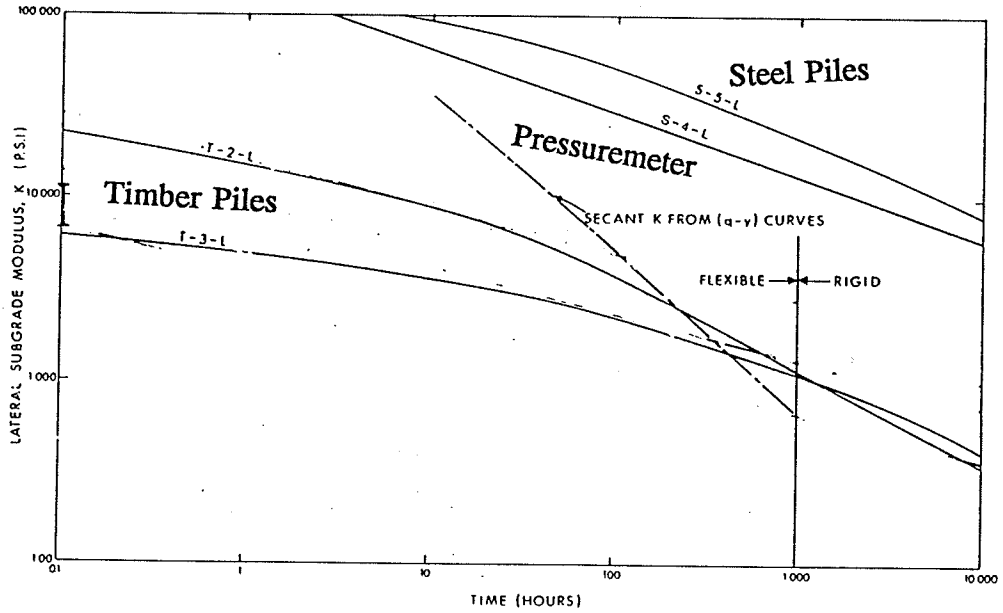

Figure 2.8 Comparison of time-dependent subgrade reaction modulus K for Inuvik, N.W.T. pile load tests. K has been calculated from the pile load tests, and from pressuremeter creep tests (after Rowley et al., 1975).

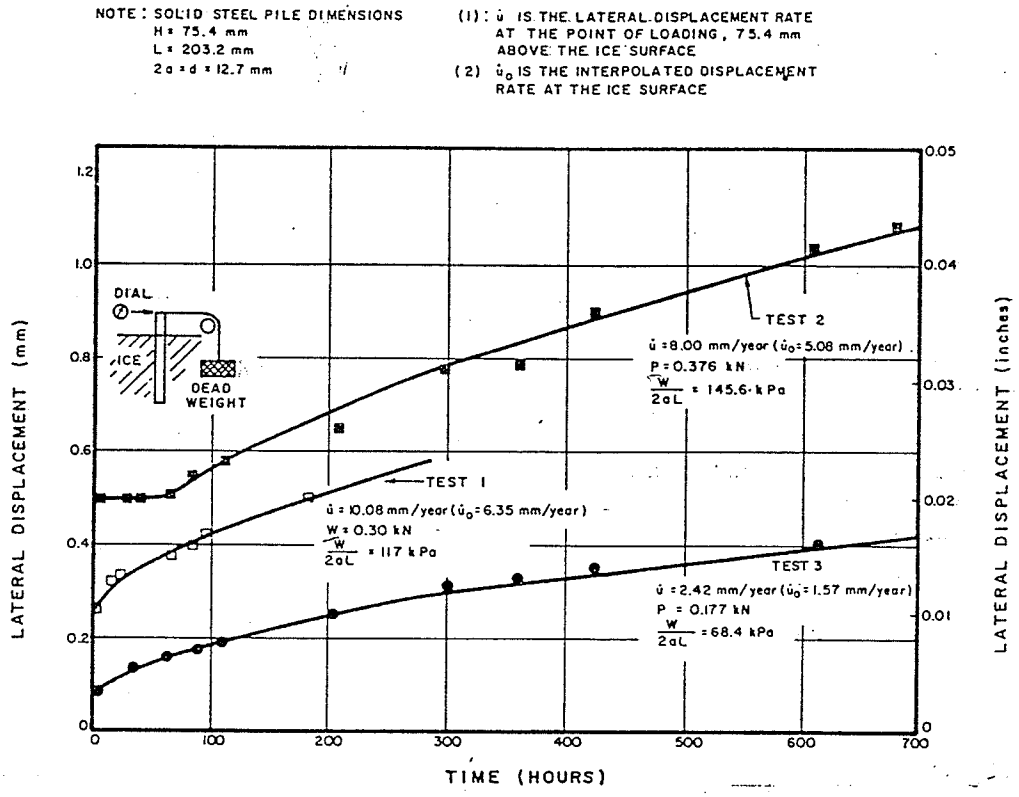

Figure 2.9 Summary of lateral model pile load test results in ice (after Nixon, 1984).

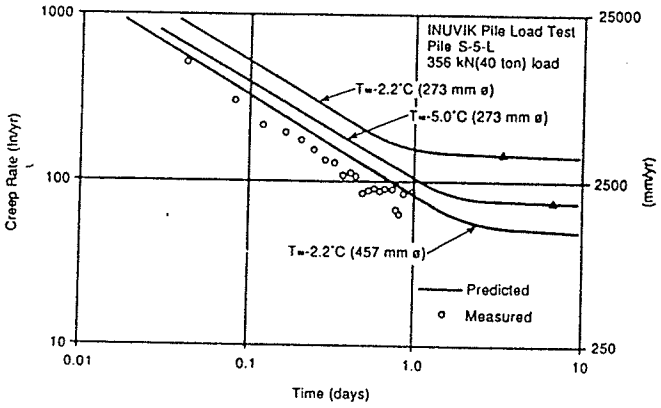

Figure 2.10 Comparison of Nixon's (1984) finite difference model versus steel pipe pile test data from Inuvik pile load tests (after Neukirchner and Nixon, 1987).

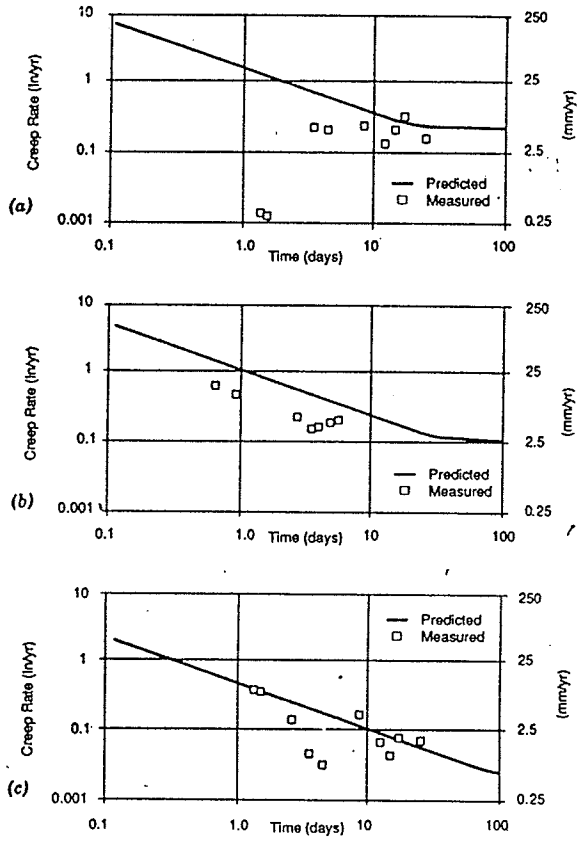

Figure 2.11 Comparison of Nixon's (1984) finite difference model versus Nixon's (1984) model pile test data (after Neukirchner and Nixon, 1987).

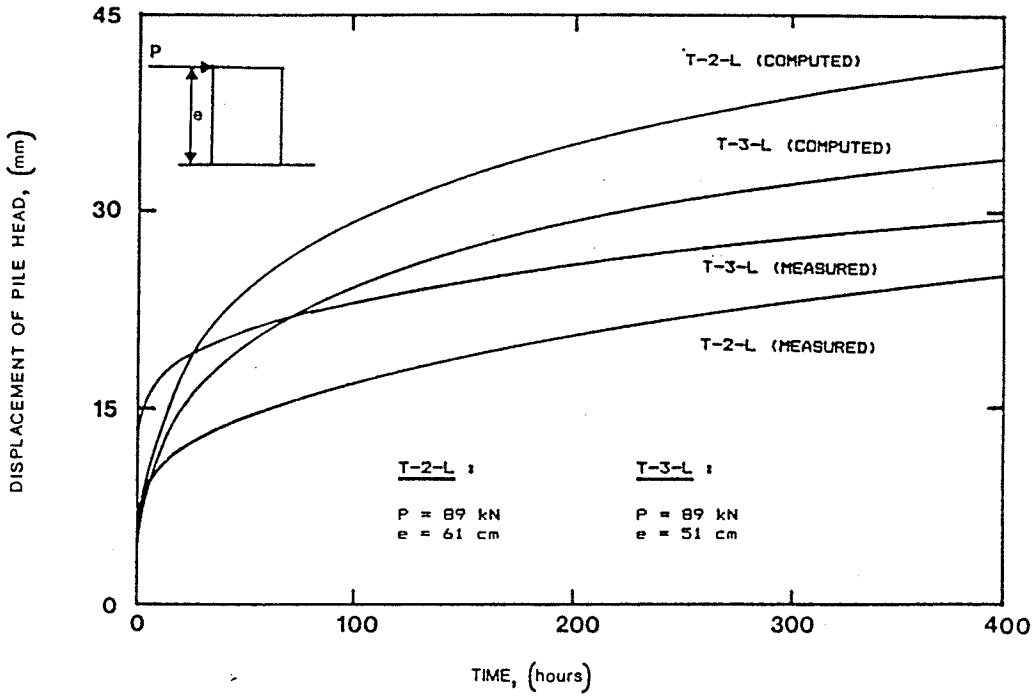

Figure 2.12 Comparison of Foriero and Ladanyi's finite element model versus timber pile test data from Inuvik pile load tests (after Foriero and Ladanyi, 1990).

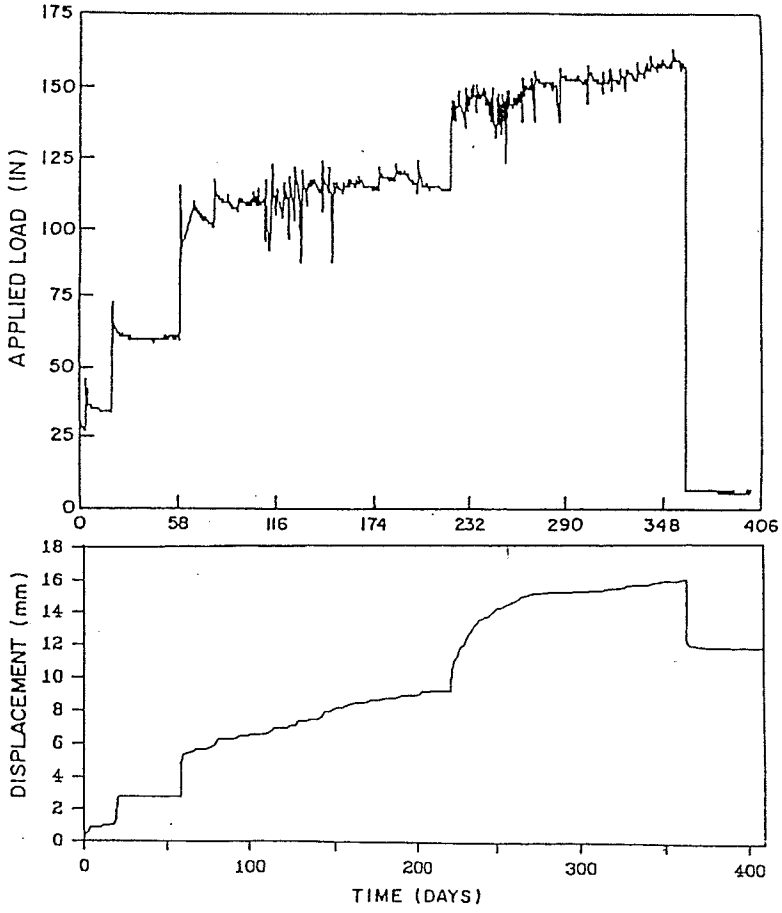

Figure 2.13 Load versus displacement test results from a large-scale model pile load test in frozen sand (after Domaschuk et al., 1991).

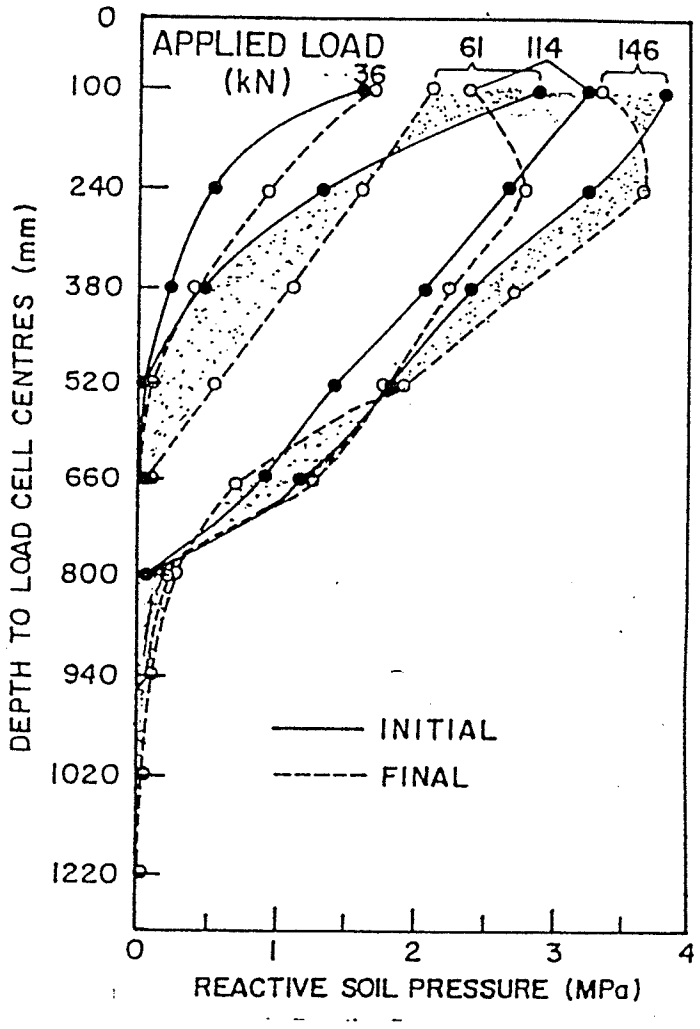

Figure 2.14 Measured evolution of reactive pressures due to creep (after Domaschuk et al., 1991).

CHAPTER 3

EXPERIMENTAL SETUP AND TEST PROCEDURES

3.1 INTRODUCTION

The objective of the experimental program was to create a single Winkler layer of ice, and to force a single Winkler pile element to translate laterally through this layer. Analytically, the experiments were designed to investigate, under controlled laboratory conditions:

1. The validity of conducting pressuremeter creep tests in order to model the creep behaviour of a laterally loaded pile element (Rowley et al., 1973, 1975).
2. The validity of current engineering solutions (Rowley et al., 1973; Nixon, 1984; Foriero and Ladanyi, 1989) in modelling long-term creep of a single Winkler element.
3. The validity of conducting multi-stage tests to determine the load-displacement-time relationship of a laterally loaded pile, as compared to single-stage tests.

3.2 PRELIMINARY DESIGN CONSIDERATIONS

The decision to investigate the validity of using pressuremeter creep tests to model the creep behaviour of a laterally loaded Winkler element imposed some practical experimental constraints:

1. In order to eliminate scale effects, the Winkler element must have

approximately the same diameter as the initial cavity diameter of the pressuremeter test.

2. The same frozen material must be tested, and at the same temperature.
3. The boundary conditions imposed by the pressuremeter tank and the Winkler element tank must be as similar as practical.

This researcher did not intend to conduct both pressuremeter creep tests and Winkler element tests. Three different researchers had previously completed and documented carefully controlled pressuremeter creep tests in large diameter tanks of laboratory prepared frozen soil or ice. Both Ladanyi and Eckardt (1983) and Fensury (1985) had conducted laboratory creep and relaxation tests on thick-walled cylinders of frozen sand, while Kjartanson (1986) had conducted pressuremeter tests on thick-walled cylinders of laboratory prepared polycrystalline ice.

After reviewing the experimental programs and test data from each of the three researchers, the testing by Kjartanson was selected for the following reasons:

1. Polycrystalline ice more correctly satisfies the assumptions inherent to the solution of power law creep theory. Power law creep theory assumes a material which deforms in an incompressible, frictionless manner (Hult, 1966). Polycrystalline ice is considered to deform in an incompressible frictionless manner (Glen, 1955; Ladanyi and St. Pierre, 1978; Sego and Morgenstern, 1983, 1985). Saturated frozen sand, on the other hand, exhibits volume change (dilation or contraction) during shear, and deforms through a combination of intergranular friction plus creep of the pore ice (Ladanyi, 1981).

2. This author concluded that it was easier to make homogeneous, isotropic and reproducible samples of polycrystalline ice, than it was to make samples of frozen sand. Kjartanson (1986) had concluded that it was "relatively easy to make homogeneous, isotropic, reproducible samples of ice", whereas Eckardt (1981) had attributed the large scatter in his test data to variability in the sand density.

The next three subsections present the test apparatus developed for the experiments, the ice sample preparation, and the experimental test procedures. To this author's knowledge, the experimental apparatus described in the following subsections is unique, as are the experimental results presented in the following chapter.

3.3 TEST EQUIPMENT

Plate 3.1 shows an overview of the cold room, the data acquisition system (DAS), and the tanks inside the cold room. Figure 3.1 shows a schematic layout of the experimental apparatus. The major components consisted of:

1. The steel bar or Winkler element.
2. The tanks and sample freezing system.
3. The loading system.
4. The data acquisition system (DAS).
5. The instrumentation.

Only one testing apparatus is shown in Figure 3.1. However, two such apparatus were used to complete the testing program. The testing sequence was to prepare and freeze two samples simultaneously, to run the two tests sequentially, and then to melt

down both samples and repeat the process. Tests were never run concurrently, due to a lack of available channels on the DAS.

3.3.1 The Steel Bar or Winkler Element

Two steel bars (referred to as Bar 1 and Bar 2) were used to model the Winkler element. Bar 1 is shown on Plate 3.2. The bars were solid circular sections of cold-rolled mild carbon steel. They were sized to have approximately the same diameters as the initial 77 mm diameter of the pressuremeter testhole reported by Kjartanson (1986). Bar 1 was 75 mm in diameter, while Bar 2 was 76.2 mm in diameter. Each bar was approximately 1.2 m in total length, with the embedded length being 0.6096 m, and approximately 0.3 m protruding freely through both the bottom and top ends of the tank.

Midway through the testing program, the Winkler bars were instrumented with strain gauges to observe the stress redistribution in the bar during the early primary creep phase (Neukirchner and Nixon, 1987; Foriero and Ladanyi, 1990). A total of seven strain gauges were aligned along the back side of the bar, spaced at 76.2 mm intervals along its length. Plate 3.2 shows the gauges mounted on the bar, and covered with two layers of waterproofing material. The strain gauges were 120 ohm resistance precision strain gauges which were mounted in a quarter bridge configuration. To optimize the accuracy of the quarter bridge, the following measures were taken:

1. The balancing strain gauges were maintained at the same temperature as the active gauges. To achieve this, the balancing gauges were wrapped in blankets of fibreglass insulation, and placed in the cold room on top of the tank.

2. The signal wire lengths from both the active and the balancing gauges were of the same length.

The steel bars were calibrated twice in bending. The first calibration was completed prior to Tests 9 and 10, and the second calibration prior to Tests 10 and 11. The calibrations were performed in the 267 kN compression testing machine of the Civil Engineering Department's Structures Laboratory. Calibrations were at ambient room temperature.

The calibration test data are summarized on Figure 3.2 showing measured bending strain as a function of applied bending moment. Readings from the middle three of the seven strain gauges are plotted, due to limited file space of the graphic software, but all seven gauges of each pile gave consistent results. The section moduli as determined from these calibrations were 330 kN-m^2 for the 75 mm diameter bar (Bar 1) and 360 kN-m^2 for the 76.2 mm diameter bar (Bar 2). These calibrated values compare to theoretical section moduli of 330 kN-m^2 for Bar 1, and 350 kN-m^2 for Bar 2, assuming a value of Young's modulus, E, of 210 GPa.

The strain gauges on the bars were checked for electronic drift at test temperatures and zero load conditions, prior to the start of each test. Table 3.1 summarizes this electronic drift as recorded prior to Tests 9, 10, 11 and 12. The maximum standard deviation of strain gauge drift under zero load ranged from 2 to 8 bits of resolution of the DAS. This represented 5 to 20 microstrains in bending, or 0.5% to 2.0% of the maximum full-scale readings during the test. Zero load readings taken immediately after the completion of each test were always within this range.

The observations of the stress redistributions were not considered one of the

primary objectives of this experimental program. Nevertheless, it was decided to collect some preliminary data to confirm or refute the postulates of Neukirchner and Nixon (1987) and Foriero and Ladanyi (1990). Since this program was initiated, similar observations have been reported by Domaschuk et al. (1988, 1991).

3.3.2 The Tanks and the Sample Freezing System

In order to compare the Winkler bar tests with the results of the pressuremeter creep tests, both tests must be performed in containers which imposed as similar boundary conditions as practical. In this regard, the essential boundary conditions of Kjartanson's tanks were:

1. The tanks were constructed from sections of steel pipe (abandoned high pressure gas pipeline was used) which was 890 mm in diameter by 11.7 mm wall thickness. A 9.5 mm thick circular plate was welded on to the bottom of the tank.
2. No lid was used during the pressuremeter testing. Hence the pressuremeter tank can be visualized as a very large "can" with the lid removed, which was full of a carefully prepared sample of polycrystalline ice. The pressuremeter tests were then carried out inside these containers.

The Winkler Tanks

The Winkler tanks constructed for this study imposed similar cylindrical boundary restraint conditions as the pressuremeter tanks, but the end restraints were different. A photograph of the empty tank is shown in Plate 3.3. The cylindrical portion was

890 mm in diameter with 11.5 mm thick walls, and the cylinder was 610 mm deep in the vertical direction.

The end restraints consisted of a 12.5 mm thick circular plate welded on to the bottom, plus a 12.5 mm thick lid bolted on to the top. In order to fasten the top lid, a 76 mm wide circular flange was welded to the top of the tank. These end restraints differed from those of the pressuremeter tanks, where no top restraint was imposed.

Finally, a 150 mm diameter hole or cutout was removed from the top and bottom plates, so that the free ends of the Winkler bar could protrude through the top and bottom of the tank. The 150 mm diameter hole allowed the bar approximately 37.5 mm of lateral travel (roughly one-half the bar diameter), before the bar would stop against the edge of the cutout. The tanks were supported off the floor by three legs bolted to the sides of the tank.

The influence of the sides of the tank on the behaviour of the Winkler bar was estimated by applying the solution by Baguelin et al. (1977). Baguelin et al. proposed an elastic engineering solution for the distribution of stresses in front of a Winkler element, assuming it was embedded in a finite disc of elastic material. The calculation suggested that a laterally loaded 75 mm or 76.2 mm diameter steel bar embedded in a 890 mm diameter disc of "elastic" ice would induce stresses at the ice-tank boundary which would be less than 5% of the equivalent frontal pressure applied at the steel bar. More recently, an undergraduate thesis by Goodman (1992) was completed, whereby the pressuremeter tank used by Kjartanson was instrumented with strain gauges and a pressuremeter test completed. The stresses measured on the tank during the pressuremeter test were negligible. Hence it is concluded that the steel tank was

sufficiently large in diameter such that the bar behaved as if embedded in an infinitely large disc of ice.

Because of the analytical problems that placing a pile in a pre-drilled hole had appeared to cause Rowley et al. (1973, 1975), it was decided to place the Winkler bar in the tank first, and then to form the ice sample around the bar. Therefore, during sample preparation and freezing, a water-tight collar was required to hold the bar in the middle of the cutout. This collar or insert is shown in Plate 3.4. The collar fit snugly around the bar and inside the 150 mm cutouts. O-rings were placed on the inside and outside circumference of the collar to ensure water-tightness. This collar was removed once the ice had frozen, leaving the bar free to translate within the limits of the cutout.

Finally a box-shaped load frame of 12.5 mm thick plate steel was welded to the side of the tank. Hydraulic cylinders were mounted on the top and underneath the load frame as shown in Plate 3.5 and were used to apply the lateral loads.

3.3.3 The Sample Freezing Apparatus

The samples were frozen one-dimensionally, from the bottom upwards, to allow the sample to expand freely as freezing progressed, and to prevent the buildup of stresses within the ice sample (Sego, 1980; Kjartanson, 1986). Freezing was achieved by fastening a freezing coil to the underside of the tank during sample freezing, and then removing it prior to the test.

The freezing coil was constructed of 12.5 mm diameter copper tubing which was coiled and sandwiched between a disc of 50 mm thick styrofoam insulation and a 4 mm thick plate of aluminum. Plate 3.6 shows the freezing plate. When the sample was

ready to start freezing, the plate was placed on the underside of the tank, and fastened to its top flange using long threaded rods.

The freezing coil was connected, via quick connect couplers, to a half-horsepower Tecumseh condensing unit located outside the cold room. This unit had a rated heat flow capacity of 344 watts at an evaporator temperature of -40°C, and 996 watts at an evaporator temperature of 0°C.

3.3.4 The Loading System

A photograph of the loading system is shown on Plate 3.7. The loading system consisted of loading collars placed around the Winkler element, and the load cells which connected the loading collars directly to hydraulic cylinders. The system was designed to place a lateral load on the Winkler element as close as possible to the top and bottom surface of the disc of ice, and to impose the load in a free-headed condition. The base of the loading collar was in fact 12.5 mm removed from the ice surface, and the centre of the pin connecting the load cell to the loading collar was 50 mm removed from the ice surface. Top and bottom loads could be controlled separately. Details of the load cell calibration are discussed in section 3.3.6.

3.3.5 The Data Acquisition System

The data acquisition system (DAS) used in this study was a 32 channel Neff 620 S multiplexer, with a 12-bit analog to digital converter. The multiplexer was controlled by a Hewlett Packard Model 9825 A (64 K RAM) desk top calculator. The Hewlett Packard contained a real time clock so that all channels could be scanned automatically

at preset time intervals. Readings were stored on the Hewlett Packard's cassette cartridge.

Because the Hewlett Packard was dedicated to controlling the multiplexer, it could not be used to actively monitor the test progress. Previous researchers using this system had printed out the data periodically, and later transferred it manually to another computer for manipulation and analysis.

As part of this study, the Hewlett Packard was connected to an IBM compatible computer, via an RS232 cable, so that data could be transferred from the Hewlett Packard to the IBM compatible. Typically, data was transferred every 4 to 6 hours during testing.

Each channel of the Neff multiplexer could be programmed to scan one of twelve different voltage ranges, depending on the voltage outputs from the individual electrical instruments. Thus the single bit resolution for each instrument could be optimized according to its signal output voltage. The measuring voltage range, and corresponding single bit resolution for each of the instruments used during the experiments is summarized on Table 3.2.

3.3.6 Instrumentation

The instrumentation monitored during a typical test consisted of:

1. Type T thermocouples to record temperatures (total of seven to nine per test).
2. Load cells machined and instrumented by the Civil Engineering Department's support staff.
3. Linear variable displacement transducers (four per test).

4. Strain gauges mounted on the steel bar (total of seven).

5. Excitation voltages for the load cells and strain gauges on the steel bar.

Typically, therefore, a total of 22 to 24 instruments were monitored throughout the test. The DAS was limited to 32 channels, making it impossible to run two tests concurrently without sacrificing one-third of the instrumentation per individual test.

Temperature Measurement

When the ice is maintained close to its melting temperature (say -2°C as for this test program), it is critical to have temperature measurements accurate to within plus or minus 0.1 to 0.2°C (Sego, 1980). This subsection details how the required accuracy was achieved through both careful calibration procedures, and by checking the temperature measuring system during individual tests.

Temperature measurement was achieved using Type T (copper-constantin) thermocouples. The measuring junction of the thermocouples was welded in mercury, and a Kaye Instruments Ice Point Reference provided the reference junction in the thermocouple circuit. The Kaye Ice Point Reference maintained the reference junction to within plus or minus 0.05°C. The DAS measured the thermocouples using a single bit resolution of plus or minus 0.06°C.

As shown on Figure 3.1, a string of five thermocouples was embedded vertically in the ice at vertical intervals of approximately 100 mm. As well, a thermocouple was welded to each load cell, so that the temperature of the load cell could be monitored and its calibration coefficients could be adjusted to reflect the operating temperature of the load cells. Finally, during the test, two reference thermocouples were taped to the bulb

of a Brooklyn Calorimeter Thermometer and then placed in a container of glycol which sat in the cold room beside the tank. In this way the accuracy of the thermocouples were visually monitored throughout the test.

The thermocouples were calibrated four times throughout the test program. They were individually calibrated in a temperature bath over a range of 0°C to -10°C. Calibration temperatures were measured by a Brooklyn Calorimeter Thermometer. The calibration of this thermometer is traceable to the National Bureau of Standards, and it is considered accurate to plus or minus 0.02°C.

This system of temperature measurement was consistently accurate, to less than plus or minus two bits of resolution of the DAS, or to plus or minus 0.12°C in temperature, as checked against the Brooklyn Calorimeter Thermometer.

Load Cells

The load cells used to measure the applied lateral load on the steel bars, were designed by this author and constructed by the Civil Engineering Department's technical support staff. A total of four load cells were fabricated. Plate 3.8 shows one of them. The calibrations of two of the four load cells (LC10 and LC20) are presented in this subsection. These two load cells (LC10 and LC20) were used for 10 of the 12 tests.

Preliminary design calculations indicated that the load cells would operate over a range of from 20 to 60 kN. Individual tests were anticipated to last as long as two months, and so it was necessary to construct a load cell that would be stable in its output signal. Because the load cell was part of the load application system, its elastic strain must be negligible when compared to the displacements of the pile, and it must not be

susceptible to creep itself. The intent was therefore to size the load cell such that the design loads would be achieved at relatively small accompanying strains.

The load cells were 57 mm in diameter by 250 mm long. The cells were machined from ordinary cold-rolled mild carbon steel. Under maximum loading, the strain in the steel was calculated to be in the order of 0.01%.

Four 350 ohm resistance precision strain gauges were mounted on each load cell, arranged in a full bridge configuration. An excitation voltage of 10 volts was provided by a Hewlett Packard Model 6204 B power supply. The 10 volt excitation voltage was monitored during all testing, and always remained steady to plus or minus 10 mV (2 bits). A thermocouple was welded directly to the load cell, so that its operating temperature could be monitored as required.

It was anticipated that the calibrations of the load cells (zero setting and slope) would be temperature sensitive, and it was also suspected that the zero reading would shift with time as the steel aged (personal communication Ed Lemke). The calibration program was established to account for these three factors.

All calibrations were performed using the 267 kN compression testing machine in the Structures Laboratory of the Civil Engineering Department. To account for temperature effects, the load cells were calibrated under a series of temperatures ranging from +10°C to -10°C. Temperature control was achieved by constructing a small styrofoam cooling chamber around the compression testing machine and load cells. Calibration temperatures were recorded by the thermocouples which were welded to the load cells.

The load cells were calibrated a total of four times during the testing program.

The calibration results for load cells 10 and 20 are summarized on Figures 3.3, 3.4, and 3.5. Figures 3.3 and 3.4 each present three graphs showing: load cell output versus applied load, calibration slope versus temperature, and zero load output versus temperature. Figure 3.3 applies to LC10, and Figure 3.4 to LC20. Figure 3.7 summarizes the zero load output as a function of aging of the load cells.

The pertinent conclusions regarding the calibrations are:

1. The calibrations of the load cells were repeatable during the four calibrations.
2. The slope of the load cell calibration (kN/mV) shifted by one bit resolution on the DAS for every 5°C. Therefore, under normal test conditions in the cold room, the slope of the load cell calibrations was constant.
3. The zero point of the load cells shifted by one bit resolution for each 1°C. While more temperature sensitive than the slope of the load cells, it remained negligible. Prior to starting each test, the zero load output of the load cells were monitored for one week, and this average value then input as the zero load constant.
4. The zero point did shift as the load cells aged, but not to the point where accuracy was affected during individual tests. Figure 3.7 shows that the zero point for both load cells shifted by an amount equal to 0.0001 mV per day or 0.004 mV per month. This represented approximately 1.5 bits sensitivity for each month of the test. Two of the twelve tests were maintained for periods long enough such that the zero shift changed by two bits.

Finally, immediately prior to each test, the load cells were tested for drift under no load conditions for a period of one week. Results for tests 9 through 12 are

summarized on Table 3.1. Figure 3.6 illustrates typical drift under zero load as measured prior to test 10. Under zero load, the maximum standard deviation was equivalent plus or minus one bit sensitivity of the DAS, or plus or minus 0.1 kN.

In conclusion, temperature and aging effects on the slope of the load cells were accounted for through careful calibration procedures. The load cells were considered accurate to plus or minus two bits sensitivity of the DAS or in engineering units to within 0.2 kN (0.4% of the full-scale output).

Displacement

Pile displacements were measured by four commercially available linear variable displacement transducers (LVDT)s. Calibration factors were supplied by the manufacturers of the instruments, so the calibrations served primarily to check their accuracy. The LVDTs were calibrated in the cold room, at the test temperature of -2°C, using an Otto Wolpert Werke vernier available from the Structures Laboratory of the Civil Engineering Department. Vernier readings were corrected to allow for thermal contraction of the steel vernier. The calibration curves thus derived were able to reproduce the calibrations readings to within 0.06 mm which was within the single bit resolution of 0.1 mm of the DAS. Under zero load conditions (Table 3.1), instrument drift was usually plus or minus one bit of sensitivity, but always measured to within two bits resolution or 0.2 mm travel. Figure 3.7 illustrates typical drift under zero load as measured prior to test 10. Hence it is concluded that bar displacements were measured to an accuracy of 0.2 mm.

3.4 ICE SAMPLE PREPARATION

3.4.1 A Brief Review of Ice Sample Making Techniques

Some form of the seed crystal technique is generally followed to make laboratory samples of polycrystalline ice (Glen, 1955; Cole, 1979; Kjartanson, 1986). Following this technique, a sample mould is placed in a cold room at 0°C, filled with ice crystals of uniform crystal size, placed under a vacuum, and then saturated with 0°C water. Various freezing techniques, as discussed below, are used to freeze the sample.

The seed crystals act as nucleation points and cause a random orientation of the c-axis of the individual ice crystals in the bulk sample. Thermal strains due to freezing are reduced by the matrix of seed ice crystals which do not undergo phase change, by greasing the inside of the mould, and by freezing the sample unidirectionally from one end and allowing the sample to expand at the opposite.

Generally these techniques have been applied to smaller sized (<1 kg) samples such as uniaxial compression test samples (Glen, 1955; Cole, 1979) or direct shear or simple shear samples (Sego, 1980), but Kjartanson (1986) adapted the procedure to make much larger pressuremeter samples, in the order of 450 kg in size.

Glen (1955)

Glen (1955) described using the following seed crystal technique to produce homogeneous, isotropic laboratory samples of polycrystalline ice (see also Sego, 1980). A sample mould was packed with individual ice crystals which had been screened to provide a uniform grain size. Glen collected hoar frost crystals from the condenser unit of the cold room until the necessary volume of crystals had been accumulated. A

vacuum was attached to one end of the mould for several hours, and supercooled de-aired, de-ionized water was introduced at the other end. The sides of the mould were insulated, the mould was placed on a freezing plate, and frozen unidirectionally.

Glen did not report measured densities, but Sego (1980) followed this procedure and reported an average sample density of 0.891 Mg/m^3. Both researchers reported that the samples were cloudy, visually, with air bubbles trapped throughout the sample. Studies of thin sections prepared from the samples concluded that the ice was, however, polycrystalline in structure.

Cole (1979)

Cole (1979), reduced the visual cloudiness of the sample and increased sample density by following the procedures outlined above, until the sample was saturated. Then the sample was frozen radially inward, while constantly flushing the unfrozen centre core with more distilled de-aired water at 0°C.

Bulk densities in the order of 0.913 Mg/m^3 were reported, versus 0.891 Mg/m^3 by Sego, and versus the theoretical bulk density of polycrystalline ice of 0.917 Mg/m^3.

According to Cole, some air bubbles remained visible throughout the sample but the ice was not described as cloudy in appearance. Cole concluded that his modification to Glen's technique diminished bubble formation by minimizing the supersaturation of dissolved gases that leads to bubble nucleation and growth.

Fransson (1986)

Researchers in ice mechanics from the University of Luleå, Sweden (personal

communication, L. Fransson) account for the cloudiness by hypothesizing that air bubbles remain attached to the crystals' sharp extremities, attached by a surface tension which is greater than the suction applied to evacuate the mould. Their technique (unpublished) is to pre-wet the seed crystal very briefly with de-aired water at +4°C to +5°C to slightly melt and round the sharp lattice points of the individual seed crystals. The sample is then saturated under vacuum using 0°C water. As discussed in Appendix A, this technique was employed for two of the early tests in this study (tests 3 and 4), and did reduce visual cloudiness.

Kjartanson (1986)

Kjartanson's adaptation of the seed crystal technique was to use commercially available finely-crushed party ice as the seed crystal. The fine-grained party ice was frozen from filtered tap water, and sieved to yield individual ice particles between 6.4 mm and 12.7 mm in size. Approximately 280 kg of such party ice was used per sample.

The ice making procedures used in this thesis follows the technique of Kjartanson. Step by step procedures are outlined below.

Preparation for Ice Making

1. The cold room thermostat was set to 0°C. The cold room temperature was then monitored by placing several containers of anti-freeze on top, underneath, and beside the tanks. Thermocouples were immersed in the anti-freeze, and the thermostat adjusted until the air temperatures around the tanks were within 0.25°C of 0°C. Depending on outside room temperatures, this could take one

to three days, including time to ensure that the temperature was likely going to remain steady.

2. A large water reservoir, inside the cold room, was filled with cold tap water, and was chilled to 0°C. Care had to be taken that the water did not becomes supercooled. When this occurred, large ice crystals tended to plug the saturating hose as soon as water was drawn from the reservoir.

3. On the day of the sample pouring, the sides, bottom, and lid of the tank were coated with petroleum jelly. The freezing plate was positioned to the underside of the tank and the Tecumseh condensing unit was turned on.

4. Thermocouples were checked and the string of thermocouples placed in the tank. During initial tests, two sets of vertical thermocouple strings were placed on opposite sides of the tank to check that the ambient room temperatures did indeed provide a uniform lateral sample temperature. Temperatures were uniform, and so the number of strings was reduced to one.

5. Twelve 20 kg bags of fine-grained party ice was placed in the cold room. Table 3.3 lists the chemical properties of the filtered water used to make the fine-grained party ice.

Making the Sample

1. The bottom freezing collar was placed in its cutout, and the Winkler bar placed vertically through the collar. This action fixed the bottom of the bar in the exact centre of the sample. The bar's verticality was adjusted to centre the bar approximately.

2. A small circular piece of 6 ml clear plastic, about 200 mm in diameter (larger than the 150 mm cutout in the bottom of the tank), was forced over the top end of the steel bar, and pushed down flush with the bottom of the tank. Once the freezing collar was removed to start the test, this plastic remained frozen to the ice and prevented sublimation from the ice-bar interface.

3. The hose from the pore water reservoir was placed in the bottom of the tank, and the tap from the reservoir was opened.

4. Forty kg of the seed crystals were immediately placed in the bottom of the tank, and compacted 100 times with the wooden tamper used by Kjartanson (1986).

5. As the pore water surface rose close to the top of the layer of seed crystals, additional bags of ice were placed and compacted at 100 blows per 20 kg. The rate of placing was controlled by the rise of the porewater. Additional ice was not placed until the porewater surface was close to the top of the seed crystal surface.

6. The level of the compacted ice crystals and pore water was brought up to the top of the tank.

7. The lid to the tank was lifted over the top end of the bar and bolted to the top flange.

8. The top freezing collar was slipped over the top of the Winkler bar, and pushed down the bar close to the lid of the tank. Until this time the position of the top of the bar was close to the centre of the sample, but had not been centred. The bar and its top freezing collar were centred until the freezing collar would fit into the cutout. Now the lid was on the tank and the bar was fixed in the middle of

the sample.

9. The steel bar was rotated by hand to bring the line of strain gauges on the back side of the bar in line with the direction of the applied lateral load. The top end of the pile had been scored to mark the front and back of the pile, and plumb bobs were used to align the pile with the projected line of travel of the hydraulic cylinders.

10. A pencil line was scribed on the pile at its interface with the top lid of the tank. This was done as a visual measure of pile heave during freezing. In twelve tests, no heaving of the pile was observed.

11. Blankets of heating duct insulation were fastened by duct tape around the sides of the tank, and pillows of fibreglass insulation were placed over the top of the tank.

12. Sample freezing typically was completed in four to seven days. Figure 3.8 shows a typical record of the upward progression of the freezing front during freezing of the sample for test 5.

13. During the freezing period, the top lid was loosened once per day, and the sample was visually examined to ensure that a crust of ice had not formed on top. It was difficult to maintain the room temperature at exactly 0°C, and so it was quite often necessary to break up the top several millimetres of the sample and adjust the room temperature accordingly.

14. Once the freezing front had progressed approximately two-thirds of the way up the sample, the lid was removed to allow the sample to expand above the top of the tank. Generally the finished frozen ice surface would be several millimetres

above the top flange of the tank at the completion of freezing.

15. At the completion of freezing, the cold room temperature was adjusted to -2°C, and the untrimmed ice sample was allowed to come to thermal equilibrium.

16. The top of the sample was then trimmed flush with the top of the tank using a large drawknife shown in Plate 3.9. The drawknife was fabricated as part of this testing program.

17. The lid was placed back on the tank, and the bolts torqued to 200 foot lbs.

Following completion of step 17, the sample was ready for testing. The following subsection describes the test procedures.

3.5 TEST PROCEDURES

The procedures used to carry out both the single stage creep tests, and the multistage test are discussed in this subsection. As in any new experimental program where the test equipment is untried, and where the development of the test procedures constitute part of the testing program, it took a number of tests (tests 1 to 4) to establish procedures which would yield results that were repeatable, reproducible, and which were suitable for analysis. Details of those four preliminary tests, including what "went wrong", are included as Appendix A. The following description of procedures applies to tests 5 to 12, which yielded data in a form suitable for analysis.

1. Sample temperatures were monitored for approximately one week prior to starting the test. This monitoring period was used to establish that the sample temperature had indeed stabilized to -2°C. The monitoring period was also used to check the electronics for drift.

2. The tests were load controlled tests. Design or target loads were calculated such that the magnitude of the equivalent frontal reaction, p, (total lateral load/projected frontal area), was equal to the magnitude of the radial borehole pressure from the pressuremeter tests.

3. The pressuremeter tests had been performed at cavity pressures ranging from 1.0 MPa to 2.5 MPa, in 0.25 MPa increments. The calculated equivalent loads, Q, to be applied at both ends of the bar, are listed and compared to the corresponding pressuremeter test pressures on Table 3.4.

4. For all these tests a slightly larger load was applied at the top end than was applied at the bottom. This slight differential was necessary, because without it the bottom end tended to translate faster than the top. This problem is discussed in detail in Appendix A.

5. The magnitude of this differential loading was generally quite small. For example, the target load for test 10 was Q = 40.6 kN (p = 1.75 MPa). The actual average bottom load was 40.0 kN, while the average top load was 41.6 kN. In other words, the difference between the top and bottom loading was 1.5 kN or 3.9% of the actual target load.

6. At the appropriate time the test was started. The DAS was programmed to scan the instruments every 15 seconds for the first 5 minutes. The load application began after two or three scans. Loads were typically ramped on (Mellor, 1979) over a one to two minute period. While the Hewlett Packard was actively scanning, it stored individual scans in sequence on its data cartridge, but could not be programmed to print out the results.

7. At the five minute period, the data was printed out on the Hewlett Packard's internal thermal printer. The results were quickly scanned and the loads adjusted as required. The data was then transferred to a data base program in the IBM compatible computer, where the accumulated ongoing test data would actually be stored. During this time the DAS was not monitoring the test. This step typically required five minutes to complete.

8. The Hewlett Packard was then reprogrammed to scan every ten to fifteen minutes for an hour or so, at which time the process of printing out the data, adjusting loads, and transferring data from the Hewlett Packard to the IBM compatible was repeated.

9. As the test proceeded, the loads were adjusted independently at the top and bottom as required. The loading system could accurately apply target loads to within 0.2 kN, but the magnitude of this load tended to drift if left unattended. Hence, the load settings were checked and adjusted at a frequency determined by the rate at which the bar was translating. The load monitoring and adjusting frequency were more frequent at high loads (typically every one to two hours during the 52.3 kN test), but much less frequent during the smaller loads (every twelve hours during the Q = 29.0 kN test).

10. The single stage tests were continued in this fashion either for a time duration equivalent to Kjartanson's pressuremeter tests, or to a lateral displacement of 15 mm. The 15 mm represents the radial borehole expansion limits of the OYO pressuremeter used by Kjartanson.

11. During the multistage tests, individual stages were continued until the

displacement rate had clearly reached a steady state rate. At that time, the load would be increased and this next stage continued until the steady state creep again was achieved.

12. At the conclusion of the test, the lid was removed and the top surface was visually examined for cracking patterns around the pile.

13. Next the ice was cored, using a modified CRREL core barrel. Generally two vertical coreholes were drilled. The cores were visually examined for structure (cloudiness versus clarity), and representative samples were carefully trimmed for bulk density measurement.

14. The diameter and lengths of the ice cores were carefully measured using laboratory steel calipers corrected for the thermal contraction of steel from 20°C to -2°C.

15. After test 2, a crystallographic examination of thin sections of representative ice was undertaken as an undergraduate thesis (Thompson, 1987), and completed under the direct supervision of this author. Thin sections were prepared, photographed under cross-polarized light, and measurements of average crystal diameter for each section were completed. Details of the thin section equipment, and test procedures are detailed in the undergraduate thesis, and are discussed in Appendix A.

16. It is to be noted, that as the bar translated through the ice, a void formed behind the bar. The ice did not flow around the back of the bar, and did not remain in contact with it.

TABLE 3.1 Check Electronic Instruments for Drift at Zero Load at Test Temperatures

Instrument	Single Bit Resolution (mV)	Test 9 86 Readings/116 hr			Test 10 42 Readings/89 hr			Tests 11 and 12 100 Readings/100 hr		
		Avg. (mV)	Std. Dev. (mV)	Std. Dev. (Bits)	Avg. (mV)	Std. Dev. (mV)	Std. Dev. (Bits)	Avg. (mV)	Std. Dev. (mV)	Std. Dev. (Bits)
Load Cells:										
LC10	.0024	-	-	-	.830	.0019	1	.789	.0019	1
LC20	.0024	-	-	-	-.998	.0021	1	-.992	.0019	1
LC18	.0024	.577	.0025	2	-	-	-	.5834	.0024	1
LC19	.0024	.252	.0029	2	-	-	-	.2546	.0032	2
Linear Variable Displacement Transducers (LVDT)										
LV1	.625	-	-	-	-980.44	.9231	2	-	-	-
LV3	.625	-558.01	.8621	2	-555.51	.8434	2	-894.46	.9922	2
LV4	1.250	-	-	-	-1690.92	.5496	1	-613.95	3.0193	3
LV5	1.250	-	-	-	543.13	.7345	1	-	-	-
Strain Gauges on Steel Bar:										
S2	.0024	-	-	-	1.498	.0026	2	1.043	.0046	
S3	.0024	-	-	-	0.845	.0030	2	.922	.0049	
S4	.0024	-	-	-	1.272	.0024	1	1.451	.0061	
S5	.0024	-	-	-	1.412	.0026	2	1.911	.0069	
S6	.0024	-	-	-	2.764	.0023	1	2.809	.0107	
S7	.0024	-	-	-	3.181	.0034	2	3.228	.0122	
S8	.0024	-	-	-	3.160	.0026	2	3.050	.0117	
S11	.0024	3.210	.0093	4	-	-	-	3.535	.0167	
S12	.0024	2.430	.0115	5	-	-	-	2.140	.0103	
S13	.0024	1.998	.0111	5	-	-	-	-	-	
S14	.0024	2.876	.0117	5	-	-	-	1.661	.008	
S15	.0024	3.269	.0095	4	-	-	-	2.784	.0133	
S16	.0024	-	-	-	-	-	-	3.282		
S17	.0024	-	-	-	-	-	-	3.484		

TABLE 3.2

Summary of Single Bit Resolution of Neff Multiplexer

Instrument	Gain Code Number	Single Bit Resolution (MV)	Single Bit Resolution (Engineering Units)
Load cells	11	.0024	.097 kN
LVDT	3 2	.625 1.250	.0097 mm
Power supply 10 volt excitation voltage for load cells	0	5	5 mv
Thermocouples	11	.0024	.063°C
Strain gauges on bar	11	.0024	$2.4 \times 10^{-6}\ \epsilon_x$*

* ϵ_x is bending strain.

TABLE 3.3

Chemical Properties of City of Winnipeg Tap Water and Arctic Ice Co. Ltd. Ice Crystals

Parameter	Tap Water (1) (mg/l)	Ice Crystals (2) (mg/l)
Fluoride	0.90	0.27
Total Hardness ($CaCO_3$)	83	8.46
pH	8.0	N.A.
Nitrate	<0.04	0.02
Chloride	2	2
Sulfate	<10	1
Calcium	22.5	5
Magnesium	6.2	0.54
Sodium	1.8	0.63
Potassium	1.4	N.A.
Iron	0.06	0.08
Manganese	0.01	0.02

N.A. Not available.

(1) Data from "Water Quality Monitoring Report", 1984, City of Winnipeg Waterworks and Waste Disposal Department, Laboratory Services Branch.
- average values of 1984 given.

(2) Data from Arctic Ice Co. Ltd.; report prepared by W.M. Ward Technical Services, August 1982.

Table 3.4

Comparison of Winkler Bar Applied Loads Versus Pressuremeter Pressures

Cavity Pressures From Kjartanson's (1986) Pressuremeter Tests (MPa)	Equivalent Load Applied to Winkler Bar* (kN)
1.0	23.3
1.25	29.0
1.50	34.8
1.75	40.7
2.00	46.5
2.25	52.3
2.50	Not tested

* Load quoted is at one end of bar only. Multiply by 2 to obtain total load pulling the bar sideways. Two different bars of diameters 75.0 mm and 76.2 mm, respectively, were used in the testing. Calculations for the equivalent load to be applied to the Winkler Bar assumed a bar diameter of 75.6 mm.

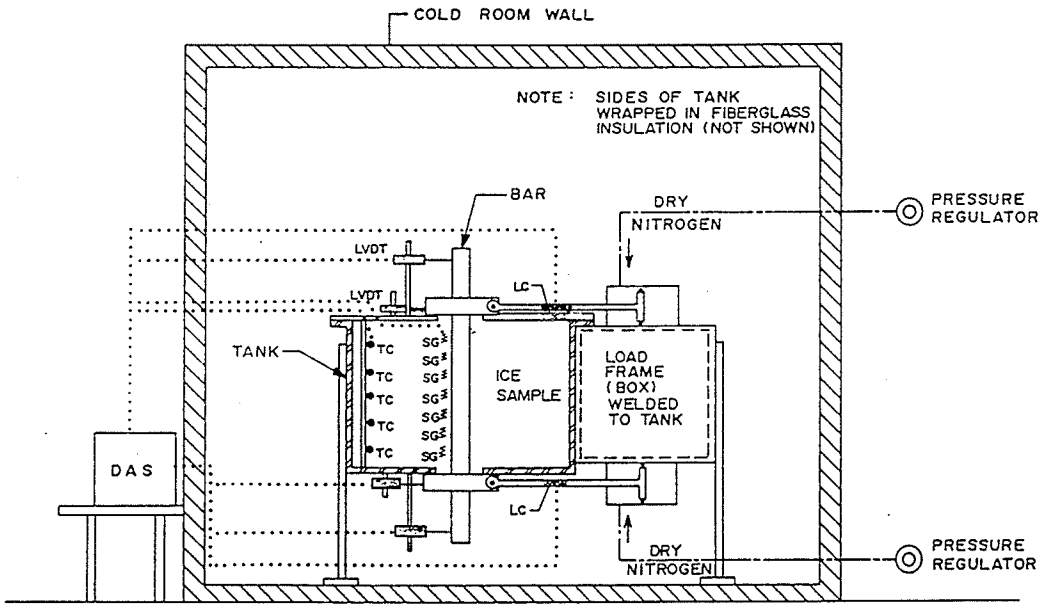

SCHEMATIC LAYOUT OF SINGLE 'WINKLER' PILE SEGMENT TESTING SYSTEM

LEGEND

TC	- THERMOCOUPLE
SG	-STRAIN GUAGE
LC	-LOAD CELL
DAS	-DATA AQUISITION SYSTEM

Figure 3.1 Schematic layout of Winkler bar test apparatus.

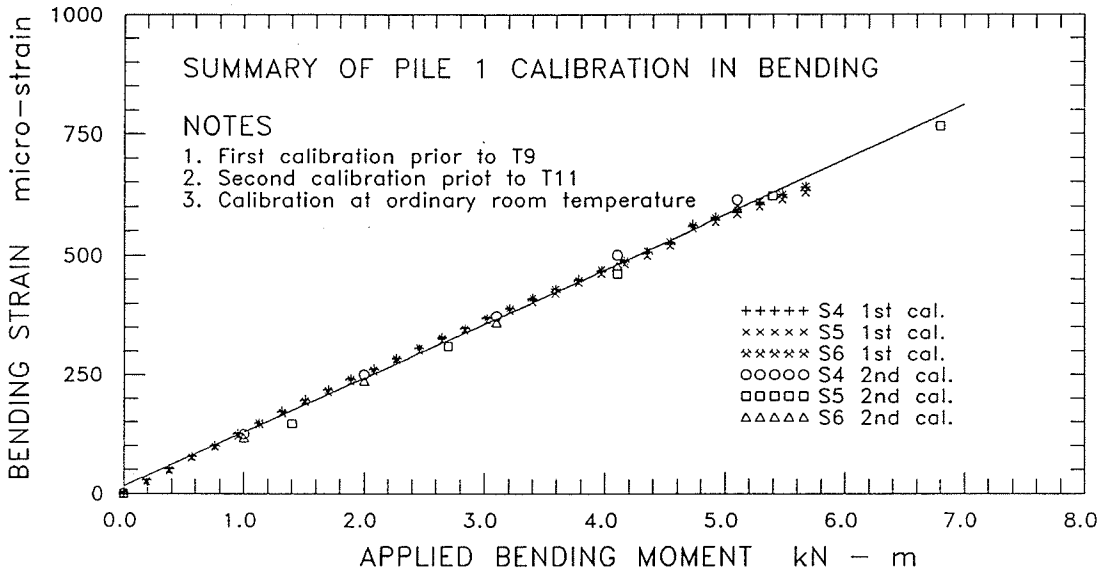

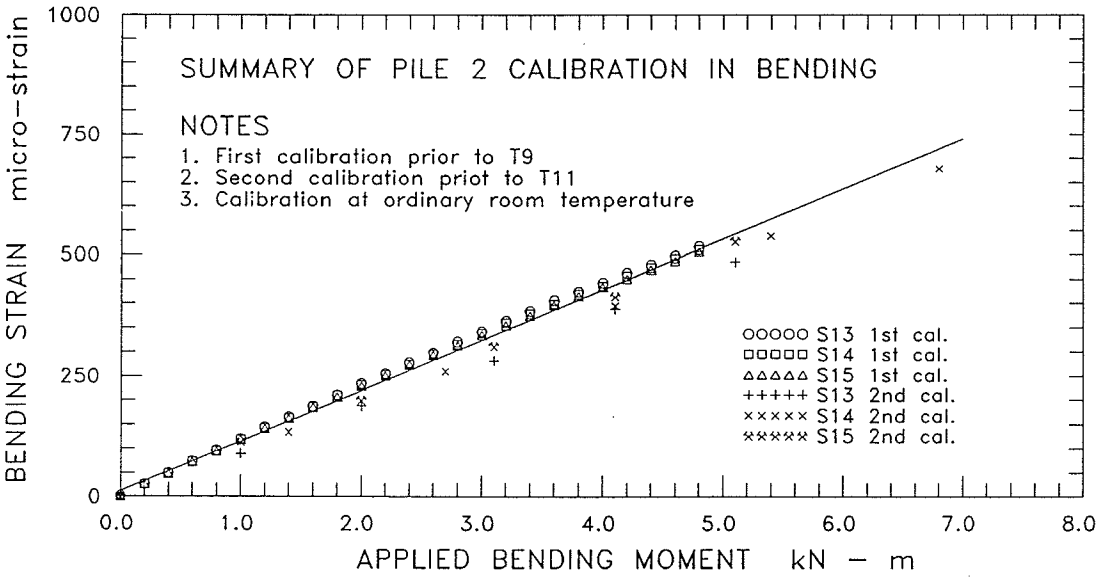

Figure 3.2 Calibration of Winkler piles (bars) in bending.

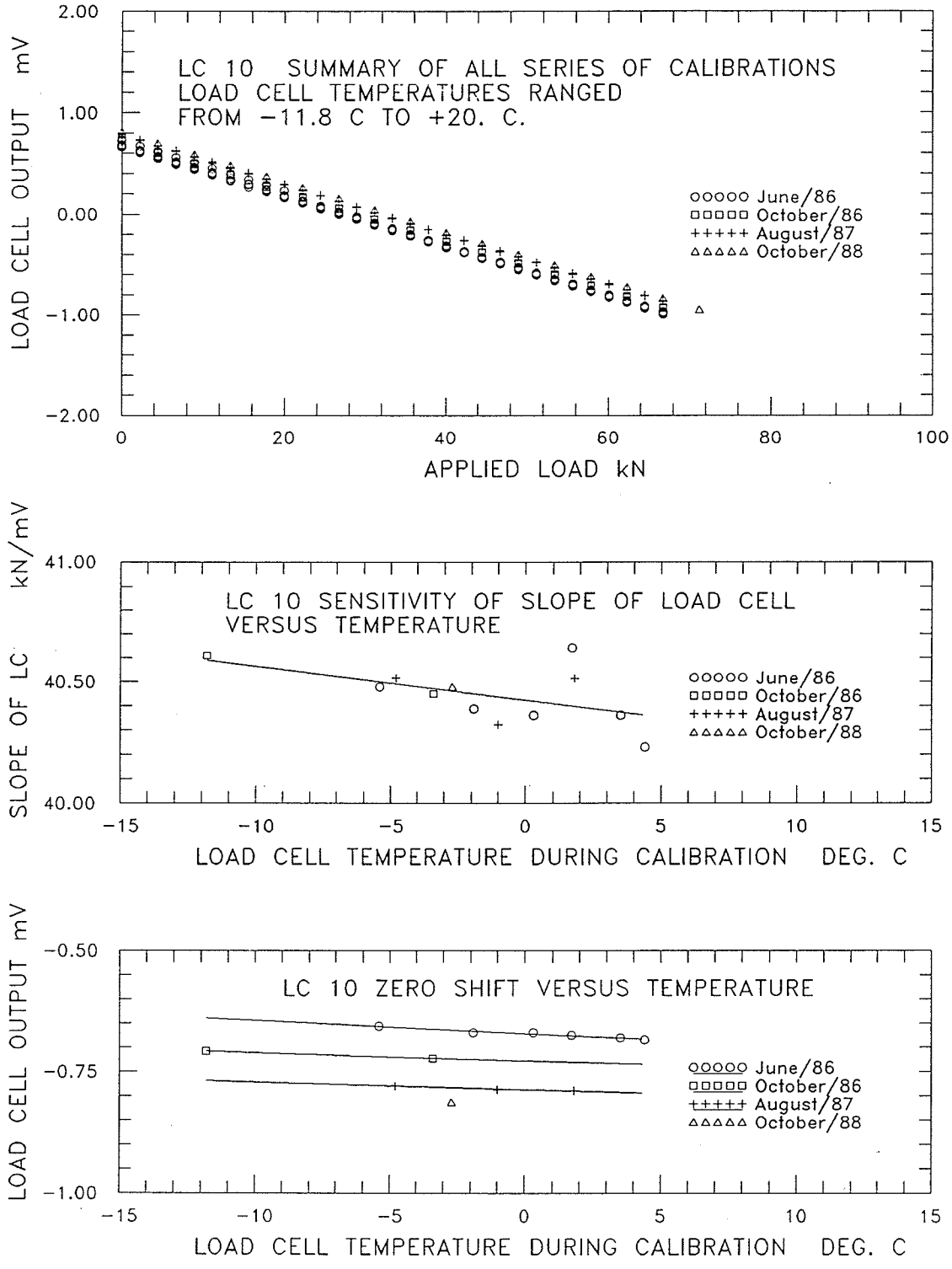

Figure 3.3 Calibration of load cell 10.

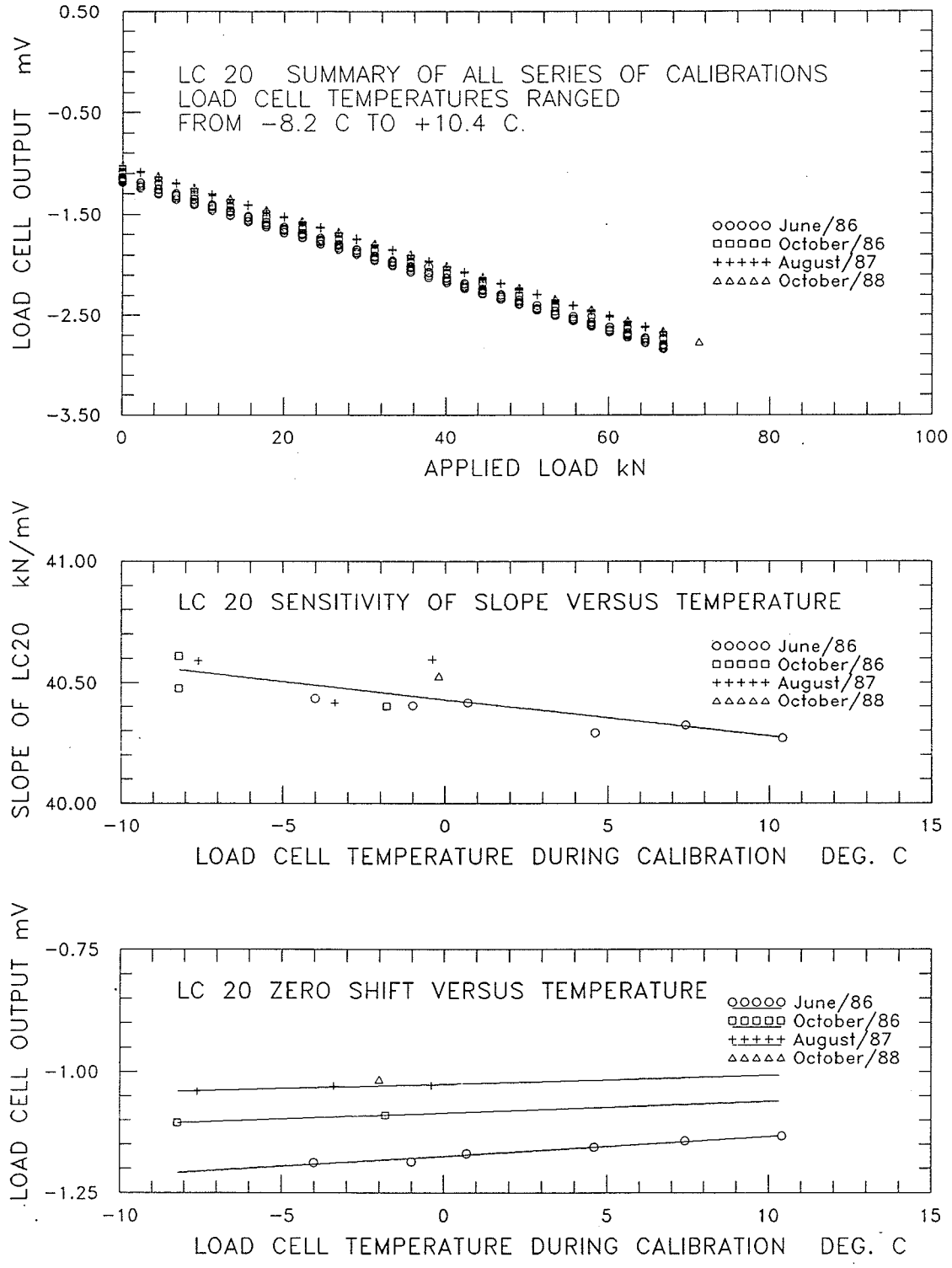

Figure 3.4 Calibration of load cell 20.

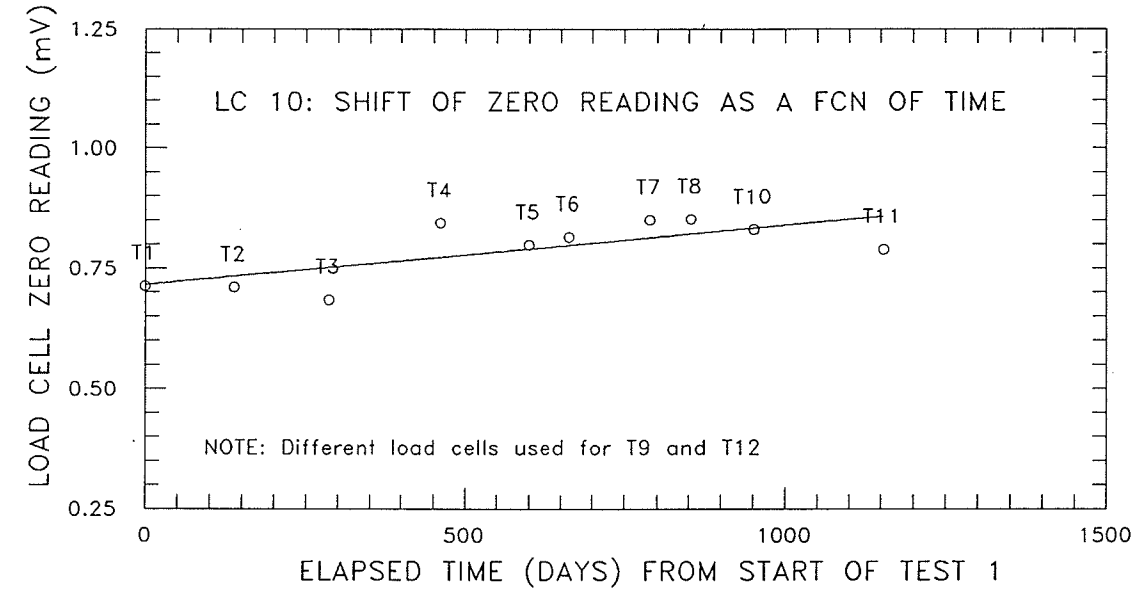

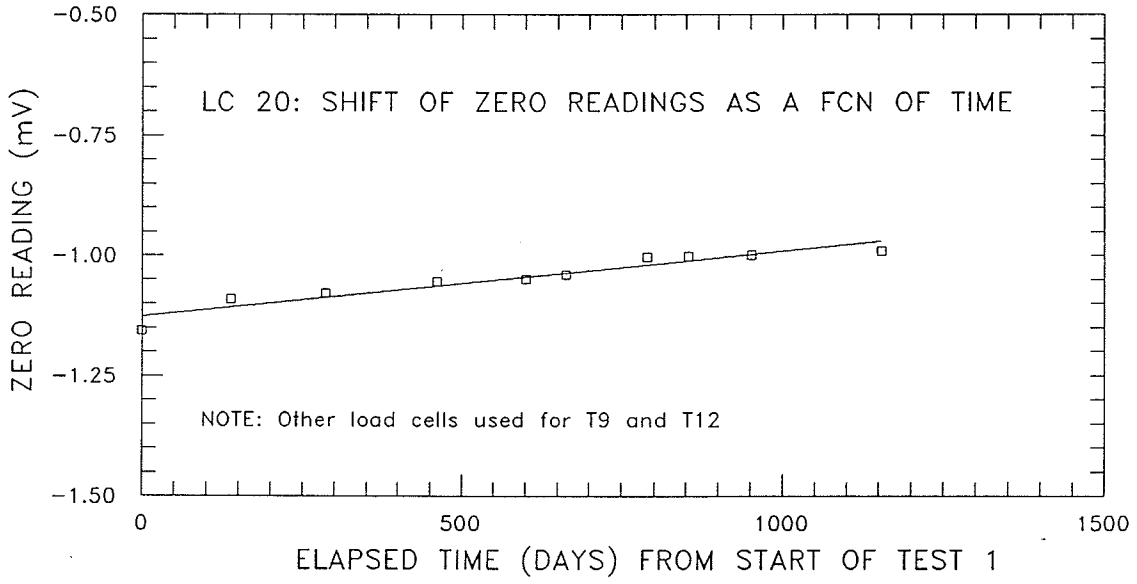

Figure 3.5 Shift of zero load output as a function of aging of the load cell.

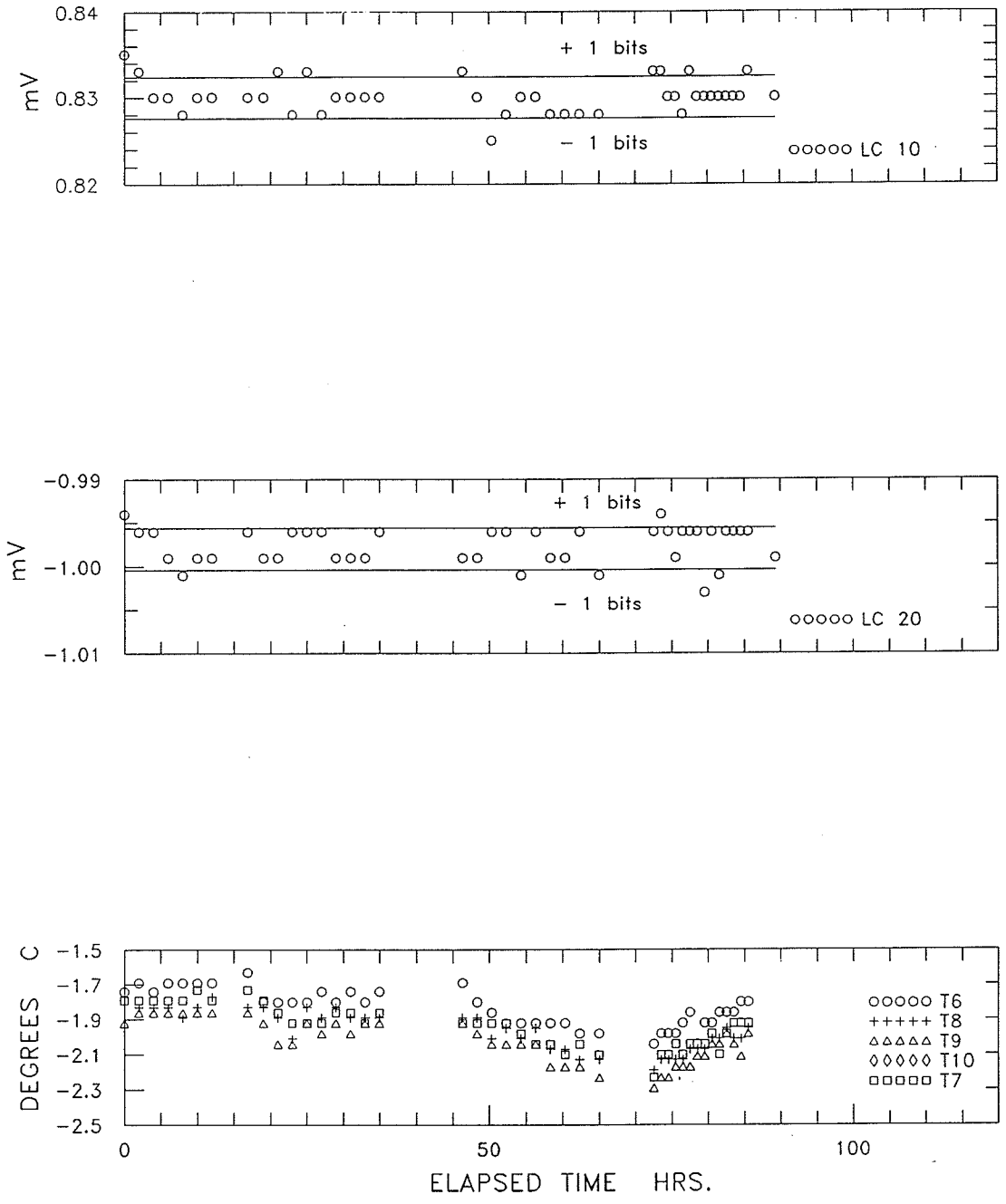

Figure 3.6 Typical drift of load cells under zero load conditions.
(Test 10 results shown).

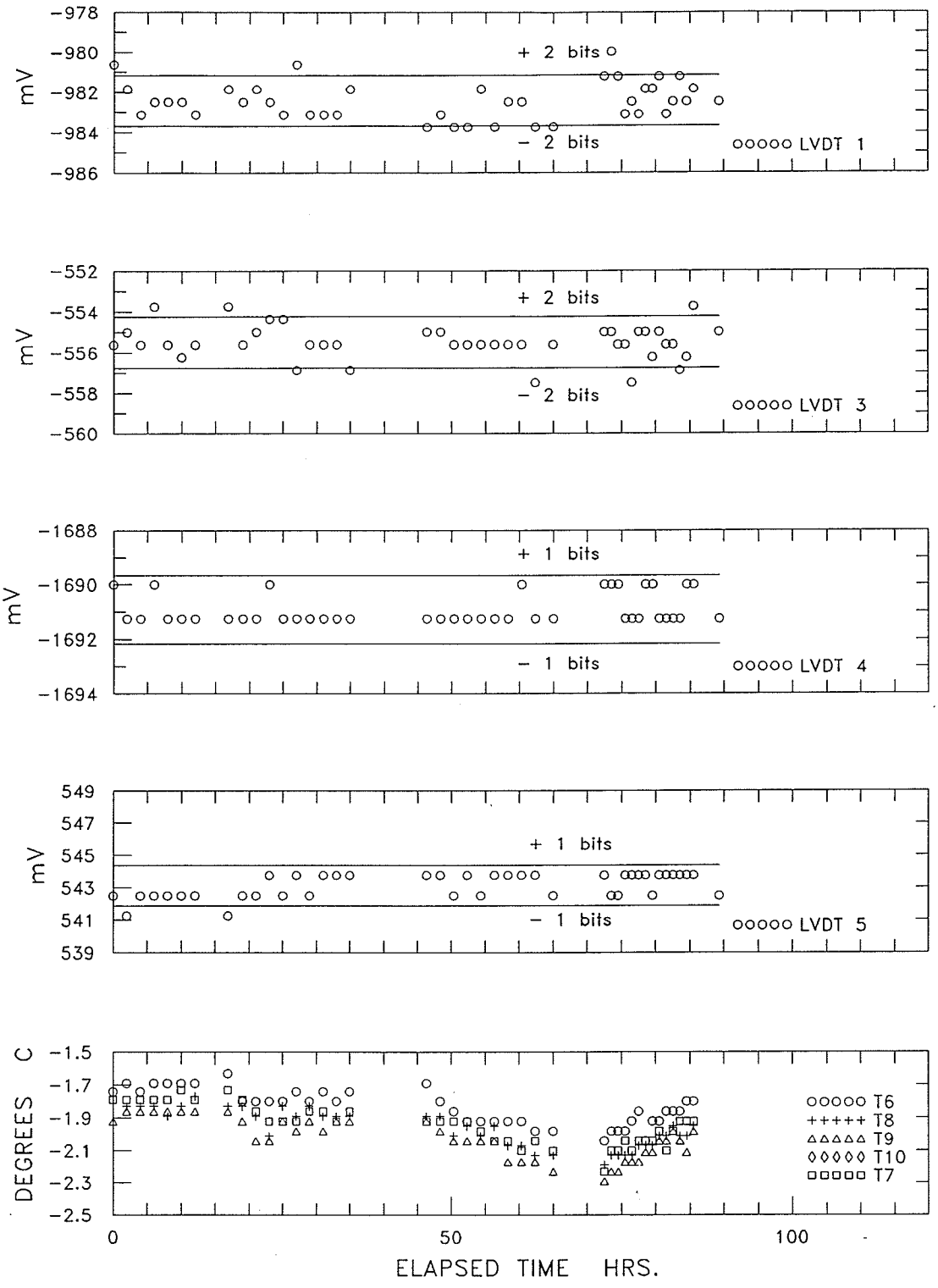

Figure 3.7 Typical drift of LVDT's under zero load conditions.
(Test 10 results shown.)

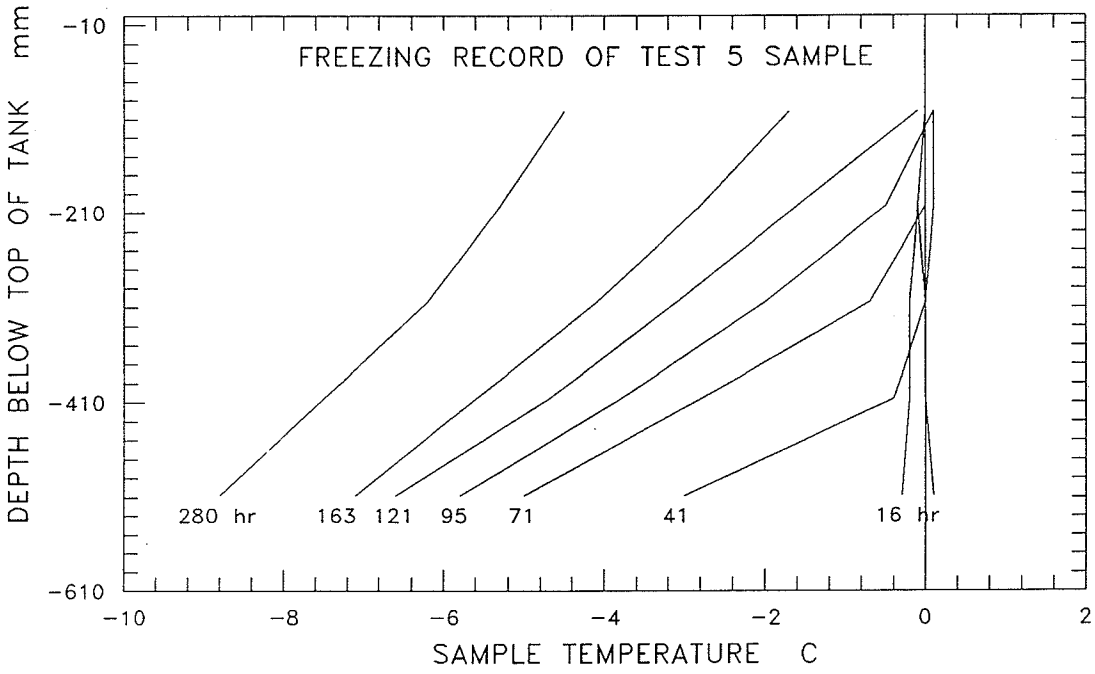

Figure 3.8 Typical freezing of the sample.

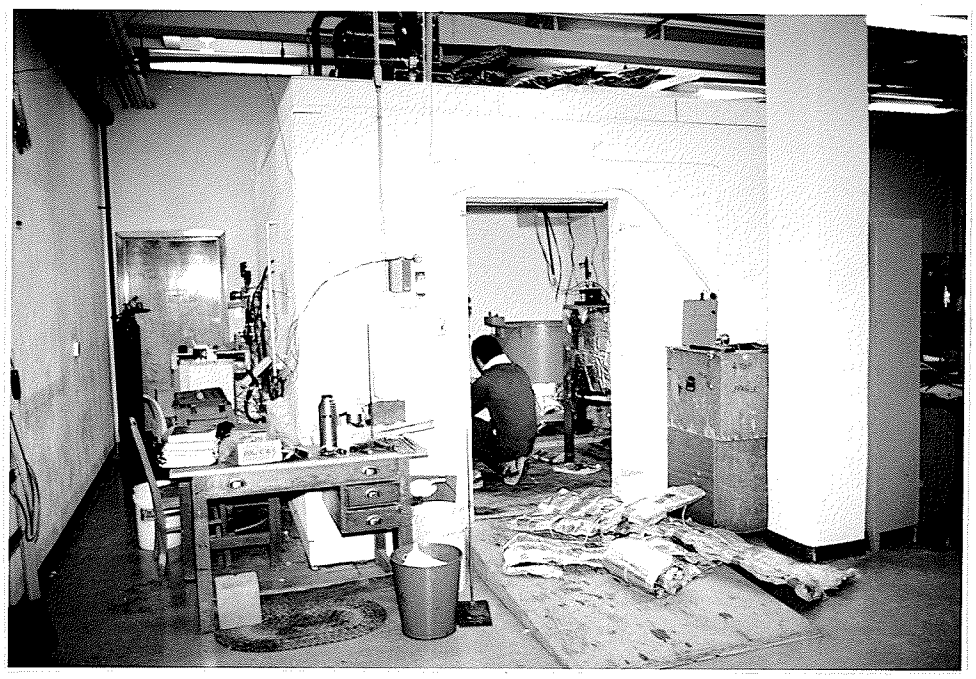

Photo 3.1 An overview of the research area including the cold room, data acquisition system, and tanks inside the cold room.

Photo 3.2 The steel bar used to represent the Winkler element. Note the plastic collar at the top of the bar to prevent sublimation. Strain gauges were mounted on the bar and covered with water proofing.

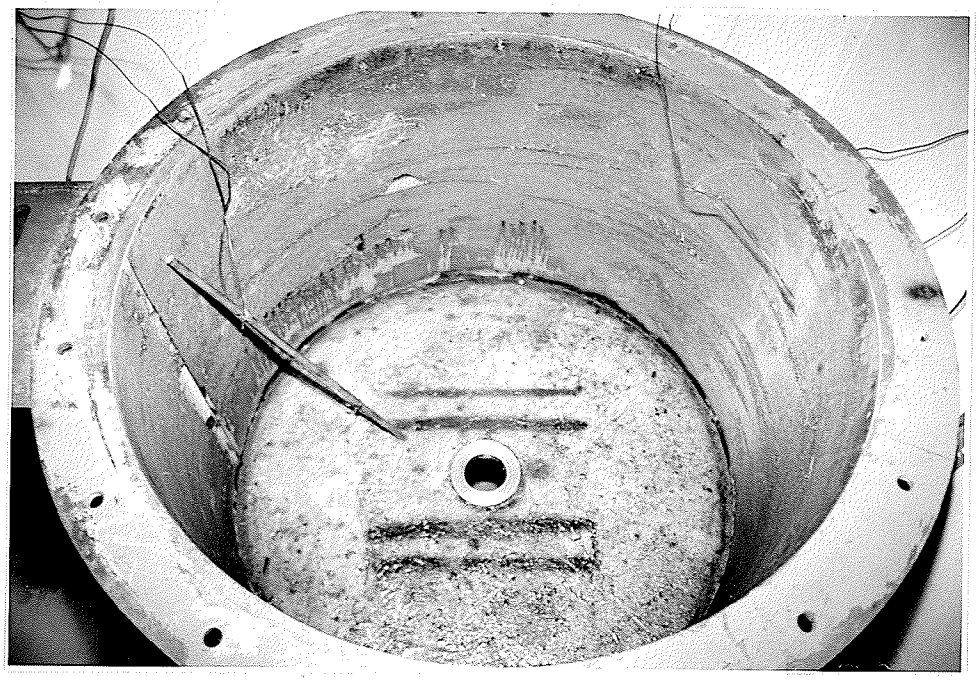

Photo 3.3 View looking inside the empty Winkler tank from the top. Note that the freezing collar (Plate 3.4) is in place in the bottom cut-out.

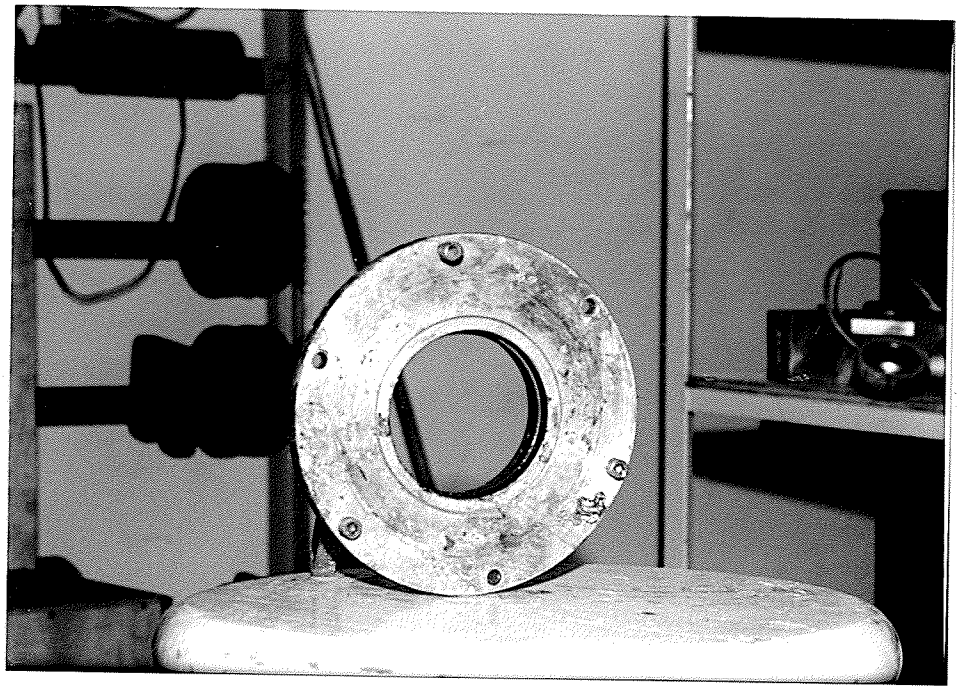

Photo 3.4 The freezing collar used to hold the bar in place during sample freezing.

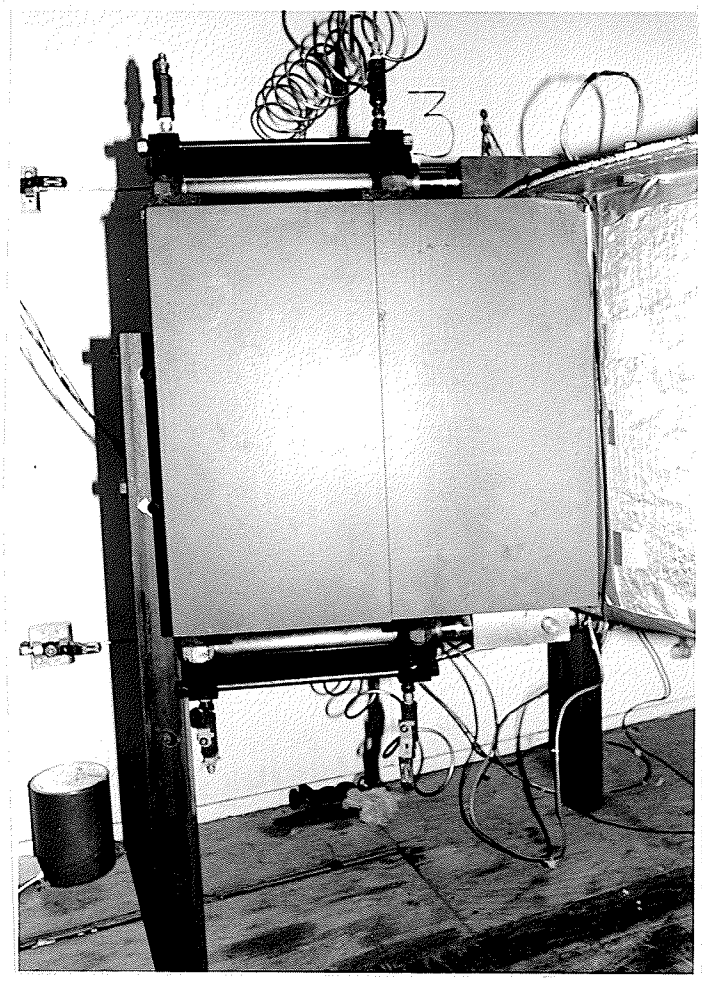

Photo 3.5 The box-shaped loading frame welded to the side of the tank. Note the hydraulic cylinders mounted to the top and bottom of the load frame.

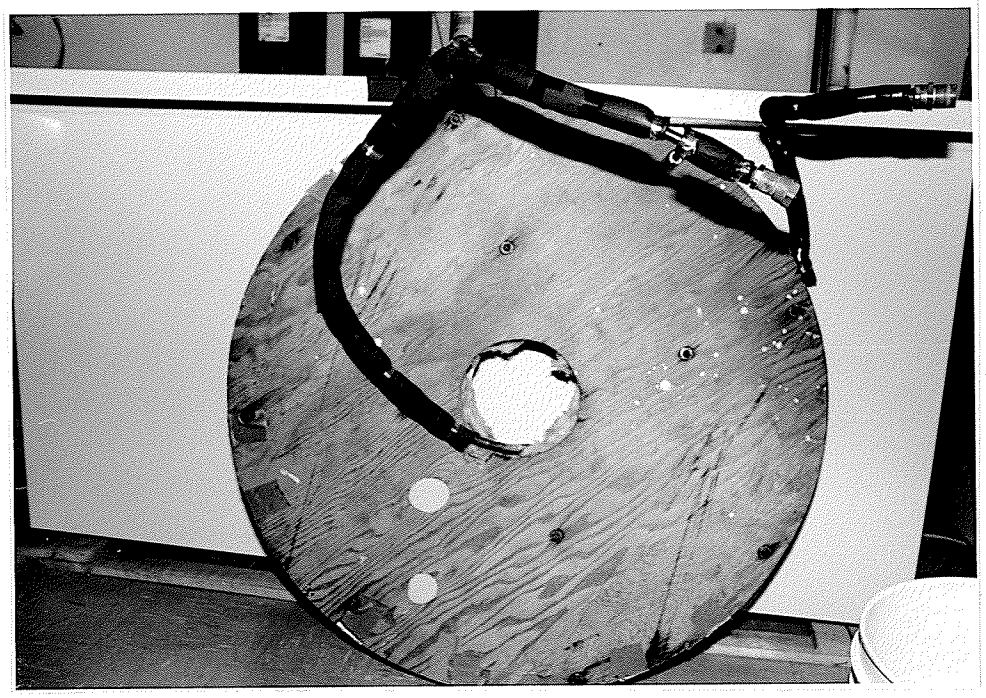

Photo 3.6 Freezing plate used to freeze the ice. To freeze the sample, the plate was fastened to the underside of the tank.

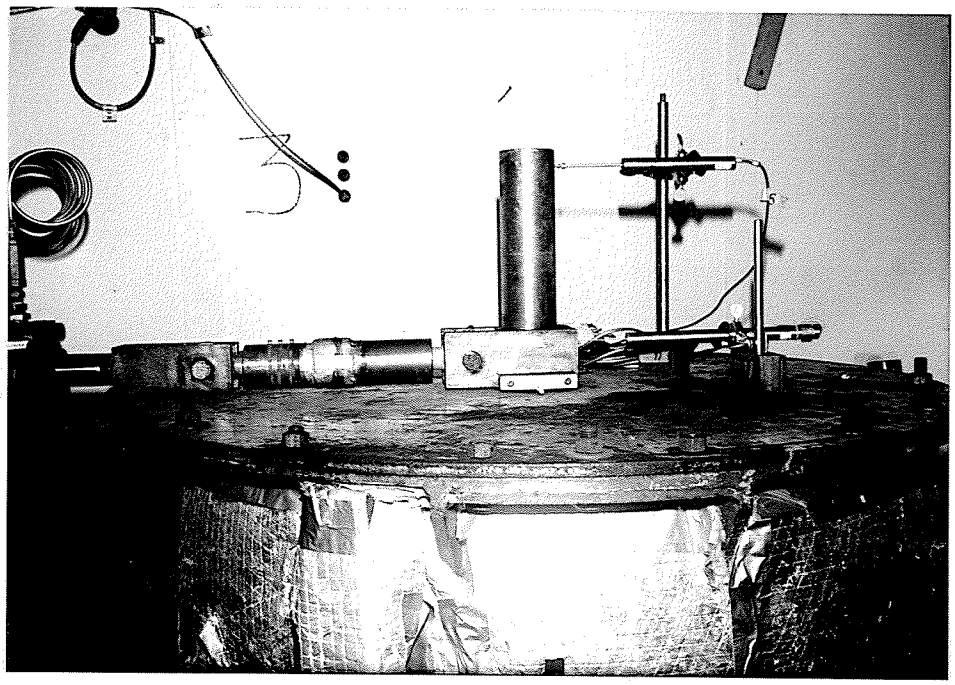

Photo 3.7 Loading system in place on the top of the tank. An identical loading apparatus was in place on the underside of the tank.

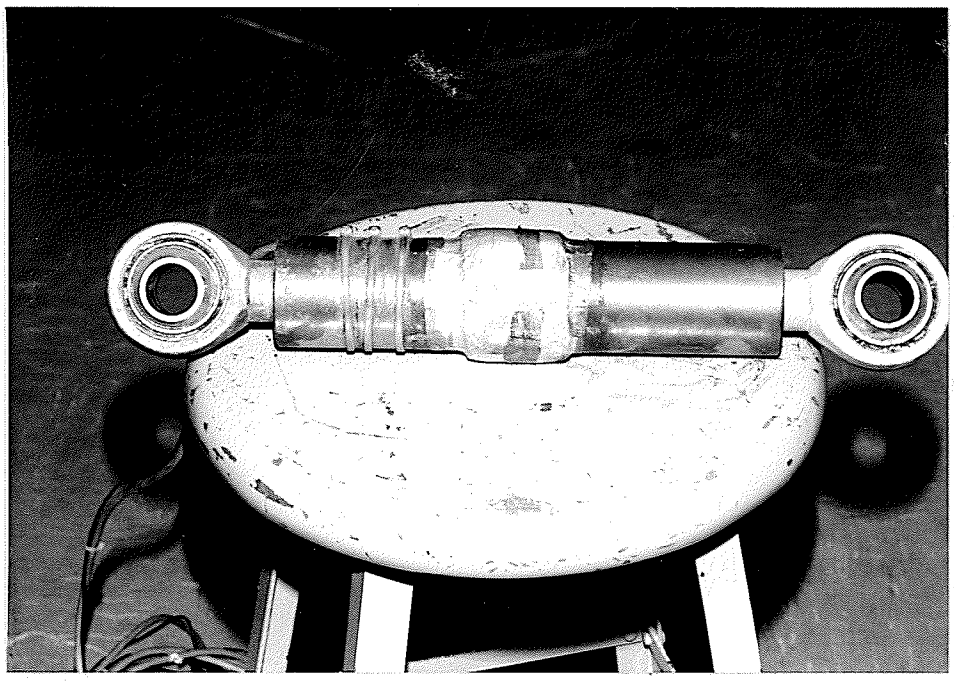

Photo 3.8 Load cell.

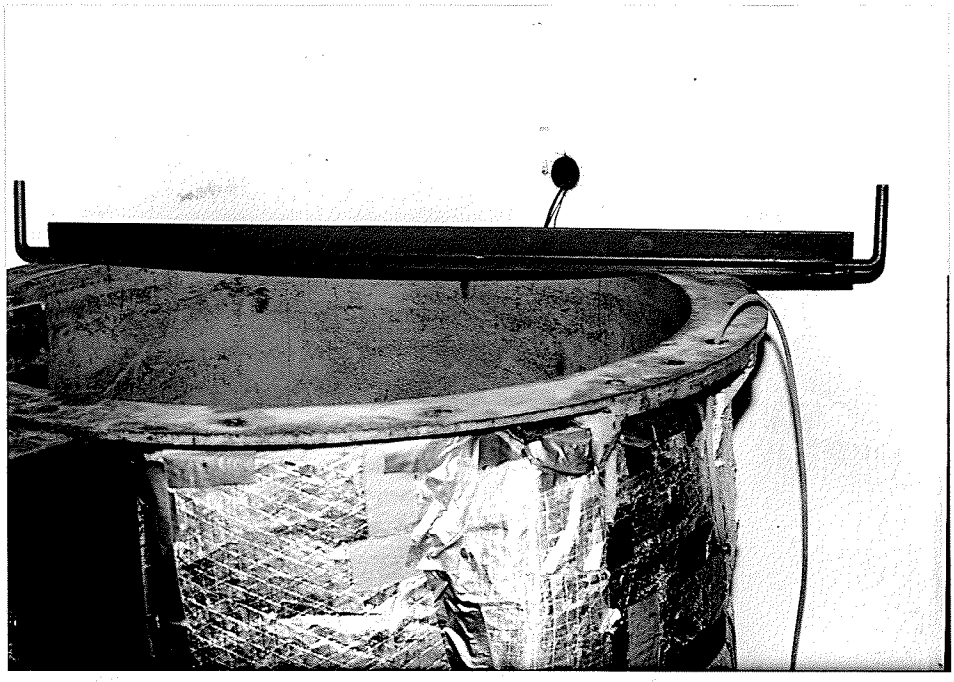

Photo 3.9 Drawknife used to trim the top of the ice sample flush with the top of the tank.

CHAPTER 4

TEST RESULTS

4.1 INTRODUCTION

This Chapter presents the experimental results of the test program. The program consisted of a total of twelve tests, of which eleven were single stage tests, and one was multi-stage. Of the twelve tests, the first four were considered preliminary in nature, and not suitable for analysis. A detailed discussion of the preliminary four tests, including "what went wrong", is placed in Appendix A. Details of each test, including applied lateral loads, Q, equivalent frontal pressure, p, and test duration are shown on Table 4.1.

This Chapter presents in detail the test results for one of the eight single stage tests (test 10), and for the multi-stage test (test 12). The Chapter also summarizes the data from all of the tests. Complete experimental results for all tests are placed in Appendix B.

4.2 EXPERIMENTAL RESULTS OF THE SINGLE STAGE TESTS

A total of eight single stage tests were completed: including test numbers 5 to 11, plus the first stage of the multi-stage test (Test 12, Stage 1). Equivalent frontal pressures, p, ranged from 1.0 to 2.25 MPa, in 0.25 MPa stages. The applied loads, Q, and calculated equivalent frontal pressures, p, are shown on Table 4.1.

Individual tests were continued either until a lateral displacement of 15 mm had occurred, or for a length of time equal to the elapsed time of the corresponding pressuremeter creep test.

Typically, results for each of the tests included plots of:

1. Deflection versus elapsed time.
2. Deflection rate versus elapsed time.
3. Applied load versus elapsed time.
4. Ice temperatures versus elapsed time.
5. Rotation of the free end of the Winkler bar versus elapsed time.
6. Bending strain versus elapsed time.

The results of tests 5 to 8 include only the first four plots. Following test 8, additional LVDT's were added so that the rotation of the free end of the bar could be monitored (Plot 5). In addition, strain gauges were mounted on the Winkler bar to measure the information required for Plot 6.

Figures 4.1 to 4.4 present typical single stage test results, using test 10 as an example. Test 10 was conducted at an applied lateral load of 40.65 kN, or p = 1.75 MPa.

Displacement Versus Time

The top graph of Figure 4.1 illustrated the displacement versus time behaviour for Test 10. As the graph illustrates, there is typically an instantaneous displacement, followed by a short period of rapidly decreasing displacement rates. The displacement rate then appears to become constant or steady with time (Fig. 4.2). In terms of classical creep behaviour, the pile appears to undergo instantaneous displacement, followed by primary creep and then by secondary creep. There is no evidence from this testing of the bar undergoing tertiary creep, i.e. an accelerating displacement rate.

Analysis of the instantaneous, primary and secondary components of the displacements are included in Chapter 5. Figure 4.4 presents a summary of displacement versus elapsed time for all single stage tests. Displacement behaviour was similar for each test.

Load Versus Time

The middle graph of Figure 4.1 illustrates the loading history of Test 10. As discussed in Chapter 3, it was necessary to maintain a slight differential between the top and bottom load in order to keep both ends of the bar moving at the same rate. However, if the load at one end were increased, the load at the other end was decreased by the same amount so that the average of the top plus bottom load was maintained at the target load (40.65 kN in this case). For Test 10, the average differential in loading was 1.6 kN or 3.9% of the target or nominal load. As shown on Table 4.2, the magnitude of the differential ranged from 1.2% of the target load for Test 8 to 9.3% of the target load for Test 11. Figure 4.5 summarizes the loading history for all single stage tests.

This manipulation of the loading was required because the four preliminary tests showed that when the same magnitude of lateral loading was applied to the top and bottom ends of the bar, then the bottom end of the bar would start moving faster than the top. The reason for the difference in rates is thought to be slight differences in the properties of the ice at the top and bottom of the tank (section 4.5).

Temperature Versus Time

The bottom graph of Figure 4.1 summarizes the ice sample temperatures during Test 10. The average test temperature, as measured at five different vertical positions in the ice, was -1.96°C. The standard deviation was 0.09°C. A summary of test temperatures for all tests is shown on Table 4.3, and illustrated on Figure 4.6. For eleven of the twelve tests the average sample temperature was maintained within -1.8°C and -2.2°C, that is to say, within 0.2°C of the target temperature of 2°C.

Displacement Rates

Displacement rates for Test 10 are shown on the bottom graph of Figure 4.3. The rates were calculated using a data sorting program called SORT, and a sliding polynomial curve fitting program SLOP which was developed by Sun (1987). The program SORT was written by this author; Sun's program SLOP was adapted by this author to run on microcomputers.

The SORT program analyzed the displacement versus time data to reduce the amount of data to manageable proportions. The sorting criteria assumed that the LVDT's measured displacements accurately to 0.1 mm. Following this criterion, SORT stored the first data point and then scanned the data to find the next data point where there had been a measured displacement of at least 0.1 mm. The second data point was then stored, but any points in between the first and the second points were deleted. This process continued to the end of the data set, leaving a data file where sequential data points represented at least 0.1 mm displacement. The SORT program was necessary because the scanning frequency was governed by the need to measure and adjust the load

on the ends of the bar on a frequent basis, due to drift in the loads.

The data smoothing program SLOP, developed by Sun (1987), incorporated a moving point polynomial least squared regression curve fitting technique. The length of the fitted segment was typically nine sorted data points. The program fitted a polynomial through the first nine points and calculated its first derivative at the middle point. Then the program shifted the data segment one data point and repeated the process. This iteration continued until all data were evaluated. The quality of fit was examined by comparing the calculated displacement versus each measured displacement. In almost all cases the calculated deflection was within 0.1 mm of the measured displacement.

The lower graph of Figure 4.2 shows that the displacement rate of the bar decreased rapidly from its initial rate for a period of 10 to 20 hours, when the rate became more or less constant to the end of the test. The rates shown on this graph were calculated using SLOP.

A detailed analysis of when primary creep ended is presented in the following Chapter. Figure 4.7 summarizes displacement rates for each of the single stage tests, and Table 4.4 summarizes the steady or secondary displacement rates. Appendix C contains displacement and displacement rate plots for all tests during the primary creep phase.

Rotation of Free Ends of the Bar and Bending Strain Along the Bar

Figure 4.2 summarizes the rotation of the free ends of the bar during Test 10, and also the bending strain in the embedded portion of the bar. The rotation is shown in radians measured from the vertical. The lower graph summarizes the bending strain

measurements along the bar as a function of elapsed time. Bending strain measurements were taken to obtain: (1) information regarding stress redistribution in the bar (Neukirchner and Nixon, 1987; Foriero and Ladanyi, 1990), and (2) the true shape of the bar at any time.

The redistribution of bending strain with time is illustrated on Figure 4.8. This figure shows the distribution of bending strain along the bar at selected time intervals up to the end of primary creep (12 hrs), plus the bending strain distribution at the end of the test (399 hrs). The conclusion drawn from this figure is that the redistribution of bending strains, from initial loading to the end of primary creep, is quite extensive.

Graphs similar to Figure 4.8 have been prepared for each of Tests 9 through 12, and are included with the complete test data in Appendix B.

4.3 EXPERIMENTAL RESULTS OF THE MULTI-STAGE CREEP TEST

One multi-stage test (Test 12) was completed as part of this experimental program. Figures 4.9 through 4.13 summarize the test behaviour of this test. As was done with the single stage test results, the figures include graphs of displacement, displacement rate, load, temperature, rotation of the free ends of the bar, and bending strain versus elapsed time. A complete breakdown of stage by stage test results is presented in Appendix B.

Examination of the top graph of Figure 4.9 suggests that well developed instantaneous and primary creep periods occur only in the first stage of the multi-stage test. The second and succeeding stages show much smaller instantaneous displacements, followed by a very short phase of primary creep. This observation is reinforced by examining the

displacement rates for each stage as shown on Figure 4.11. If Figure 4.11 is compared to the corresponding Figure 4.7 for the single stage tests, it appears that primary creep is less pronounced for the multi-stage tests.

As discussed in Chapter 3, each stage was maintained until displacement rates, as shown on Figure 4.11, had stabilized to a steady state condition. The secondary creep rates for each stage of the multi-stage test are summarized and compared to the single stage test results on Table 4.4. The data indicate that the secondary rates obtained during each stage of the multi-stage test are comparable to the secondary displacement rates observed during the single stage tests.

Observations and comments regarding applied loads, ice sample temperatures, and rotation of the free end of the pile are the same as for the previous subsection on the single stage tests.

Figure 4.12 shows the evolution of the distribution of bending strain along the bar during stage 1, and Figure 4.13 presents the same information for stage 5. The figures demonstrate that stress redistributions along the bar were much lower during the second and subsequent stages of the multi-stage test, than for the equivalent single stage tests.

4.4 TEST REPEATABILITY

Two sets of repeat single stage tests were completed, to test the repeatability of the testing program. Tests 6 and 10 were each completed at equivalent frontal pressures of 1.75 MPa, and Tests 8 and 9 were each completed at pressures of 2.25 MPa. Figure 4.14 summarizes displacements versus elapsed time for the repeat tests. The displacements of Tests 6 and 10 superimpose one upon the other, while the agreement

between Tests 8 and 9 was not as good.

4.5 ICE PROPERTIES AND SAMPLE HOMOGENEITY

Following each test, a minimum of two continuous ice cores were retrieved, and ice densities were measured from the cores systematically from top to bottom of each borehole. Table 4.5 summarizes the measured ice densities for each of the twelve tests. The ice had an average measured density of 0.904 Mg/m^3, based on fifty-six core samples. The standard deviation in density was 0.007 Mg/m^3. For no test did the average ice density fall beyond one standard deviation. There was no systematic measured density variation either vertically or laterally in the ice.

A crystallographic examination of the ice structure undertaken as an undergraduate thesis (Thompson, 1987), concluded that the ice was polycrystalline and its densities were uniform. It also concluded, however, that the crystallography was not homogeneous. Thompson found that the ice crystal diameters varied systematically from top to bottom, and he found a systematic variation in the pattern of entrained air bubbles within the mass of ice. Details of Thompson's study are found in the undergraduate thesis, and are synthesized in Appendix A.

Thompson measured the average crystal diameters from nineteen thin sections which had been trimmed from core samples of the Test 1 ice and photographed under cross-polarized light. In each thin section, from fifteen to forty-seven crystal diameters were measured. The measurements showed that the average crystal diameter near the top of the ice sample was 1.24 mm, while the corresponding crystal diameter near the bottom of the sample was 1.46 mm. This difference represented a variation of 18.5%

in crystal diameter.

The study also examined intact ice cores under ordinary white light for variation in the distribution in entrained air bubbles. Thompson found that the ice near the bottom had a distinct nuggety appearance, while near the top the ice appeared cloudier. The nuggety appearance was caused by tiny air bubbles which were concentrated on the surfaces of the individual seed ice cubes. The seed ice cubes were clear, as was the pore ice. The nuggety appearance was due to the air bubbles giving sharp visual definition to the ice cubes. On the other hand, the ice in the upper portion of the sample was almost cloudy in appearance. Here the air bubbles were randomly distributed throughout the ice, such that there was no visual definition of the individual ice cubes.

TABLE 4.1

Description of Laterally Loaded Pile Creep Tests

Test Number	Type of Test	Applied Load, Q, (kN)	Equivalent "Frontal" Pressure, p, (MPa)	Test Duration (Days)
PRELIMINARY TESTS - See Appendix A				
1	SST	46.5	2.0	3.5
2	SST	46.5	2.0	4.0
3	SST	23.25	1.0	86.2
4	SST	46.5	2.0	5.6
TESTS USED FOR ANALYSIS				
5	SST	46.5	2.0	13.9
6	SST	40.6	1.75	22.0
7	SST	34.8	1.50	36.1
8	SST	52.3	2.25	7.7
9	SST	52.3	2.25	18.6
10	SST	40.6	1.75	18.9
11	SST	23.3	1.0	43.5
12	MST			
	Stage 1	29.0	1.25	4.2
	Stage 2	34.5	1.50	5.7
	Stage 3	40.6	1.75	4.4
	Stage 4	46.5	2.00	2.1
	Stage 5	52.3	2.25	1.7

Notes:

1. SST Single stage test

2. MST Multistage test

3. Equivalent frontal pressure, $p = 2Q$ / (projected frontal area)

TABLE 4.2

Summary of Applied Loads

Test Number	Nominal Q (kN)	Avg. Q Top (kN)	Avg. Q Bot. (kN)	$\frac{Q_{top}-Q_{bot}}{Q_{nominal}}$ (%)
1	46.5	46.5	46.5	0.0%(1)
2	46.5	46.4	46.5	0.0%
3	23.25	23.3	23.2	0.0%
4	46.5	46.4	46.4	0.0%
5	46.5	48.0	46.1	4.1
6	40.6	41.9	39.4	6.1
7	34.8	35.8	33.9	5.5
8	52.3	52.7	52.0	1.2
9	52.3	53.5	51.2	4.4
10	40.6	41.6	40.0	0.4
11	23.2	24.2	22.0	9.3
12				
Stage 1	29.0	29.8	28.1	6.1
Stage 2	34.8	35.3	33.9	4.1
Stage 3	40.6	41.2	39.8	3.5
Stage 4	46.5	48.6	46.1	5.2
Stage 5	52.3	54.1	52.4	3.3

Note:

1. During Tests 1-4, identical loads were applied at the top and bottom.

TABLE 4.3

Summary of Sample Temperatures

Test Number	Avg. Temp. (°C)	Std. Dev. (°C)	Avg. Top (°C)	Avg. Bot. (°C)
1	-2.01	.14	-2.03	-1.98
2	-1.86	.17	-1.85	-1.86
3	-1.96	.12	-1.93	-1.96
4	-2.08	.16	-1.99	-2.07
5	-2.00	.15	-1.97	-2.01
6	-2.00	.18	-2.15	-1.88
7	-2.08	.18	-1.95	-2.00
8	-2.19	.18	-2.07	-2.09
9	-2.31	.07	-2.37	-2.28
10	-1.96	.09	-2.03	-1.85
11	-1.92	.13	-1.99	-1.84
12 S1	-2.01	.10	-2.07	-1.94
12 S2	-2.09	.10	-2.14	-2.04
12 S3	-2.21	.05	-2.27	-2.15
12 S4	-2.20	.11	-2.26	-2.14
12 S5	-2.24	.11	-2.28	-2.19

Notes:

1. Top temperature measured 100 mm below top of ice.

2. Bottom temperature measured 100 mm above bottom of ice.

TABLE 4.4

Summary of Secondary Displacement Rates

Test Number	Q (kN)	Equivalent "p" (MPa)	$\dot{y}$ (mm/hr)
5	47.1	2.03	0.054
6	40.6	1.75	0.033
7	34.8	1.50	0.018
8	52.3	2.25	0.098
9	52.3	2.25	0.082
10	40.6	1.75	0.031
11	23.3	1.00	0.004
12			
Stage 1	29.0	1.25	0.009
Stage 2	34.8	1.50	0.020
Stage 3	40.6	1.75	0.031
Stage 4	47.1	2.00	0.061
Stage 5	52.3	2.25	0.107

TABLE 4.5

Summary of Ice Densities

Test Number	Average Density (Mg/m^3)	Number of Cores Measured
1	.898	13
2	-	-
3	.909	10
4	.903	6
5	.908	6
6	.907	5
7	-	-
8	.903	9
9	.903	4
10	.898	3
11	Sample melted before ice was cored.	
12	Sample melted before ice was cored.	

Average Density	.904 Mg/m^3
Std. Dev.	.007 Mg/m^3
No. of Samples	56

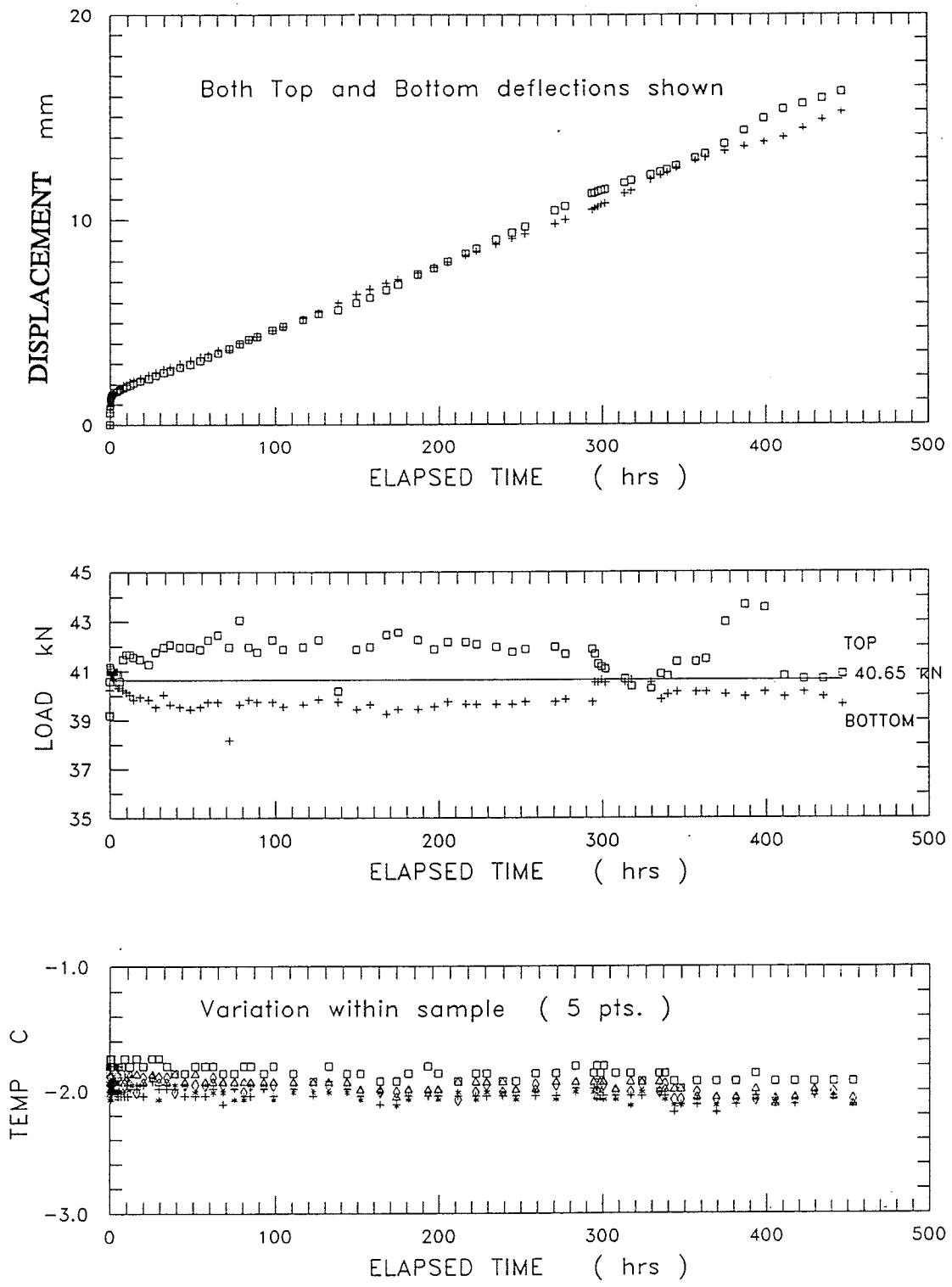

Figure 4.1 Single stage Test 10: displacement, load, and sample temperature versus elapsed time.

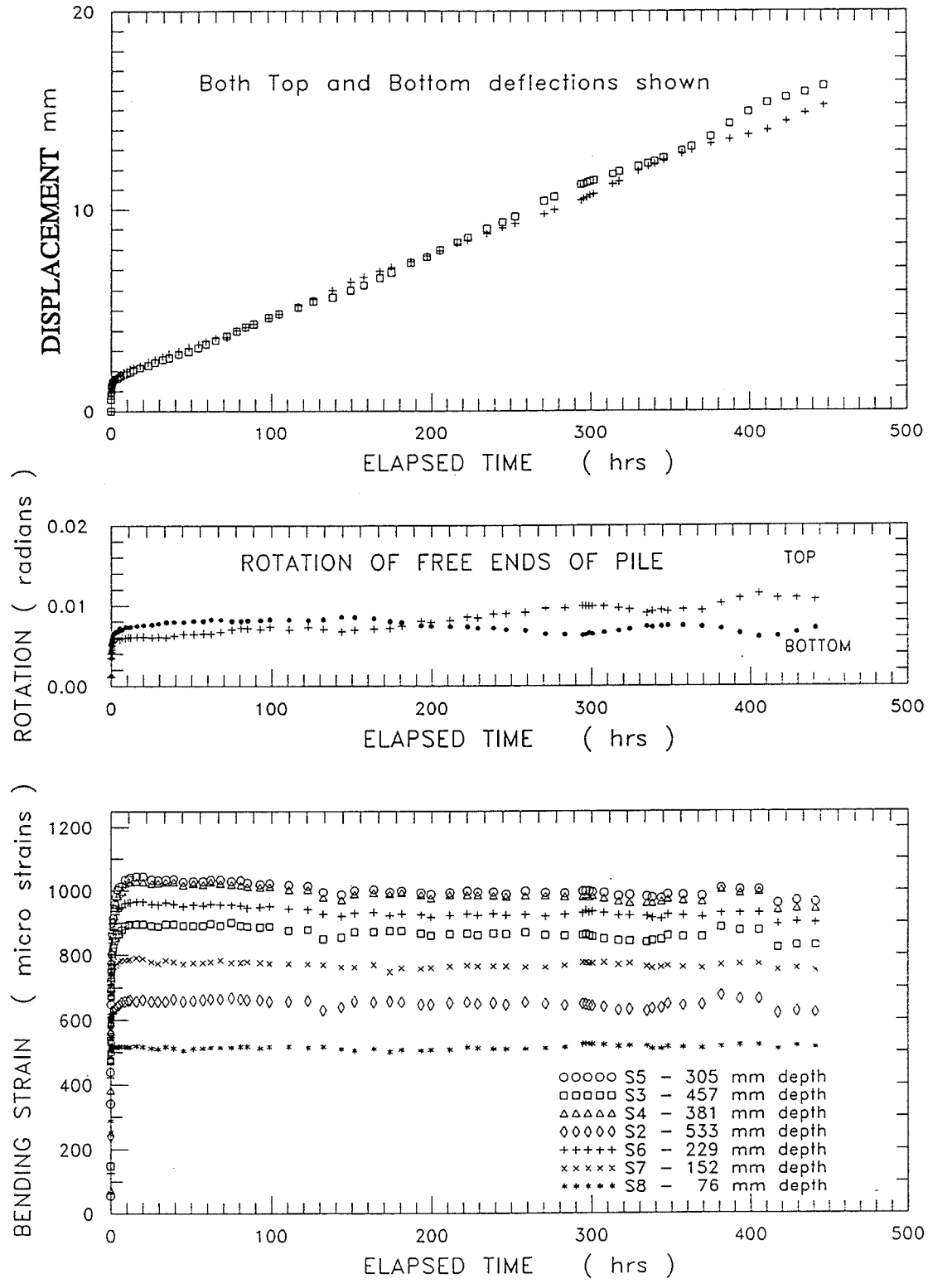

Figure 4.2 Single stage Test 10: rotation of free ends of the Winkler bar and bending strain versus elapsed time.

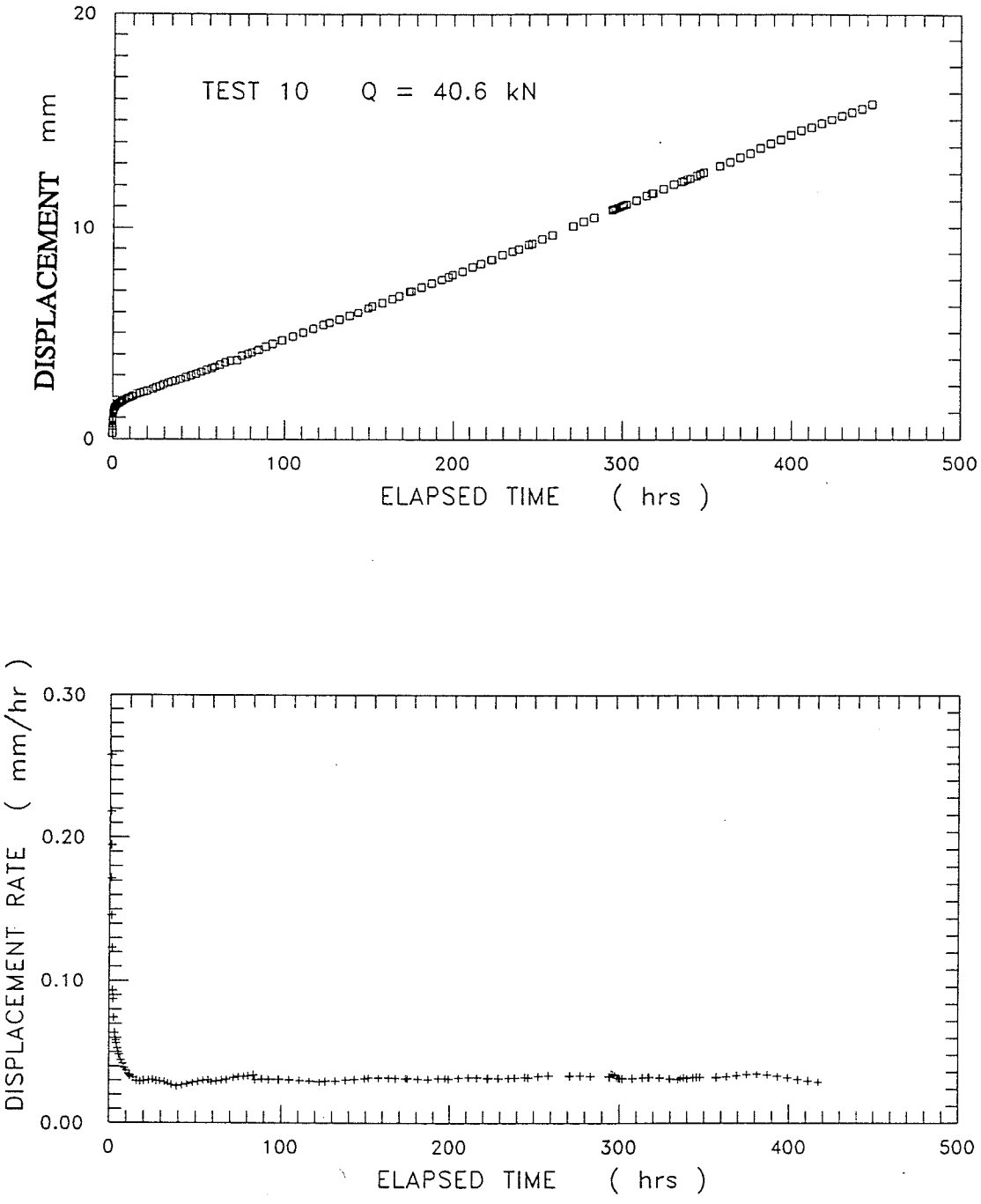

Figure 4.3 Single stage Test 10: displacement rate versus elapsed time.

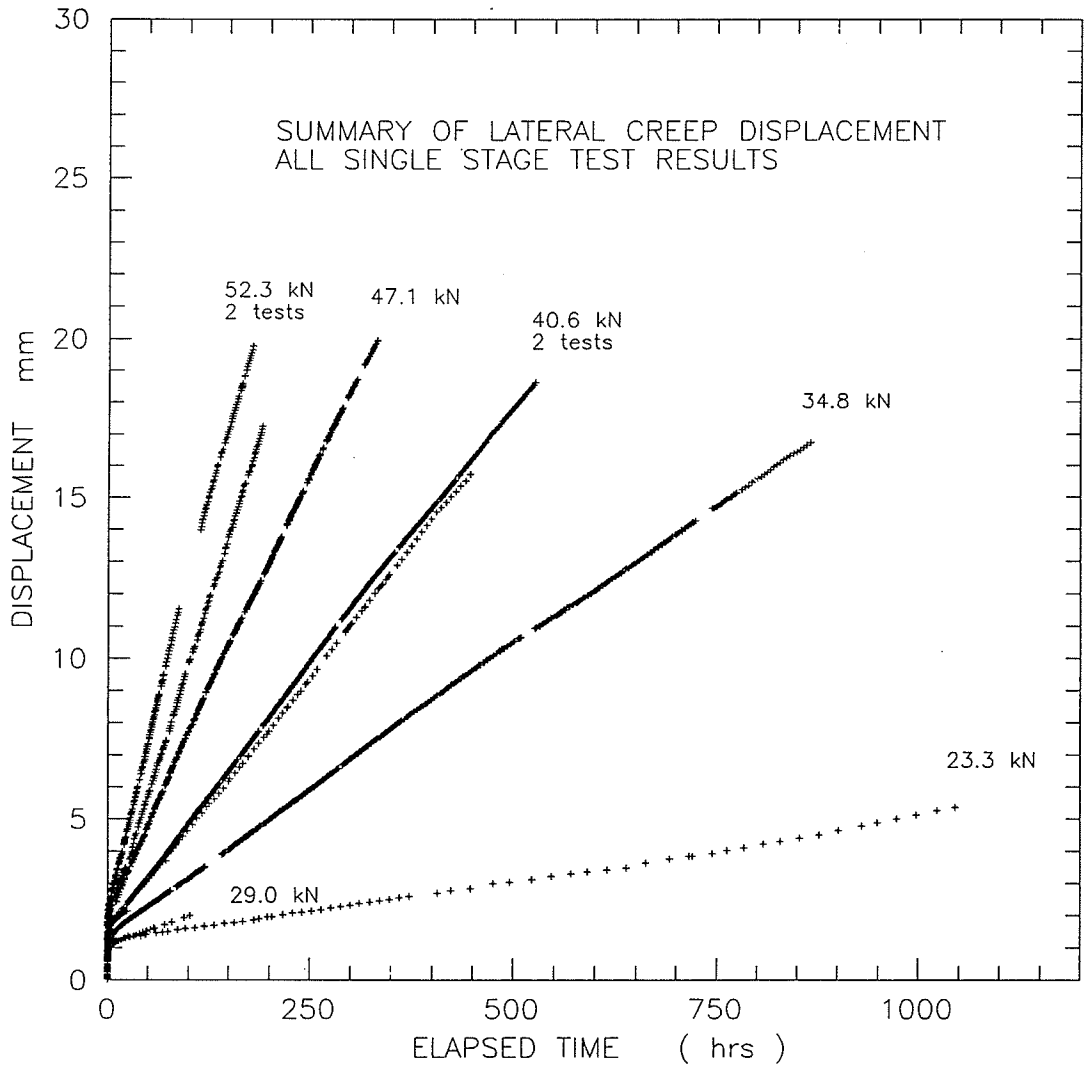

Figure 4.4 Summary of displacement versus elapsed time for all single stage tests.

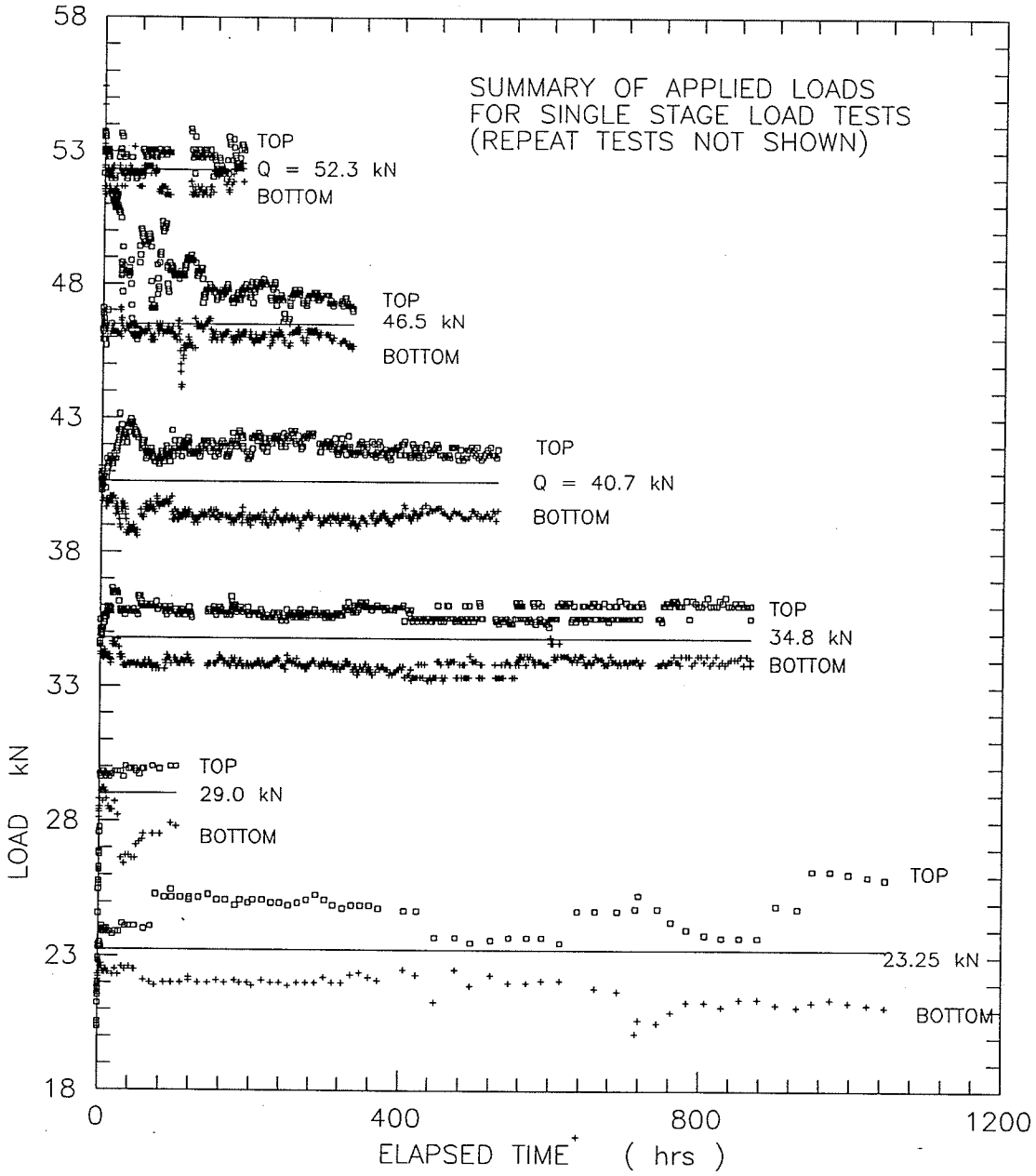

Figure 4.5 Summary of load versus elapsed time for all single stage tests.

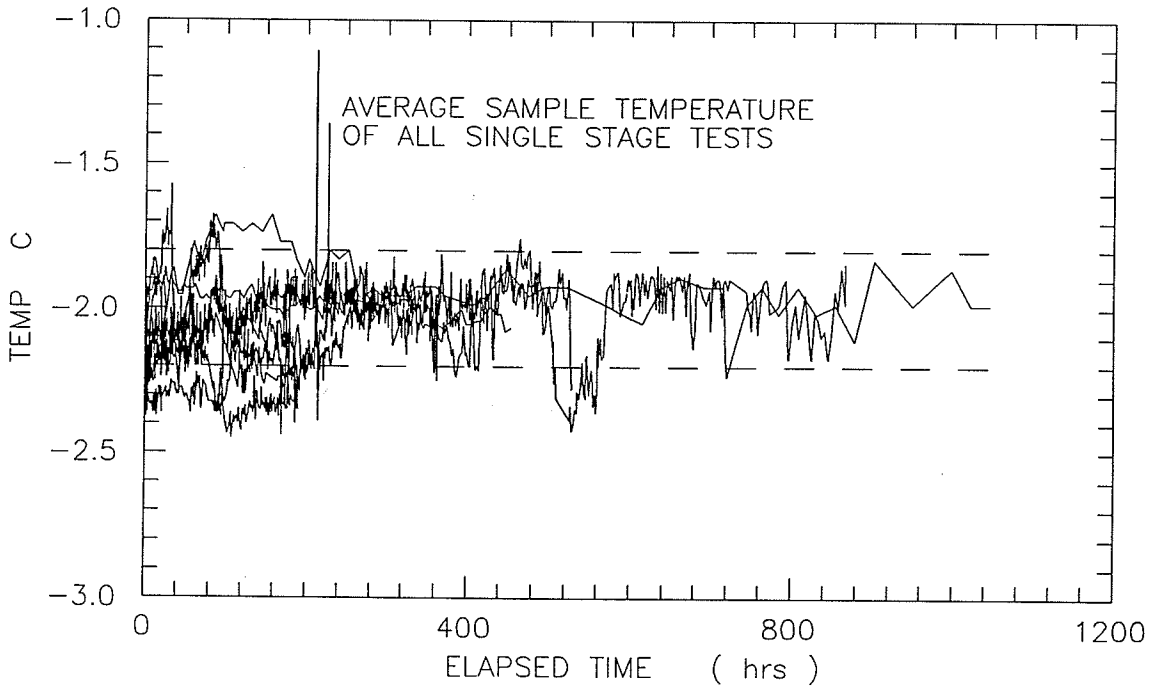

Figure 4.6 Summary of average sample temperature versus elapsed time for all tests.

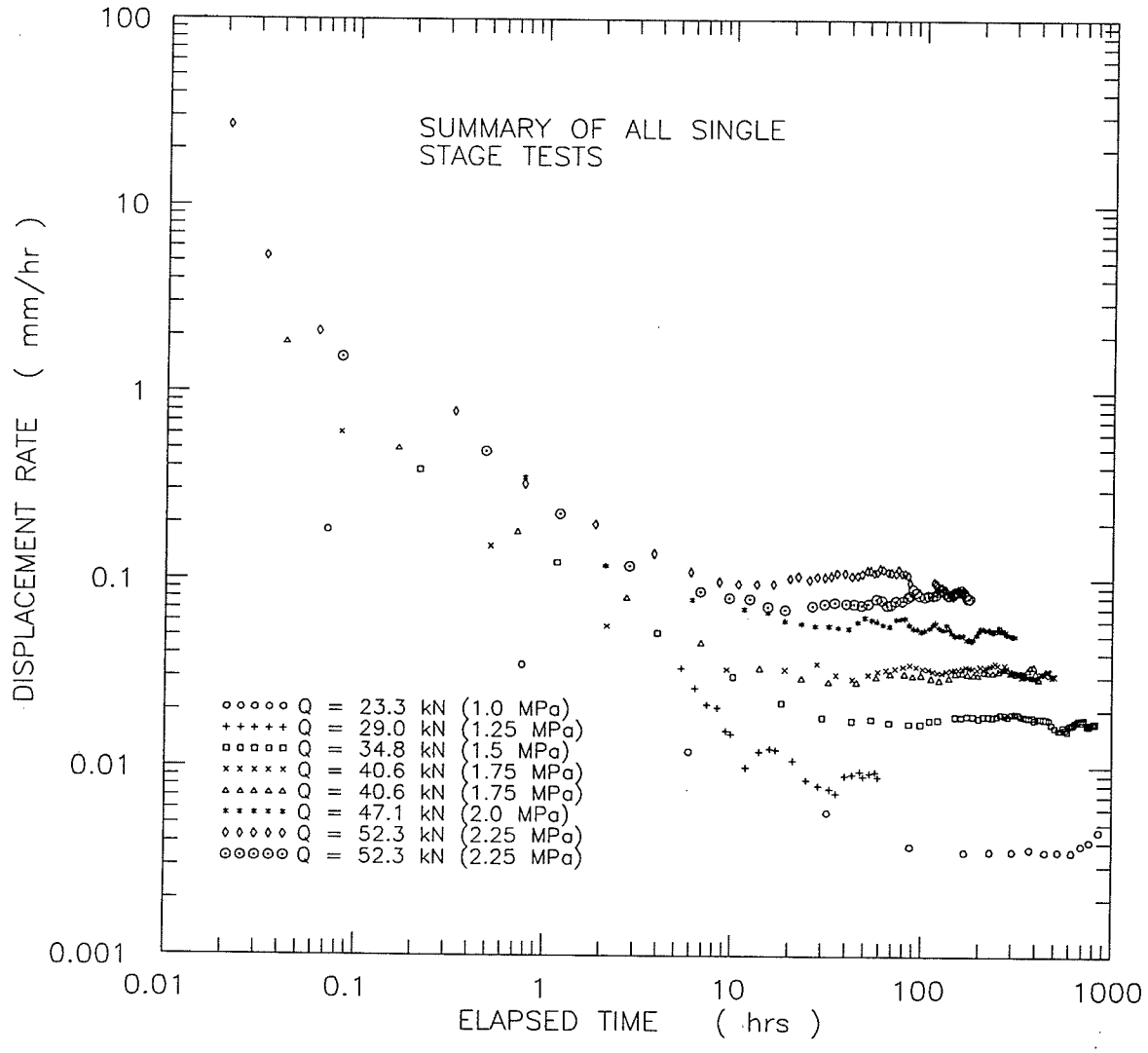

Figure 4.7 Summary of displacement rates versus elapsed times for all single stage tests.

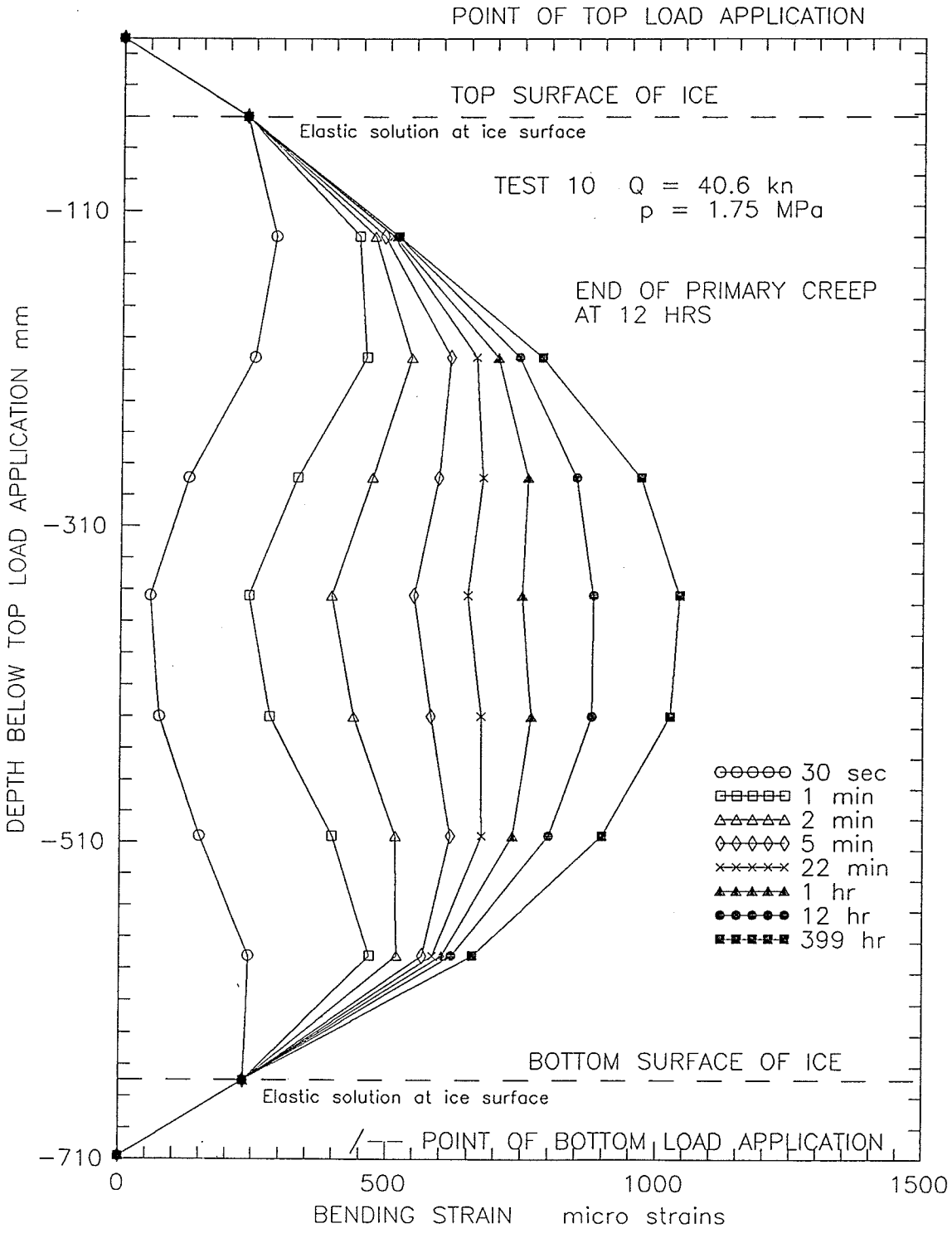

Figure 4.8 Redistribution of bending strains during single stage Test 10.

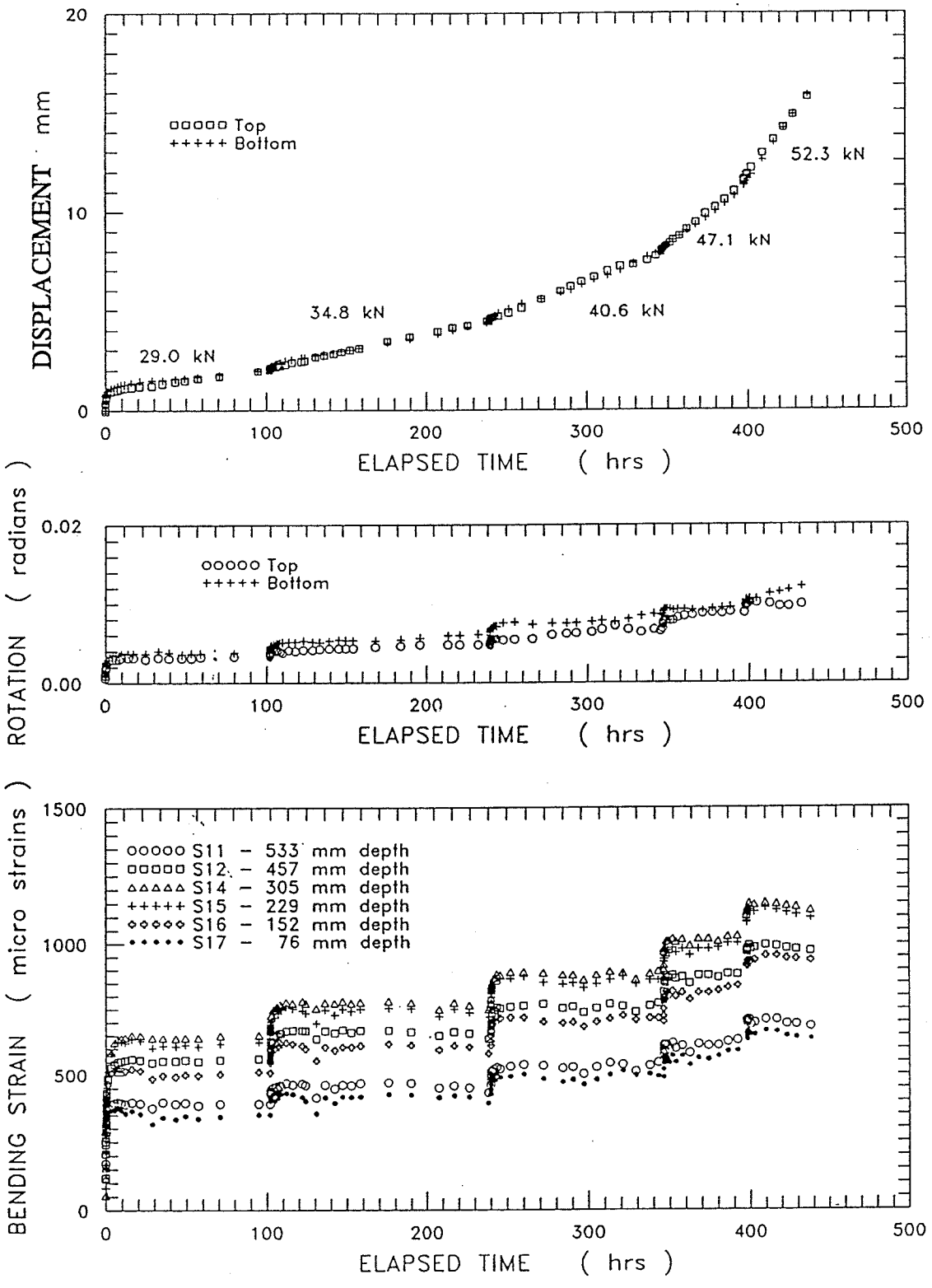

Figure 4.9 Multi-stage Test 12: displacement, load, and sample temperature versus elapsed time.

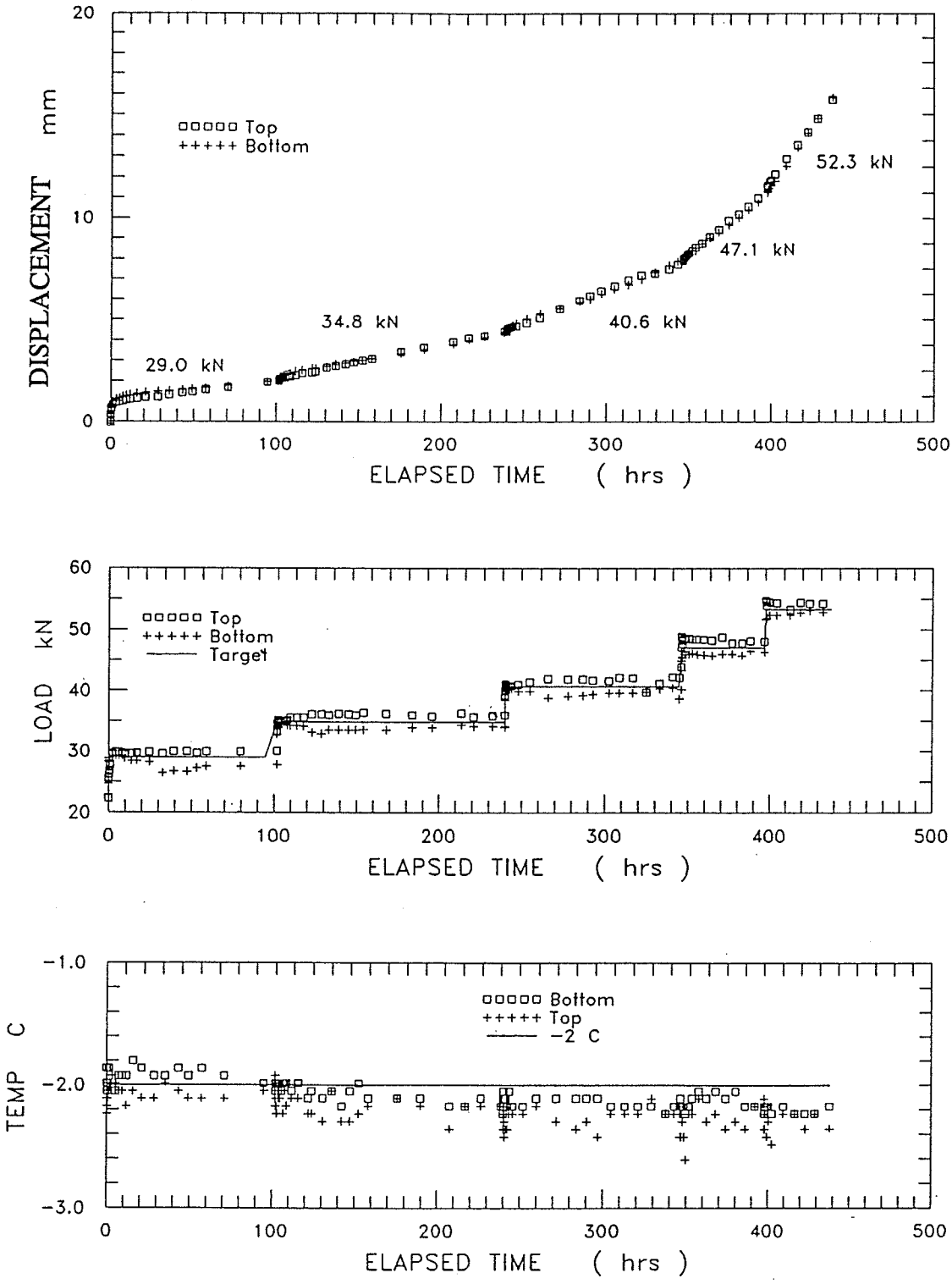

Figure 4.10 Multi-stage Test 12: rotation of free ends of Winkler bar and bending strain versus elapsed time.

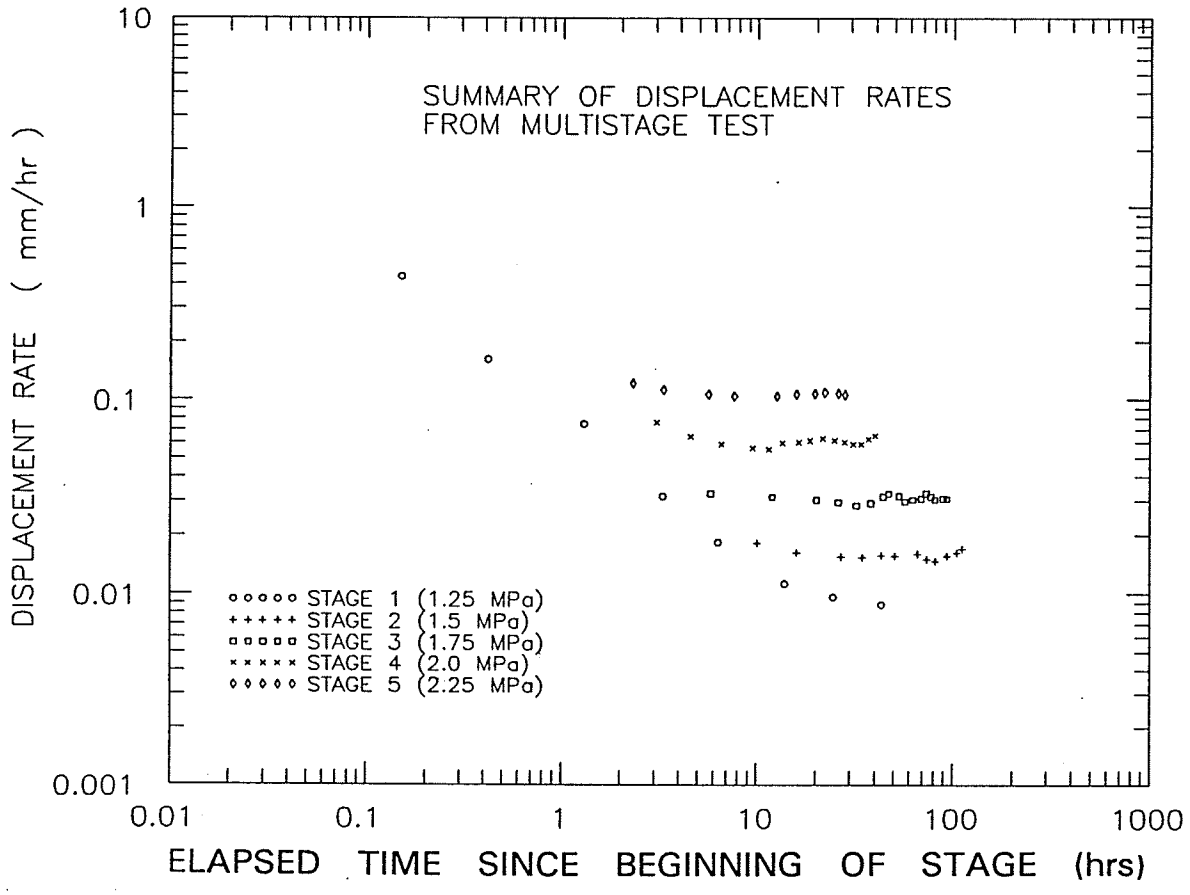

Figure 4.11 Summary of displacement rates versus elapsed time for multi-stage Test 12.

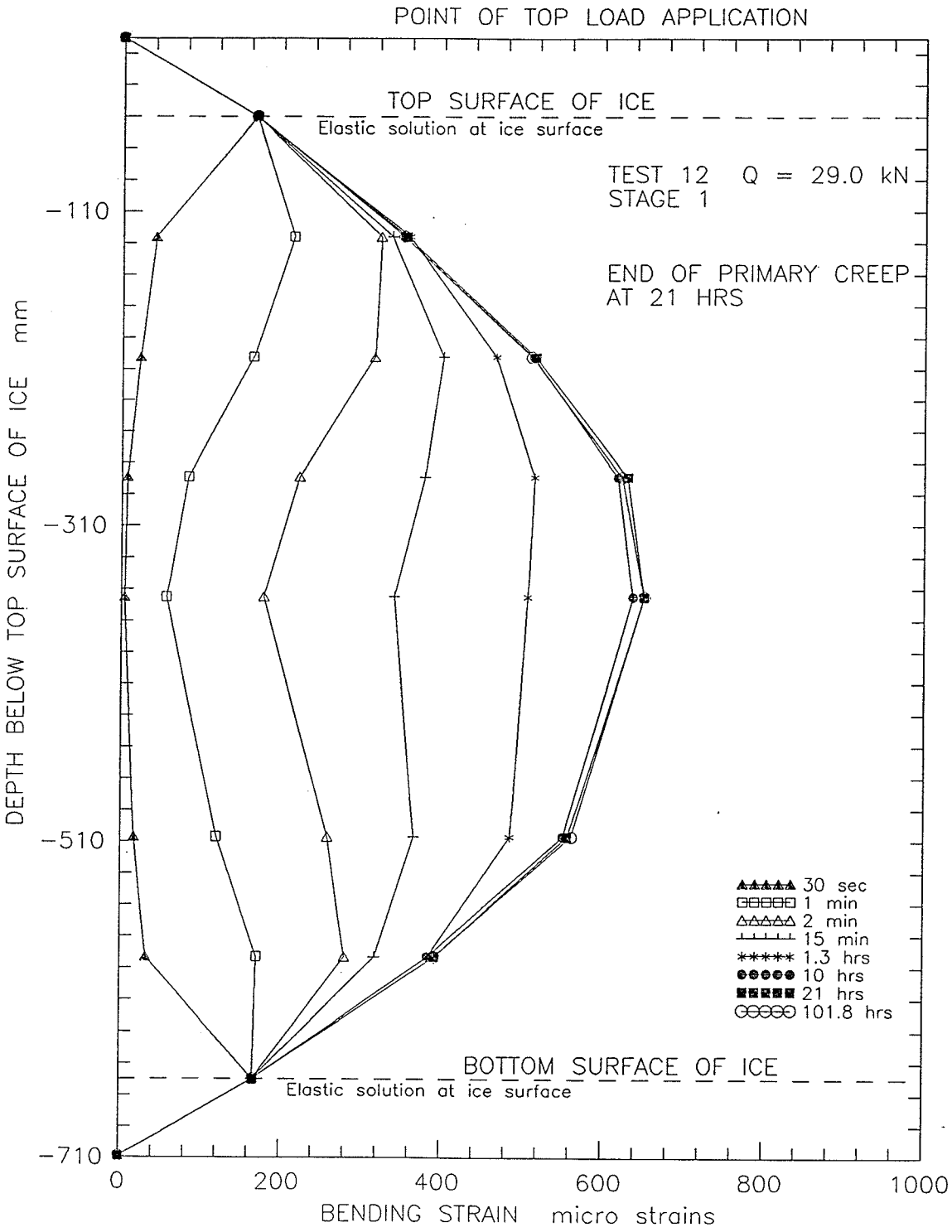

Figure 4.12 Redistribution of bending strains during Stage 1 of multi-stage Test 12.

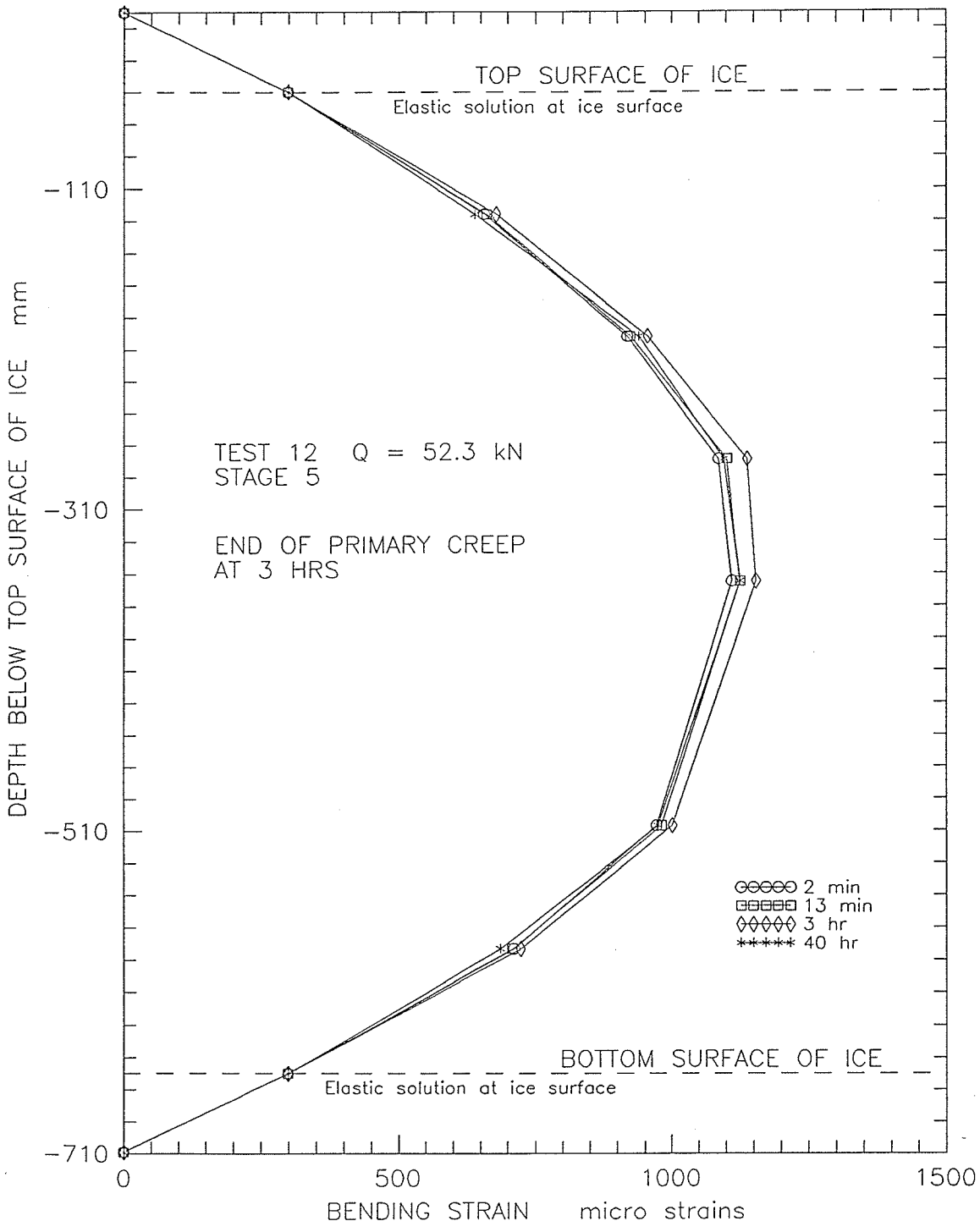

Figure 4.13 Redistribution of bending strains during Stage 5 of multi-stage Test 12.

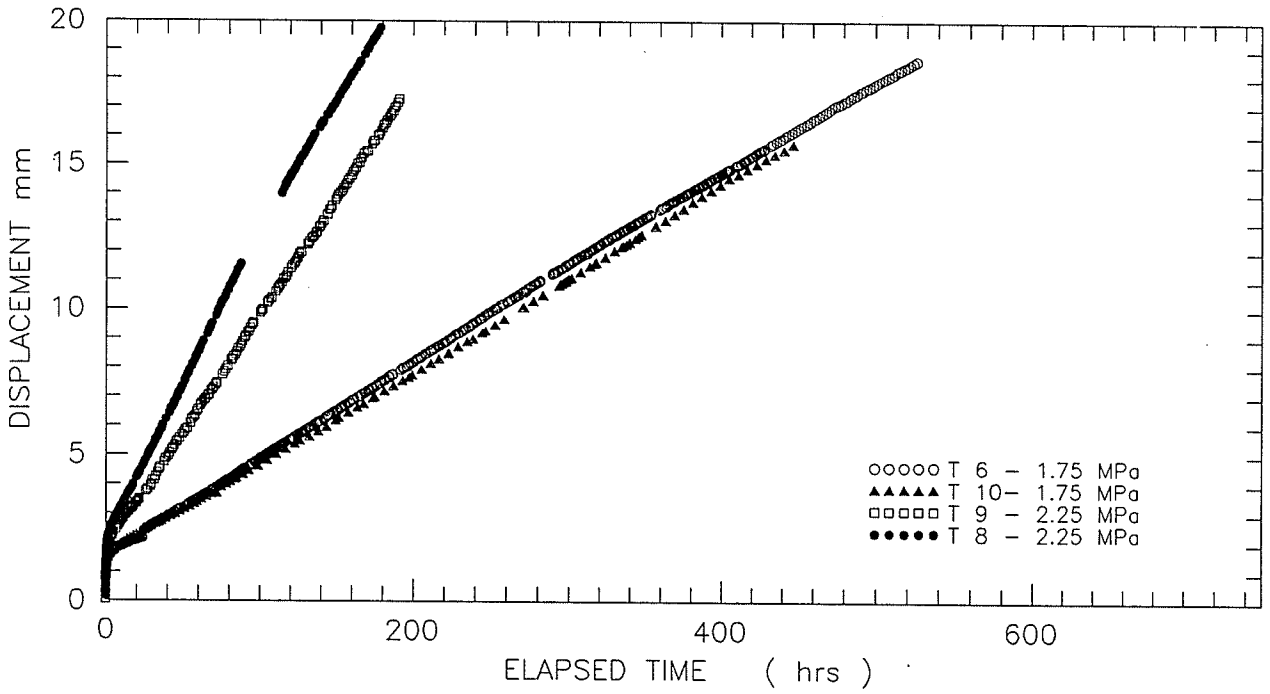

Figure 4.14 Repeatability of single stage tests: displacements versus elapsed time.